UCLA
UCLA Electronic Theses and Dissertations

Title

Electric Vehicle Integration for Grid services using AI, optimization, and blockchain

Permalink

https://escholarship.org/uc/item/51f5b4d6

Author

Narayana Gowda, Shashank

Publication Date

2024

Peer reviewed|Thesis/dissertation

eScholarship.org Powered by the California Digital Library
University of California

UNIVERSITY OF CALIFORNIA

Los Angeles

Electric Vehicle Integration for Grid services using AI, optimization, and blockchain

A dissertation submitted in partial satisfaction

of the requirements for the degree

Doctor of Philosophy in Mechanical Engineering

by

Shashank Narayana Gowda

2024

© Copyright by
Shashank Narayana Gowda
2024

ABSTRACT OF THE DISSERTATION

Electric Vehicle Integration for Grid services using AI, optimization, and blockchain

by

Shashank Narayana Gowda
Doctor of Philosophy in Mechanical Engineering
University of California, Los Angeles, 2024
Professor Rajit Gadh, Chair

The rapid adoption of electric vehicles (EVs) presents both challenges and opportunities for modern power grids. This dissertation advances EV integration within power grid systems through four interconnected contributions. First, the application of transfer learning and model-agnostic meta-learning techniques enhance short-term EV charging load forecasting in an evolving EV landscape, reducing forecasting errors by up to 61% compared to traditional machine learning approaches. These improvements enable grid operators to better manage dynamic charging patterns across diverse geographical conditions with limited historical data.

Second, an optimization framework leveraging Vehicle-to-Grid (V2G) technology demonstrates potential for grid congestion relief through strategic charging and discharging based on congestion component of Locational Marginal Prices. While EVs can contribute to grid stability, economic analysis reveals that participation typically results in net monetary losses under current market models when accounting for seasonal variations and battery degradation costs.

Third, a blockchain-based framework addresses battery degradation concerns in V2G ap-

plications through real-time tracking and assessment. The framework dynamically updates degradation cost parameters based on charging activities and environmental conditions, enabling transparent management of battery lifecycle costs and informed V2G participation.

Fourth, an optimal sizing method for Battery Energy Storage Systems (BESS) integration with electric bus charging infrastructure in urban transit networks optimizes is discussed for both depot and en-route charging scenarios. The resulting framework demonstrates how strategic storage deployment manages peak loads and reduces operational costs, enhancing the economic viability of electric public transit.

These contributions advance the development of efficient and resilient electrified transportation systems through innovative solutions in load forecasting, grid services, battery management, and infrastructure cost reduction, supporting the global transition to sustainable energy.

The dissertation of Shashank Narayana Gowda is approved.

Samanvaya Srivastava

Khalid Jawed

Xiaochun Li

Rajit Gadh, Committee Chair

University of California, Los Angeles

2024

To my family ...

for their love and support.

TABLE OF CONTENTS

1 Introduction **1**

1.1 Background and Motivation 1

1.1.1 Advanced EV load forecasting 3

1.1.2 Congestion Relief 4

1.1.3 Blockchain for EV battery management 5

1.1.4 BESS to support electric bus charging 5

1.2 Dissertation Outline 6

2 Advanced EV Load forecasting **8**

2.1 Datasets 10

2.1.1 Colorado Dataset 11

2.1.2 ACN Dataset 11

2.1.3 Norway Dataset 12

2.1.4 Data Pre-processing 14

2.2 Models 15

2.2.1 Neural networks 15

2.2.2 LSTM 16

2.2.3 Transfer Learning 18

2.2.4 Model-Agnostic Meta-Learning 19

2.2.5 Classical Machine Learning Baselines 21

2.2.6 Experimental setup 23

2.3 Results 24

2.3.1 ACN dataset . . . 24
2.3.2 Norway shared charger dataset . . . 27
2.3.3 Norway private charger dataset . . . 31
2.4 Discussion . . . 31

3 Congestion Relief . . . 35
3.1 Framework and methodology . . . 38
3.1.1 Congestion Relief and Financial Transmission Rights . . . 38
3.1.2 Utility Scale Energy Storage Projects for Congestion Relief . . . 40
3.1.3 Locational Marginal Price . . . 42
3.1.4 Node Selection Process . . . 44
3.1.5 LMP Visualization . . . 47
3.1.6 Battery Degradation . . . 50
3.1.7 Optimization . . . 52
3.2 Results . . . 55
3.3 Discussion . . . 69

4 Blockchain for EV battery degradation . . . 72
4.1 Blockchain . . . 75
4.2 Variable Battery Degradation Model . . . 78
4.3 Optimization framework . . . 80
4.4 Results . . . 83
4.5 Discussion . . . 85

5 BESS support for electric buse charging . . . 87

5.1 E-bus charging infrastructure 89
5.2 BESS sizing optimization 90
5.2.1 Optimization objective and constraints 90
5.3 Case study 94
5.4 Results 96
5.5 Discussion 100

6 Conclusion 102
6.1 Summary 102
6.2 Future Work 104

References 106

LIST OF FIGURES

1.1 Projected growth of global renewable energy capacity. 1

1.2 Cumulative stock of EVs around the world. 2

2.1 Aggregate EV charging load distribution in the Colorado dataset. 11

2.2 Aggregate EV charging load distribution in the ACN dataset. 12

2.3 Aggregate EV charging load distribution from shared chargers in the Norway dataset. 13

2.4 Aggregate EV charging load distribution from private chargers in the Norway dataset. 13

2.5 Tabular representation of inputs and outputs used in the models. 14

2.6 Structure of an LSTM network highlighting the various gates, weights, biases and operations. 16

2.7 Schematic showcasing transfer learning 18

2.8 Adjacent time windows alternated in the support and query sets for MAML . . 20

2.9 Results from the forecasting models compared to the true load value on a subset of the ACN dataset starting from September 18, 2019 for 10 days 26

2.10 Results from the forecasting models compared to the true load value on a subset of the ACN dataset starting from November 9, 2020 for 20 days 26

2.11 Results from the forecasting models compared to the true load value on a subset of the Norway shared charger dataset starting from February 21, 2019 for 10 days 27

2.12 Results from the forecasting models compared to the true load value on a subset of the Norway shared charger dataset starting from September 17, 2019 for 20 days 29

2.13 Results from the forecasting models compared to the true load value on a subset of the Norway private charger dataset starting from February 21, 2019 for 10 days 32

2.14 Results from the forecasting models compared to the true load value on a subset of the Norway private charger dataset starting from September 17, 2019 for 20 days 32

3.1 Low congestion across the CAISO grid on a Spring morning. 38

3.2 Extremely high congestion in the MISO grid in the morning of 9/7/2011. 39

3.3 Transmission line network in CAISO. 45

3.4 Wind and solar curtailment by month in CAISO. 46

3.5 Congestion and energy components of LMP visualized for DGPAN1_7_B1. . . . 48

3.6 Congestion components of LMP visualized for the ends of the 230 kV Panoche–Gates transmission lines at nodes DGPAN1_7_B1 and HURON_6_N001. 49

3.7 Congestion and energy components of LMP visualized for DSRTHV3_7_N003. . 50

3.8 Savings from LMP_T minimization at the nodes at the ends of the transmission lines. 56

3.9 Savings from LMP_C minimization at the nodes at the ends of the transmission lines. 57

3.10 Battery capacity loss (%) from LMP_T and LMP_C minimization at the nodes at the ends of the transmission lines. 58

3.11 Savings from LMP_T minimization at the solar power plant nodes. 59

3.12 Savings from LMP_C minimization at the solar power plant nodes. 60

3.13 Battery capacity loss (%) from LMP_T and LMP_C minimization at the solar power plant nodes. 61

3.14 Monthly savings from LMP_T minimization at DGPAN1_7_B1. 62

3.15 Monthly savings from LMP_T minimization at HURON_6_N001. 63

3.16 Monthly savings from LMP_T minimization at DSRTHV3_7_N003. 63

3.17 Monthly savings from LMP_C minimization at DGPAN1_7_B1. 64

3.18 Monthly savings from LMP_C minimization at HURON_6_N001. 64

3.19 Monthly savings from LMP_C minimization at DSRTHV3_7_N003. 65

3.20 Monthly total V2G power throughput at DGPAN1_7_B1. 66

3.21 Monthly total V2G power throughput at HURON_6_N001. 66

3.22 Monthly total V2G power throughput at DSRTHV3_7_N003. 67

3.23 Congestion savings in $/kWh of V2G at DGPAN1_7_B1. 68

3.24 Congestion savings in $/kWh of V2G at HURON_6_N001. 68

3.25 Congestion savings in $/kWh of V2G at DSRTHV3_7_N003. 69

4.1 Schematic highlighting the relationship among EVAs, CSO and EVs with the grid. 74

4.2 A network fabric diagram showing the different data access authorizations for all actors in a blockchain consortium network. 77

4.3 Bar chart highlighting the remaining battery energy capacity in the EVs utilized for V2G using the constant and dynamic degradation costs. 84

5.1 Metro G Line (Orange Line) connecting Chatsworth to North Hollywood in Los Angeles. 95

5.2 BESS power, E-bus charging load, and electric grid load at the Chatsworth Depot charging station during a 24-hour cycle. The BESS load curve is non-existent since no BESS specification results in savings over 10 years. 97

5.3 BESS power, E-bus charging load, and electric grid load at the Chatsworth en-route charging station during a 24-hour cycle. The BESS responsible for the BESS load profile results in savings over 10 years. 98

5.4 BESS power, E-bus charging load, and electric grid load at the Canoga en-route charging station during a 24-hour cycle. The BESS responsible for the BESS load profile results in savings over 10 years. 99

5.5 BESS power, E-bus charging load, and electric grid load at the North Hollywood en-route charging station during a 24-hour cycle. The BESS responsible for the BESS load profile results in savings over 10 years. 100

LIST OF TABLES

2.1 Mean MAE, RMSE and R2 scores of the forecasting models on the ACN dataset 25

2.2 Mean MAE, RMSE and R2 scores of the forecasting models on the Norway shared charger dataset 28

2.3 Mean MAE, RMSE, and R2 scores of the forecasting models on the Norway private charger dataset 30

3.1 Grid-scale battery projects in the USA resulting in transmission congestion relief. 41

3.2 Congested transmission lines and nodes at the ends of the transmission lines. . . 45

3.3 Chosen solar power plants from California for analysis. 47

4.1 Results from the degradation costs at the end of three-year period. 84

5.1 BESS cost and parameter ranges per kWh and kW for Li-Ion battery types, for the year 2025 96

5.2 Optimal BESS specifications and cost savings over a 10-year period 99

ACKNOWLEDGMENTS

This dissertation would not have been possible without the endless support from many individuals. First and foremost, I would like to express my immense gratitude to my doctoral advisor, Professor Rajit Gadh, for giving me the opportunity to join the Smart Grid Energy Research Center (SMERC) and tackle challenging problems in the energy domain. His mentorship has been invaluable, offering constant support, encouraging critical thinking, and fostering my growth as a researcher. Under his guidance, I have not only developed my technical skills but have also significantly improved my communication abilities. He has also played a key role in helping me build a strong professional network by hosting events, writing grants, and connecting me with outstanding people.

I would like to extend my sincere thanks to my committee members, Professor Samanvaya Srivastava, Professor Khalid Jawed, and Professor Xiochun Li, for providing insightful feedback on my research, writing, and presentations. Thank you for dedicating your time and effort despite your busy schedules.

I am also grateful to Dr. Peter Chu for his guidance and support throughout my PhD journey. His advice has been invaluable in helping me develop a vision for large projects and break them down step-by-step. I also appreciate the support and camaraderie of the PhD students and alumni from SMERC, including Yingxi Xiong, Behnam Khaki, Zhiyuan Cao, Yu-Wei Chung, and Amirhossein Ahmadian. Special thanks to Professor Hamidreza Nazaripouya and Tianyang Zhang for mentoring me during my early projects and teaching me how to write better research papers, as well as Bin Wang for his career advice. I am especially thankful to Chen Zhang, Rachel Sheinberg, and Rafi Zahedi for fostering a wonderful lab culture—I have thoroughly enjoyed working with you and look forward to future collaborations. I would also like to acknowledge Kamini Singh, Basem Eraqi, Kevin Wiranata, and Keshav Nath for their fruitful collaborations.

I would like to thank the Life Sciences and Physics departments at UCLA for supporting

me with teaching positions throughout my PhD. These opportunities helped me grow as a teacher, leader, mentor, and communicator. I am particularly grateful to Professor Katsushi Arisaka for involving me in the development of Physics 4AL, where I was able to update a course taken by over 800 undergraduates annually and successfully adapt it for a virtual environment. I also thank Professor Jay Hauser and Professor Ni Ni for helping me become a better teacher and mentor. Although balancing teaching responsibilities with research was challenging, the experience enriched me both personally and professionally. I am honored to have received recognition from the Physics department, including teaching awards and a nomination for the Distinguished Teaching Awards at UCLA. While I did not win, I am touched by the support letters from professors and students, which are treasures I will carry with me.

I am fortunate to have wonderful friends who made Los Angeles feel like home and explored this new culture with me. I am also extremely grateful to my girlfriend and her family for being my family in the US, helping me come out of my shell, and creating cherished memories. Their support has been invaluable.

My deepest gratitude goes to my parents, whose unwavering support has made me who I am today. Being the first in my extended family to pursue a PhD and study abroad was not easy, but their encouragement has been constant throughout this journey. Finally, I want to thank my brother, the first in our family to complete a Ph.D., for being an inspiration and my greatest support. I am incredibly lucky to have my best friend as my brother.

This Ph.D. journey would not have been the same without all these amazing people. Thank you all for being there through the highs and lows.

Chapter 2 is based on the following publications-

Narayana Gowda, S., Nath, K., Zhang, C., Gowda, R., & Gadh, R. (2024). Short-term aggregate electric vehicle charging load forecasting in diverse conditions with minimal data using transfer and meta-learning. Energy Systems, 1-20.

Nath, K., Gowda, S. N., Zhang, C., Gowda, R. S., & Gadh, R. (2024, February). Short-term

Electric Vehicle Charging Load forecasting using Transfer and Meta-learning. In 2024 IEEE Power & Energy Society Innovative Smart Grid Technologies Conference (ISGT) (pp. 1-5). IEEE.

Chapter 3 is based on the following publications-

Narayana Gowda, S., Nazaripouya, H., & Gadh, R. (2023). Congestion Relief Services by Vehicle-to-Grid Enabled Electric Vehicles Considering Battery Degradation. Sustainability, 15(24), 16733.

Gowda, S. N., Zhang, T., Kim, C. J., Gadh, R., & Nazaripouya, H. (2019, February). Transmission, Distribution deferral and Congestion relief services by Electric Vehicles. In 2019 IEEE Power & Energy Society Innovative Smart Grid Technologies Conference (ISGT) (pp. 1-5). IEEE.

Chapter 4 is based on publication-

Gowda, S. N., Eraqi, B. A., Nazaripouya, H., & Gadh, R. (2021, February). Assessment and tracking electric vehicle battery degradation cost using blockchain. In 2021 IEEE Power & Energy Society Innovative Smart Grid Technologies Conference (ISGT) (pp. 1-5). IEEE.

Chapter 5 is based on publication-

Gowda, S. N., Ahmadian, A., Anantharaman, V., Chu, C. C., & Gadh, R. (2022, April). Power management via integration of battery energy storage systems with electric bus charging. In 2022 IEEE Power & Energy Society Innovative Smart Grid Technologies Conference (ISGT) (pp. 1-5).

This work has been sponsored in part by grants 69763 and 45779.

VITA

2014	B.Tech., Mechanical Engineering, National Institute of Technology, Karnataka.
2014-15	Project Assistant, Microfluidic Devices & Heterogeneous Systems Lab, Indian Institute of Science.
2015-17	Graduate Student Researcher, Micro & Nano Manufacturing Lab, UCLA.
2017-24	Graduate Student Researcher, Smart Grid Energy Research Center, UCLA.
2017	M.S., Mechanical Engineering, UCLA.
2016-19	Teaching Assistant, Physics and Astronomy/Life Sciences Core Education, UCLA.
2019-22	Lead Teaching Assistant and Course Developer, Physics and Astronomy, UCLA.
2020	Energy Analytics Intern, Apex Clean Energy.
2021	Energy Storage Engineer Intern, Apex Clean Energy.

SELECTED PUBLICATIONS

Narayana Gowda, S., Nath, K., Zhang, C., Gowda, R., & Gadh, R. (2024). Short-term aggregate electric vehicle charging load forecasting in diverse conditions with minimal data using transfer and meta-learning. Energy Systems, 1-20.

Nath, K., **Gowda, S. N.**, Zhang, C., Gowda, R. S., & Gadh, R. (2024, February). Short-term Electric Vehicle Charging Load forecasting using Transfer and Meta-learning. In 2024 IEEE Power & Energy Society Innovative Smart Grid Technologies Conference (ISGT) (pp. 1-5). IEEE.

Narayana Gowda, S., Nazaripouya, H., & Gadh, R. (2023). Congestion Relief Services by Vehicle-to-Grid Enabled Electric Vehicles Considering Battery Degradation. Sustainability, 15(24), 16733.

Gowda, S. N., Ahmadian, A., Anantharaman, V., Chu, C. C., & Gadh, R. (2022, April). Power management via integration of battery energy storage systems with electric bus charging. In 2022 IEEE Power & Energy Society Innovative Smart Grid Technologies Conference (ISGT) (pp. 1-5). IEEE.

Gowda, S. N., Eraqi, B. A., Nazaripouya, H., & Gadh, R. (2021, February). Assessment and tracking electric vehicle battery degradation cost using blockchain. In 2021 IEEE Power & Energy Society Innovative Smart Grid Technologies Conference (ISGT) (pp. 1-5). IEEE.

Gowda, S. N., Zhang, T., Kim, C. J., Gadh, R., & Nazaripouya, H. (2019, February). Transmission, Distribution deferral and Congestion relief services by Electric Vehicles. In 2019 IEEE Power & Energy Society Innovative Smart Grid Technologies Conference (ISGT) (pp. 1-5). IEEE.

CHAPTER 1

Introduction

1.1 Background and Motivation

Global population growth and development have driven unprecedented energy demand. Despite their environmental and health impacts, fossil fuels remain the primary energy source worldwide, contributing significantly to air pollution and climate change [1]. The global pursuit of sustainable solutions has created a transformative era in electrical grid systems, with renewable energy systems (RES) and electric vehicles (EVs) leading this revolution. Figure 1.1 shows the rise in installed global solar and wind energy capacity with a combined capacity of 1800 GW as of 2022 [2]. Figure 1.2 illustrates the rapid increase in the stock of EVs around the world, with China emerging as the leading market [3].

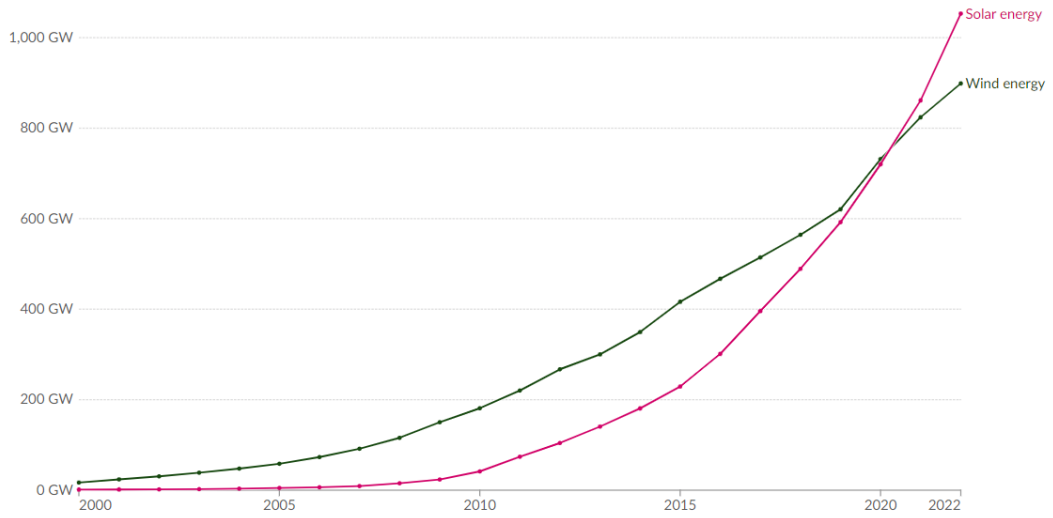


Figure 1.1: Projected growth of global renewable energy capacity.

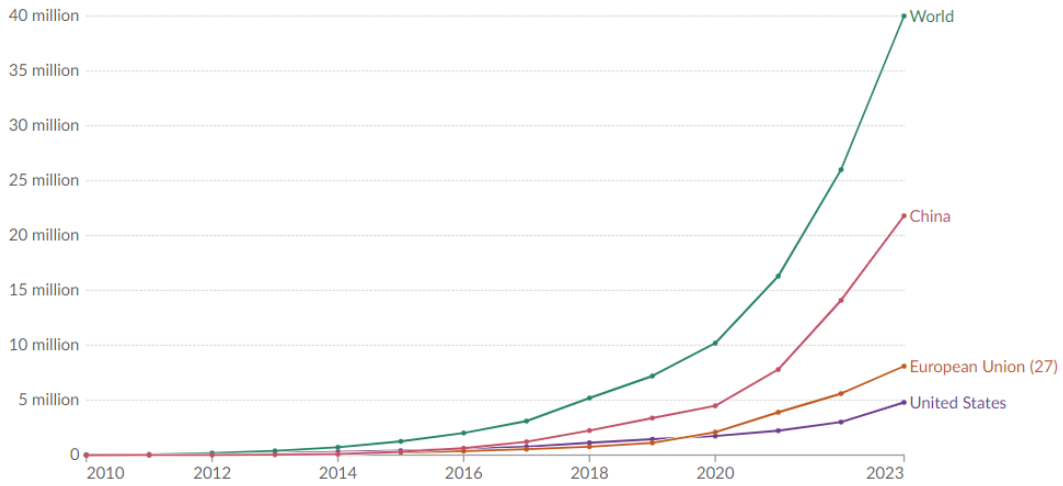


Figure 1.2: Cumulative stock of EVs around the world.

The growing integration of RES and EVs introduces new complexities in coordinating electricity supply and demand due to inherent uncertainties. Renewable energy fluctuations can compromise grid stability through supply-demand mismatches. During low renewable generation periods, utilities must either activate expensive, polluting peaker plants or implement load shedding. Conversely, excess renewable generation requires power curtailment, leading to monetary losses. Both scenarios risk equipment damage or power outages through voltage and frequency fluctuations [4]. Similarly, uncontrolled EV charging creates challenges for power systems by increasing load peaks and operational costs while threatening transformer and distribution line overload, potentially resulting in decreased power quality, grid instability, blackouts, and costly infrastructure upgrades [5].

Accurate forecasting of electricity supply and demand is crucial for maintaining grid stability amid these challenges. The modern smart grid, leveraging advanced sensors, automation, communication, and control systems, enables precise matching of supply and demand across various time scales [6]. While EVs initially present significant challenges for grid stability, energy management, and infrastructure planning, they also offer unique opportunities for grid support and optimization [7]. This thesis comprehensively explores the multifaceted role of EVs in the evolving smart grid landscape through four interconnected areas: ad-

vanced EV load forecasting, grid congestion relief using EV flexibility, blockchain-based EV battery health management, and the integration of battery energy storage systems to support heavy-duty EV charging infrastructure. Together, these research areas address critical aspects of EV integration to advance a more sustainable and resilient energy future.

1.1.1 Advanced EV load forecasting

Maintaining a seamless balance between electricity supply and demand requires accurate forecasting models that can effectively account for uncertainties in both RES and EV charging across various time scales [6]. On the supply side, RES like wind and solar are highly dependent on weather conditions, leading to intermittent power generation that complicates grid operations and makes accurate supply prediction challenging, particularly during periods of fluctuating energy production [4]. On the demand side, the growing number of EVs, each with unique charging patterns, creates additional complexity in load prediction, further complicating grid management.

The evolving energy landscape, characterized by rapidly increasing EV adoption, presents unique challenges for traditional forecasting approaches. Modern algorithms must perform effectively with limited historical data while adapting quickly to changing conditions, including the addition of new EV users, expanding charging infrastructure, emerging establishments, diverse environments, and varied charging behaviors [8]. These capabilities are crucial for successful demand-side management, enabling grid operators to mitigate peak loads, optimize energy distribution, and reduce operational costs while minimizing RES curtailment. Furthermore, accurate forecasting facilitates better integration of demand-side flexibility, reducing costs in both planning and operational phases thereby ensuring grid stability and efficiency in modern energy systems.

1.1.2 Congestion Relief

Line congestion occurs when transmission lines operate at their limits due to thermal, voltage, or stability constraints. This congestion creates barriers to efficient electricity flow, particularly from low-cost RES to end-users. In various electricity markets worldwide, this congestion necessitates differential pricing, resulting in additional operational costs when transmission lines operate near capacity [9]. When congestion occurs, grid operators must activate more expensive generation sources to deliver power through non-congested routes, leading to increased electricity prices in affected regions.

Battery Energy Storage Systems (BESS) are a promising solution due to their declining costs and improved battery lifespans [10]. Simultaneously, EVs, which rely entirely on battery power for transportation, present new opportunities for grid support, especially when combined with Vehicle-to-Grid (V2G) technology [11]. V2G allows EVs to engage in two-way power flow with the grid, transforming parked vehicles into modular mobile energy resources. When strategically coordinated, EVs can contribute to grid efficiency by participating in services like frequency regulation [12], energy arbitrage [13], and congestion relief [14]. Moreover, EVs can help balance supply and demand by charging during periods of excess renewable generation and discharging during peak demand, thereby reducing curtailment and alleviating grid congestion. This capability is particularly relevant in regions like California, where the "duck curve" phenomenon highlights the challenges of managing variable renewable energy.

Despite the extensive exploration of BESS and EVs in grid applications, the potential of EVs with V2G for addressing congestion has been relatively underexplored. Optimal charging and discharging strategies for EVs located at the end nodes of congested lines can provide congestion relief.

1.1.3 Blockchain for EV battery management

One of the major challenges in adopting V2G to support the grid lies in battery degradation caused by frequent charging and discharging [15]. The economic impact of this degradation introduces uncertainties in determining the cost-effectiveness of V2G participation. Factors such as battery degradation costs, electricity prices, revenue from grid services, and the availability of renewable energy must be carefully considered when deciding on V2G deployment. While fleet operators may overlook battery degradation to maximize revenue, this is a significant concern for private EV owners.

At the system level, charging station operators host EV charging stations, while an aggregator manages and controls the charging stations across multiple facilities. Grid services typically require power in the range of hundreds of kW to a few MW which cannot be provided by an individual EV, so the aggregator bids for the necessary services in the market and fulfills the commitments by aggregating the power from multiple EVs [16]. In such a scenario, the interests of different actors can conflict if left unregulated. For instance, an EV that could be fully charged in one hour but remains parked for eight hours might undergo multiple charging and discharging cycles, maximizing revenue for the aggregator while providing minimal compensation to the EV owner. This practice accelerates battery degradation, reducing the lifespan of the EV battery [17]. In such a system, a blockchain can track power flow, monetary transactions, and battery degradation, enabling transparent and fair management of V2G interactions while helping to prolong EV battery life.

1.1.4 BESS to support electric bus charging

In line with ambitious climate goals and regulations, various utilities are making efforts to electrify bus fleet by installing charging facilities for both depot and en-route charging as part of their journey toward achieving a 100% renewable energy. portfolio by 2030 [18]. However, the high capital costs associated with electric buses (E-bus) remain a significant barrier to

widespread adoption [19]. While the lower fuel costs of E-Buses make them competitive against traditional diesel buses, studies have shown that fast-charging technologies, essential for continuous E-Bus operation, can lead to increased electricity costs and higher operating expenses [20].

Electricity costs are largely driven by two components: energy charges and demand charges. Demand charges, which are triggered by peak power demand, can reach as high as \$90/kW in commercial and industrial sectors in the United States [21]. These charges can significantly impact the economics of E-Bus operations. Integrating E-bus charging stations with BESS can alleviate the financial burden by reducing peak demand and smoothing charging loads. Optimal BESS configurations for efficiently managing E-Bus charging demand while minimizing operational costs

1.2 Dissertation Outline

The rest of this dissertation is organized as follows:

Chapter 2 explores the use of Transfer Learning (TL) and Model-Agnostic Meta-Learning (MAML) to develop models capable of accurately forecasting short-term EV charging loads with minimal data [22] [23]. The models are fine-tuned using only 10 to 20 days' worth of data to predict the next 5 to 10 days across diverse datasets. Model robustness is ensured by testing across varying scales, geographies, and demographics using multiple datasets sourced from different locations and contexts.

Chapter 3 examines the potential of EVs with V2G capabilities to reduce congestion-related costs in aging electric grid infrastructure [14]. The focus is on strategic node locations within the Califorinia Independent System Operator (CAISO) jurisdiction, identifying those most affected by transmission congestion and large solar generation plants using historical pricing data. The study models EV charging and discharging strategies to either minimize congestion or maximize arbitrage revenue, while discussing the trade-offs between these

objectives [24].

Chapter 4 introduces a method for calculating battery degradation costs that incorporates both cycle aging (charging/discharging cycles and depth of discharge) and calendar aging (natural degradation over time) [13]. Unlike traditional approaches that treat degradation cost as a constant, this method dynamically updates the cost based on charging/discharging parameters and battery temperature conditions, offering a more accurate and timely representation of the battery's health and economic value. This dynamically updated degradation cost is integrated into optimized decision-making processes, considering the evolving condition of the battery. All transactions and degradation cost data are securely logged into a consortium blockchain accessible to relevant stakeholders, enhancing transparency and preventing abuse of EV batteries for profit maximization.

Chapter 5 investigates the optimal BESS configurations for efficiently managing E-Bus charging demand while minimizing operational costs in both depot and en-route charging scenarios [25]. The optimization considers factors such as operating range, charging schedules, flexibility, grid capacity, fleet size, and charging interfaces to reduce costs, including demand charges and facility charges.

Chapter 6 concludes the dissertation with a summary of the thesis including key results and recommendations for future research.

CHAPTER 2

Advanced EV Load forecasting

The increasing incorporation of RES and EVs introduces complexities in achieving coordination between electricity supply and demand due to their inherent uncertainties. Consequently, accurate forecasting of electricity generation and loads assumes pivotal importance in sustaining a stable smart grid, enabling the precise matching of supply and demand across various time scales [6]. On the supply side, wind and solar energy sources exhibit intermittency, relying on external weather variables outside human control. Simultaneously, the forecasting of EV charging loads becomes a necessity for long-term infrastructure planning and medium-to-short-term demand-side management. These efforts mitigate peak loads, reduce costs, and minimize the curtailment of RES [5]. Furthermore, harnessing demand-side flexibility has the potential to yield cost savings in both planning and operational aspects [7].

Traditionally, EV charging load forecasting is treated as a time series problem and involves the application of statistical and machine learning approaches [5]. Among statistical methods, autoregressive integrated moving average (ARIMA) and exponential smoothing (ETS) are popular due to their simplicity, robustness, efficiency, and accuracy [26]. Machine learning techniques, such as Long Short-Term Memory (LSTM) networks, a type of recurrent neural network (RNN) that leverages both current and stored information in memory, are widely used for time series forecasting, at times surpassing the performance of statistical methods [26]. To enhance the predictive accuracy further, the authors in [5] adopted ensemble learning techniques that combine the strengths of multiple machine learning models, effectively synergizing their capabilities to enhance the precision of EV charging load

forecasting.

The evolving energy landscape, characterized by rapidly increasing EV adoption, presents unique challenges for traditional forecasting approaches. Modern algorithms must perform effectively with limited historical data while adapting quickly to changing conditions, including the addition of new EV users, expanding charging infrastructure, emerging establishments, diverse environments, and varied charging behaviors [8]. However, neural network (NN)-based forecasting methods exhibit suboptimal performance in these scenarios characterized by limited or evolving training data. One approach to address this challenge is transfer learning (TL), which leverages pre-trained forecasting models developed using extensive and diverse datasets as initial models. These pre-trained models can then undergo fine-tuning using a limited dataset specific to the problem at hand [27]. [28] proposed the use of TL using deep generative models for cold-start forecasting of residential EV charging behavior. Generative models were used to augment the small samples in the target dataset before fine-tuning. A hybrid LSTM TL model was used in [29] to predict EV charging demand and network voltage profiles with limited data within a single city.

Another promising algorithm for mitigating the data scarcity issue is model-agnostic meta-learning (MAML). MAML is capable of training on a variety of learning tasks, enabling it to adeptly tackle new learning tasks with a limited number of available training samples [30]. [31] introduced a transferable MAML model tailored for short-term load forecasting in individual Australian households. [8] harnessed transfer and meta-learning techniques to predict personalized residential loads in Korea and substation loads in Portugal but ignored load patterns during weekends and holidays. Both [31] and [8] performed univariate load forecasting where the only feature used to predict load was historical load. [32] employed a meta-learning model to forecast load profiles at the transmission level, utilizing open-access data from Elia, a Belgian transmission system operator. In [32], the forecast was performed to find the future values in the same source dataset, meanwhile [31] and [8] forecasted loads of similar scale in the same country.

In this chapter, we employ TL and MAML techniques for short-term aggregate EV charging load forecasting. Our investigation spans two distinct geographical areas: the California Institute of Technology (Caltech) campus [33] and the Trondheim region in Norway [34]. We accomplish this by leveraging a comprehensive EV charging load dataset sourced from Boulder, Colorado for pre-training [5]. These datasets encompass varying scales, including campus-level, housing initiative-level, and city-level data. Moreover, they originate from different locations: Pasadena, CA, USA; Trondheim, Norway; and Boulder, CO, USA. Additionally, we work with aggregated EV charging data in both shared charger and private charger settings. To assess the effectiveness of our approach, we evaluate the performance of different TL, MAML, and traditional LSTM network variants on these diverse datasets at time scales of 10 to 20 days. The models are fine-tuned on only 10 or 20 days' worth of data to predict the next 5 to 10 days for each investigated dataset. We compare our results to traditional LSTM deep learning networks and other classic machine learning models.

This chapter is organized as follows:

- Section 2.1 presents the dataset collection and pre-processing methodology
- Section 2.2 introduces TL and MAML frameworks, along with their neural network architectures and experimental methodology
- Section 2.3 evaluates the performance of TL and MAML approaches against traditional deep learning and classical machine learning methods across diverse scenarios
- Section 2.4 summarizes key findings and implications

2.1 Datasets

We utilized three distinct publicly available datasets containing EV charging data from Pasadena, CA, USA; Trondheim, Norway; and Boulder, CO, USA.

2.1.1 Colorado Dataset

The Colorado dataset [35], used in [5], contains records of individual EV charging transactions from city-owned shared charging stations in Boulder, Colorado, USA, spanning January 1, 2018, to July 31, 2022. The aggregated EV charging load data is shown in Figure 2.1.

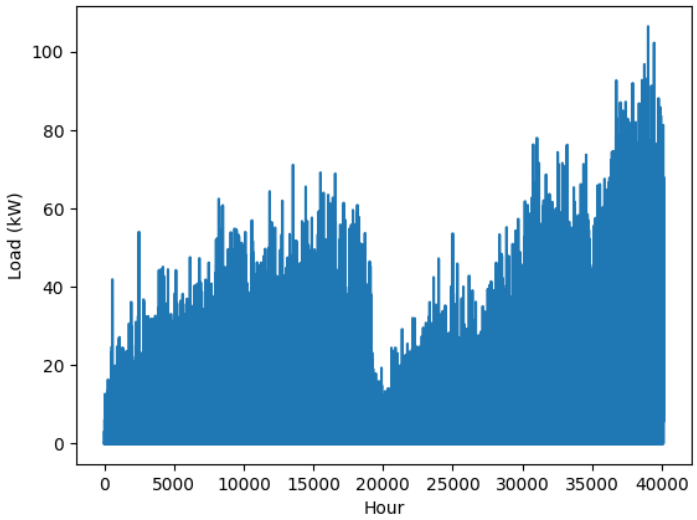


Figure 2.1: Aggregate EV charging load distribution in the Colorado dataset.

2.1.2 ACN Dataset

The Adaptive Charging Network (ACN) dataset [33] comprises EV charging transactions recorded at the Caltech and JPL campuses. Our analysis focuses on the Caltech data due to its lower EV penetration and sparser nature, as shown in Figure 2.2. This dataset spans from April 4, 2019, to September 16, 2021.

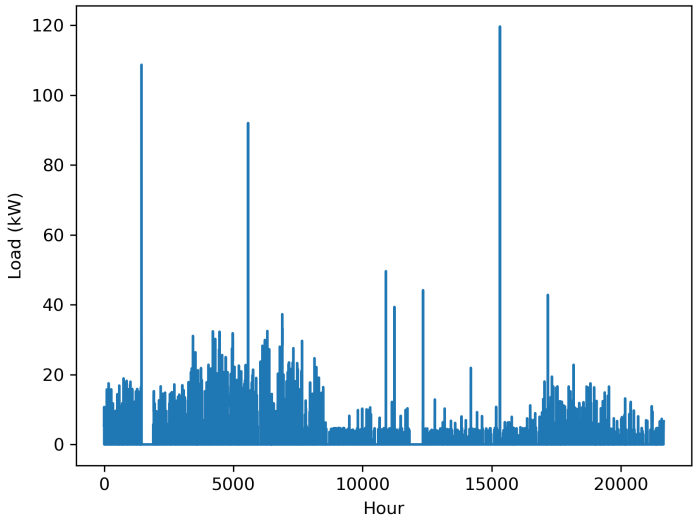


Figure 2.2: Aggregate EV charging load distribution in the ACN dataset.

2.1.3 Norway Dataset

The Norway dataset [36], analyzed in [34], contains hourly charging load data from charging stations within a residential block in the Trondheim region. The dataset comprises two components: aggregate shared charger data and aggregate private charger data, visualized in Figures 2.3 and 2.4, respectively. Both datasets exhibit irregular distribution patterns due to the incremental addition of chargers over time. The aggregate private charger data shows approximately three times the magnitude of the shared charger data. The shared charger data spans January 10, 2019, to January 31, 2020, while the private charger data covers December 21, 2018, to January 31, 2020.

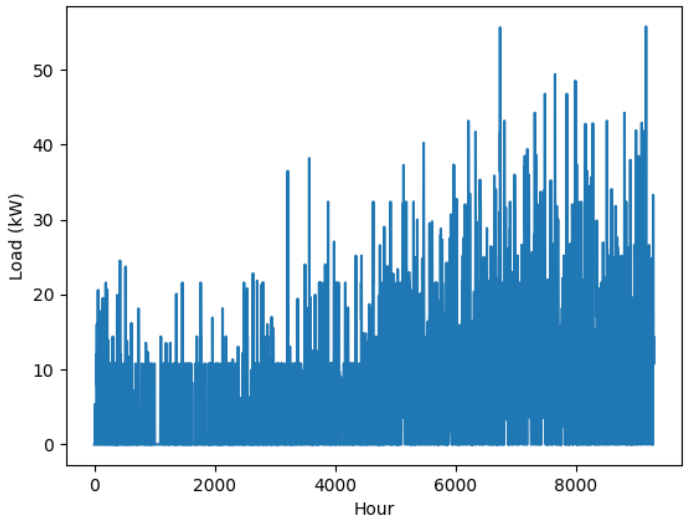


Figure 2.3: Aggregate EV charging load distribution from shared chargers in the Norway dataset.

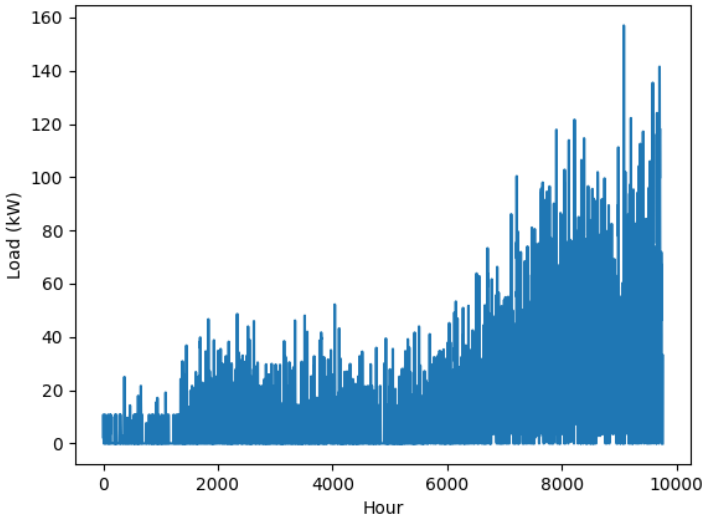


Figure 2.4: Aggregate EV charging load distribution from private chargers in the Norway dataset.

2.1.4 Data Pre-processing

We transformed the Colorado and ACN datasets from charging transactions into hourly load format. Subsequently, all four datasets (Colorado, ACN, Norway-shared, and Norway-private) underwent comprehensive pre-processing, incorporating ten features:Hour, Quarter-of-day, Day, Day-of-week, Week-of-year, Month, Quarter-of-year, Season, and Load (kW)

The data was structured into input-output pairs, with the input comprising a sequence of 24 consecutive hours as features and the load of the 25th hour serving as the target variable as shown in figure 2.5. Formally, $D = (x_t, y_t), t \in T$ with $x_t \in \mathbb{R}^{10\times24}$ and $y_t \in \mathbb{R}$. Given the substantial size and density of the Colorado dataset, we employed it for pre-training both the MAML and TL models. These pre-trained models were then fine-tuned using subsets of the ACN and Norway datasets. The fine-tuning process utilized 10-day and 20-day subsets, requiring the models to forecast hourly loads for the subsequent 10 and 20 days, respectively. This approach challenged the models to adapt to very limited historical data when predicting future trends.

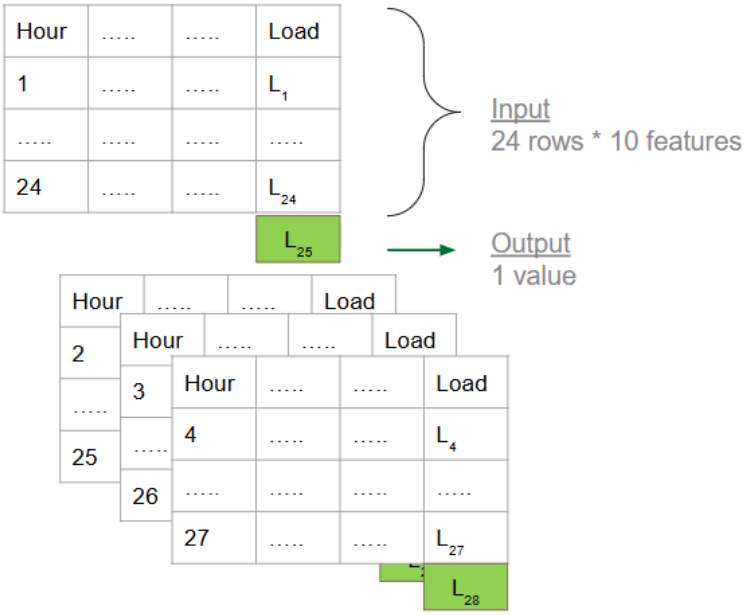


Figure 2.5: Tabular representation of inputs and outputs used in the models.

2.2 Models

2.2.1 Neural networks

In the context of forecasting, which falls under supervised learning, a neural network (NN) can be represented as $z = f_\theta(x)$, where x represents the input, z denotes the output, and $\theta \in \mathbb{R}^n$ encompasses parameters distributed across multiple layers in the network. Typically, θ comprises weights W that signify the strength between neuronal connections in adjacent layers, as well as biases b within each layer.

These parameters are subject to optimization for a specific task $\mathcal{T} = (D, L)$, minimizing a loss function L over a designated subset of data $D = (x_t, y_t) \mid t \in T$, employed for training $D_{train} = (x_t, y_t) \mid t \in T_{train}$. x_t represents the input data and y_t stands for the corresponding labels. T encompasses the total number of samples within the dataset, and T_{train} denotes the portion of samples reserved for training. The loss function L leverages a distance metric $d()$ to capture the dissimilarity between the model outputs z and the ground truth labels y.

$$L(\theta) = \sum_{t \in T} d(z_t, y_t) = \sum_{t \in T} d(f_\theta(x_t), y_t) \tag{2.1}$$

For regression problems, L1 loss and mean squared error (MSE) loss are the prevalent loss functions as shown in equations (2.2) and (2.3). The MSE loss is used when we want to penalize larger errors more heavily, while the L1 loss is used in the presence of outliers in the data and when the distribution of errors is not necessarily normal.

$$L_{L1}(\theta) = \frac{1}{T} \sum_{t \in T} |f_\theta(x_t) - y_t| \tag{2.2}$$

$$L_{MSE}(\theta) = \frac{1}{T} \sum_{t \in T} (f_\theta(x_t) - y_t)^2 \tag{2.3}$$

The optimal parameters θ^* are achieved through the iterative application of the back-

propagation algorithm, as depicted in equation (2.4), that minimizes the loss function across the training data. Here, α represents the learning rate, and $\nabla_\theta L()$ denotes the gradient of the loss function.

$$\theta \leftarrow \theta - \alpha \nabla_\theta L(\theta) \tag{2.4}$$

2.2.2 LSTM

Long Short-Term Memory (LSTM) networks, an extension of NNs are designed to handle long-term dependencies [26]. The fundamental components of LSTM units encompass a cell, an input gate, an output gate, and a forget gate, each playing a distinct role in information processing [37]. In the description below, the symbols W denote weights, while b represents biases. x_t represents the current input and h_{t-1} is the historical output. A visual representation of the various LSTM network components is provided in Figure 2.6.

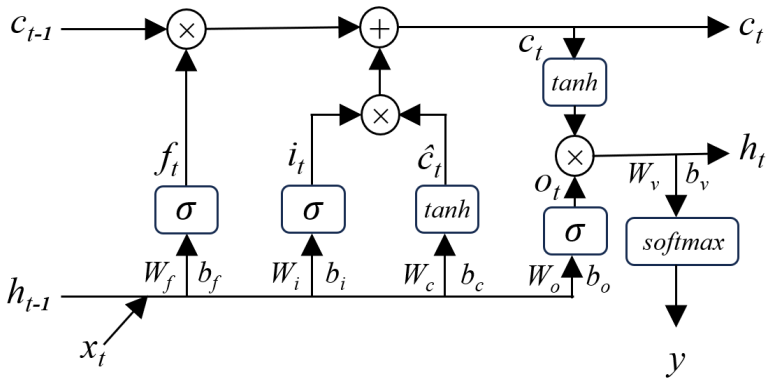


Figure 2.6: Structure of an LSTM network highlighting the various gates, weights, biases and operations.

The functioning of an LSTM network can be explained through its individual components:

Forget Gate (f_t): The forget gate determines the information discarded. It operates on x_t and h_{t-1} using weights $W_{f,x}$ and $W_{f,h}$, followed by the application of the sigmoid function $\sigma()$ which yields an output in the range (0,1).

$$f_t = \sigma(W_{f,x}x_t + W_{f,h}h_{t-1} + b_f) \tag{2.5}$$

Input Gate (i_t): The input gate determines what information should be retained in memory. Weights $W_{i,x}$ and $W_{i,h}$ associated with the x_t and h_{t-1}, facilitate this decision.

$$i_t = \sigma(W_{i,x}x_t + W_{i,h}h_{t-1} + b_i) \tag{2.6}$$

Current Cell State Estimate ($\hat{C}_t$): A hyperbolic tangent function $tanh()$, which generates outputs within the range (-1,1), is employed to compute the estimate of the current cell state. This estimation relies on parameters $W_{c,x}$, $W_{c,h}$, and b_c.

$$\hat{C}_t = tanh(W_{c,x}x_t + W_{c,h}h_{t-1} + b_c) \tag{2.7}$$

Current Cell State (C_t): C_t is updated using the previous cell state C_{t-1}, $\hat{C}_t$, and the outputs of f_t and i_t.

$$C_t = f_t \times C_{t-1} + i_t \times \hat{C}_t \tag{2.8}$$

Output Gate (o_t): The output gate interacts with x_t and h_{t-1} through weights $W_{o,x}$ and $W_{o,h}$.

$$o_t = \sigma(W_{o,x}x_t + W_{o,h}h_{t-1} + b_o) \tag{2.9}$$

Current Output (h_t): h_t is generated by combining the results of the o_t and C_t.

$$h_t = o_t \times tanh(C_t) \tag{2.10}$$

Final Output (y): The final output y is obtained by applying a softmax function to the

product of weights W_v and h_t.

$$y = softmax(W_v h_t + b_v) \tag{2.11}$$

LSTM models require access to substantial amounts of historical data to generate meaningful results. This can pose a challenge when dealing with newer or smaller hubs with limited data availability.

2.2.3 Transfer Learning

TL is designed to address challenges arising from limited training data. The TL process begins by initially pre-training models on a larger, separate dataset. These models are then fine-tuned through training on the target dataset, allowing them to extract general patterns from the larger dataset and adapt this knowledge to the smaller, intended dataset, as seen in figure 2.7 and outlined in [27]. TL is employed to enhance learning in a target task, denoted as $\mathcal{T}_T = (D_T, L_T)$, by leveraging knowledge from a different yet related task, $\mathcal{T}_S = (D_S, L_S)$.

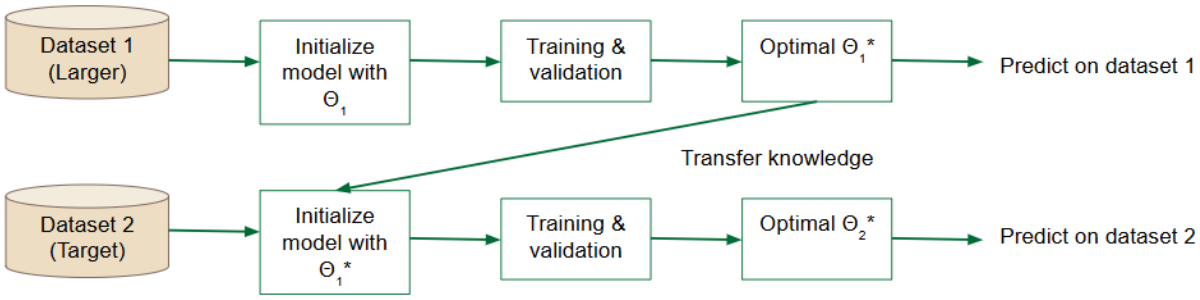


Figure 2.7: Schematic showcasing transfer learning

The optimal parameters θ_S, obtained from a NN trained on $D_{S,train}$ and validated on $D_{S,test}$, serve as the initial weights and biases for the NN model intended for the target task $\mathcal{T}_T$ as shown in Algorithm 1. Subsequently, the TL model undergoes fine-tuning by training on $D_{T,train}$ and is evaluated on $D_{T,test}$ to obtain optimal parameters θ_T specific to the target

task $\mathcal{T}_T$.

It is essential to acknowledge a primary limitation of TL models. Fine-tuning may not fully mitigate the disparities in datasets and trends, potentially resulting in sub-optimal performance when transitioning from the source to the target task.

Algorithm 1: Transfer Learning (TL)

Data: $\mathcal{T}_S = (D_S, L_S)$: Source task, α: Step size hyperparameter

Randomly initialize θ;

while *not done* **do**

  Batch load data (x_i, y_i) from $D_{S,train}$;

  Evaluate $\nabla_\theta L_{\mathcal{T}i}(f_\theta)$ using 2.2 or 2.3;

  Update $\theta \leftarrow \theta - \alpha \nabla_\theta L_{\mathcal{T}i}(f_\theta)$;

Use optimal θ_S as initial parameters for fine-tuning

2.2.4 Model-Agnostic Meta-Learning

MAML represents a recent advancement within the realm of Deep Learning (DL) that offers a solution to the limitations of conventional DL and TL, as introduced in [30]. In the context of meta-learning, specifically MAML, a large dataset is initially divided into numerous meta-tasks, each comprising only a limited number of data points. The model is subsequently exposed to these tasks, essentially becoming proficient in "learning to learn". This means that instead of directly updating its parameters based on an extensive external dataset, the model focuses on acquiring the ability to efficiently adjust its parameters in order to maximize its performance when faced with new tasks.

In the case of time series data, following the generation of features and time windows as outlined in Section 2.1.4, the dataset $D = (x_n, y_n)$ is partitioned into N tasks denoted as $\mathcal{T}_i, i \in (1, N)$ that each contain the same number of time windows $2l$. $2l$ consecutive time windows with a random starting point are selected for each task. Alternate time windows in each task $\mathcal{T}_i$ are segregated into exactly l support sets trained in an inner loop and l query sets

trained in the outer loop. This is because alternate time windows are temporally correlated [38]. For example, consider figure 2.8. The support set contains time windows beginning at even-numbered hours (2, 4, ..., 200), while the query set contains time windows beginning at odd-numbered hours (3, 5, ..., 201). This arrangement ensures adjacent, non-overlapping time-periods for training and validation.

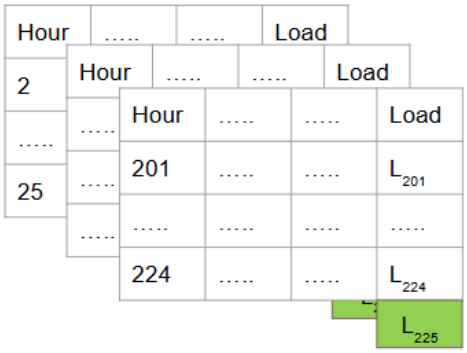


Figure 2.8: Adjacent time windows alternated in the support and query sets for MAML

The NN model utilized for MAML is initialized with random parameters θ. The time windows $(x_{i,k}, y_{i,k}), k \in (1, l)$ in the support set of each task $\mathcal{T}_i^{sup}$ are used to iteratively update temporary parameters θ_i' by using θ and the gradient of the loss function as expressed in equation (2.12) for a number of adaptation steps set by the user. α is the inner loop learning rate.

$$\theta_i' = \theta - \alpha \nabla_\theta L_{\mathcal{T}_i^{sup}}(f_\theta) \tag{2.12}$$

Following this parameter update, the meta-learning rate β, parameters θ_i' and their gradients as well as time windows $(x_{i,j}, y_{i,j}), j \in (1, l)$ from the query set of each task $\mathcal{T}_i^{que}$ are employed to adjust θ, as demonstrated in equation (2.13).

$$\theta \leftarrow \theta - \beta \sum_{i=1}^{N} \nabla_\theta L_{\mathcal{T}_i^{que}}(f_{\theta_i'}) \tag{2.13}$$

The model, now meta-trained, can be fine-tuned on smaller datasets, allowing it to adapt quickly and learn effectively without being hampered by data scarcity or external dataset influences. The entire process is shown in Algorithm 2.

Algorithm 2: Model-Agnostic Meta-Learning (MAML)

Data: Tasks $\mathcal{T}_i, i \in (1, N)$: Derived from dataset D, α, β: Step size hyperparameters

Randomly initialize θ;

while *not done* **do**

  Sample batch of tasks $\mathcal{T}_i$;

  for *all* $\mathcal{T}_i$ **do**

    Sample data $(x_{i,k}, y_{i,k}), k \in (1, l)$ from support set $\mathcal{T}_i^{sup}$;

    Evaluate $\nabla_\theta L_{\mathcal{T}i}(f_\theta)$ using equation 2.2 or 2.3;

    Compute temporary parameters with gradient descent using equation 2.12;

    Sample data $(x_{i,j}, y_{i,j}), j \in (1, l)$ from query set $\mathcal{T}_i^{que}$ for meta-update;

  Update θ using equation 2.13;

Use optimal θ_S as initial parameters for fine-tuning

2.2.5 Classical Machine Learning Baselines

To validate the necessity of complex deep learning approaches, we establish performance baselines using classical machine learning (CML) models. We focus on Random Forests (RF) and K-Nearest Neighbors (KNN) due to their established effectiveness in regression tasks, implementation simplicity, and widespread adoption [39]. While Support Vector Machines were also evaluated during experimentation, they consistently underperformed and are therefore excluded from our results.

2.2.5.1 Random Forests

Random Forests operate through an ensemble of Decision Trees (DTs). A Decision Tree is a hierarchical model that recursively partitions the feature space, beginning with a root node that represents an initial feature-based decision. This root branches into child nodes, each representing subsequent decisions, ultimately terminating in leaf nodes that provide final predictions. In our implementation, the splitting criterion is the MSE as defined in equation 2.3. The RF model creates multiple DTs, each trained on a distinct random subset of the training data. The final prediction is computed as the average of individual tree predictions, with this ensemble approach effectively mitigating overfitting risks.

2.2.5.2 K-Nearest Neighbors

KNN regression operates by mapping data points into a multidimensional feature space and making predictions based on local neighborhoods. For a given input point, the algorithm:

1. Identifies the k nearest training points using Euclidean distance
2. Computes the prediction as the average of these neighbors' target values

This process can be formally expressed as:

$$\hat{y}(x) = \frac{1}{k} \sum_{i=1}^{k} y_i \tag{2.14}$$

where:

- $\hat{y}(x)$ is the predicted value for input x
- k is the number of nearest neighbors (set to 5 in our implementation)
- y_i represents the target value of the i-th nearest neighbor

2.2.6 Experimental setup

In our experimental setup, we employ LSTM networks as the foundational architecture. We configure an LSTM network comprising of two LSTM layers, each housing 48 neurons. This is followed by a Dense layer with 48 neurons and culminating in a single-neuron output layer. To optimize the network, we employ an RMSprop optimizer with a learning rate (α) of 0.001. Our experiments are conducted using Pytorch and the learn2learn library [40] in Python, hosted on Google Colab, which provides ample resources including 12.7 GB of RAM and an NVIDIA Tesla T4 GPU. Multiple variations of the above network were trained and tested, including number of layers, number of neurons in each layer, number of LSTM layers, bidirectionality, and learning rate. The settings mentioned were selected because they provided the best results.

For our meta-learning approach, we commence by partitioning the Colorado dataset into 500 tasks (N), with each task encompassing 200 consecutive data points (2l). The number of tasks and data points per task were selected on the basis of performance by testing each of them in steps of 50 starting from 50 until 500. The LSTM network is encapsulated within a MAML module with a learning rate (β) of 0.05. We create two distinct models, one trained with L1 loss and the other with MSE loss. Our training process consists of 50 iterations. Within each iteration, the model encounters 32 tasks, where each task is further divided into query and support sets. Specifically, every alternate 24-hour input time window serves as a support set, while its subsequent time window serves as the query set. The model adapts to the support sets in the inner loop and evaluates its performance on the query sets, iteratively updating its parameters to enhance its performance across tasks. In each iteration, a new copy of the MAML model is employed. This practice involves cloning the original model before adaptation, effectively isolating changes made during adaptation to a specific task ensuring proper generalization.

Upon completing the meta-learning phase, we create fresh LSTM models, initializing them with the same parameters θ as the meta-trained LSTM. These models are then sub-

jected to fine-tuning on the remaining datasets (ACN, Norway-shared, and Norway-private). We select 20-day and 40-day subsets from these datasets, splitting them evenly into training and testing sets. Fine-tuning is carried out over 50 iterations, employing L1 loss as the objective function.

In contrast, our TL approach involves training LSTM models with the previously described architecture directly on the entire Colorado dataset. Two separate models are trained—one with L1 loss and the other with MSE loss—for 50 iterations. Subsequently, these models are fine-tuned on the ACN and Norway datasets in a manner consistent with the process outlined above.

For traditional DL, where no pretraining is involved, models are directly trained on the first halves of the selected subsets for 50 iterations using L1 loss and then evaluated on the remaining halves. The CML models are also directly trained on the same portions of the data after flattening the input vector. The evaluation metrics include mean absolute error (MAE), root mean squared error (RMSE), and coefficient of determination (R2) scores. To ensure robustness, each experiment is conducted five times, and the average values of all metrics are reported.

2.3 Results

This section is divided into 3 subsections pertaining to each of the datasets under investigation. Tables 2.1, 2.2 and 2.3 provide the metrics for the seven EV charging load forecasting models: TL with MSE and L1 loss, MAML with MSE and L1 loss, DL with L1 loss, RF and KNN.

2.3.1 ACN dataset

Analyzing the ACN dataset results presented in Table 2.1, it becomes evident that TL L1 exhibits the most favorable performance, particularly in terms of MAE and RMSE. Notably,

Table 2.1: Mean MAE, RMSE and R2 scores of the forecasting models on the ACN dataset

Specification		**Mean Scores**		
Subset	**Model**	***MAE***	***RMSE***	***R2***
18th September 2019, 10 Days	TL MSE	1.48	***2.97***	***0.83***
	TL L1	***1.40***	3.03	0.82
	MAML MSE	1.58	3.17	0.81
	MAML L1	1.53	3.19	0.81
	DL	1.95	3.53	0.75
	RF	1.51	2.99	0.74
	KNN	2.27	3.93	0.54
9th November 2020, 10 Days	TL MSE	0.18	0.76	0.72
	TL L1	***0.14***	***0.70***	***0.76***
	MAML MSE	0.20	0.78	0.70
	MAML L1	0.18	0.79	0.69
	DL	0.19	0.78	0.70
	RF	0.34	0.93	0.16
	KNN	0.5	1.27	0.01
18th September 2019, 20 Days	TL MSE	1.52	3.42	0.68
	TL L1	***1.37***	3.37	0.69
	MAML MSE	1.47	3.38	0.69
	MAML L1	1.47	3.38	0.69
	DL	1.46	3.39	0.69
	RF	1.51	***3.21***	0.68
	KNN	1.93	3.79	0.54
9th November 2020, 20 Days	TL MSE	0.30	***0.96***	***0.72***
	TL L1	***0.29***	1.00	0.70
	MAML MSE	0.34	1.05	0.67
	MAML L1	0.31	1.03	0.68
	DL	0.33	1.03	0.67
	RF	0.39	1.10	0.52
	KNN	0.8	1.60	0.09

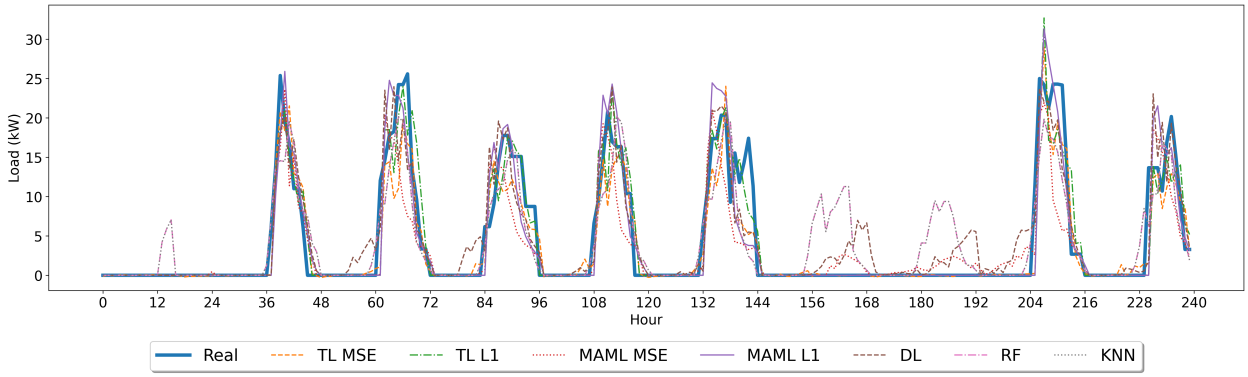


Figure 2.9: Results from the forecasting models compared to the true load value on a subset of the ACN dataset starting from September 18, 2019 for 10 days

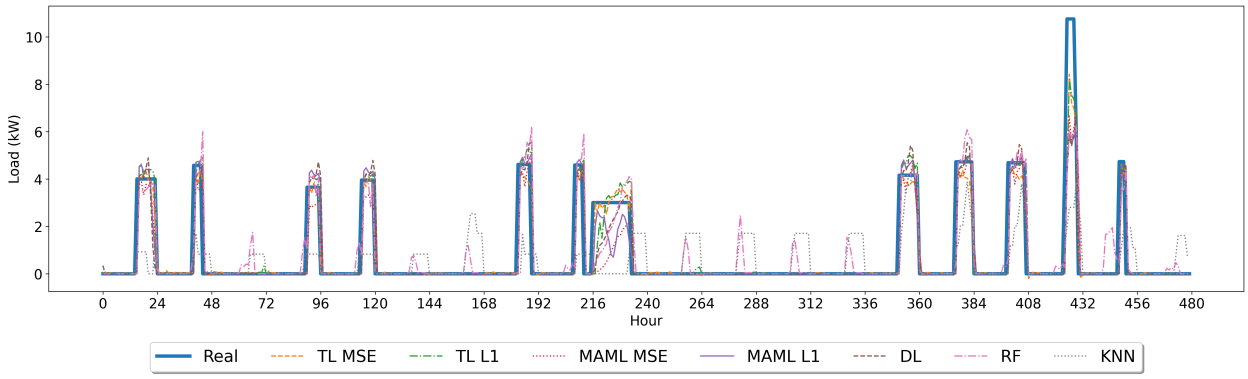


Figure 2.10: Results from the forecasting models compared to the true load value on a subset of the ACN dataset starting from November 9, 2020 for 20 days

TL L1's RMSE score is surpassed only by TL MSE in two subsets of the ACN dataset considered. In contrast, DL consistently lags behind the performance of competing models across all metrics. With the exception of the first and third subsets wherein RF performs competitively, CML models are well-beaten by the deep learning models.

Furthermore, when comparing L1 variants to their MSE counterparts within the MAML and TL models, it becomes apparent that L1 variants outshine their MSE counterparts. Additionally, examining the R-squared (R2) scores reveals that TL models excel in capturing and adhering to the underlying trends in the data.

Analyzing the trends depicted in Fig. 2.9 and 2.10, we can evaluate how well each model aligns with the actual hourly load patterns. It is evident that, in general, models tend to exhibit suboptimal performance during peak load periods, occasionally either overestimating or underestimating the peak values. Interestingly, models display a higher level of accuracy in predicting periods of zero load, with some exceptions noted in the case of DL and MAML L1, as illustrated in Fig. 2.9. From both figures, we see that the CML models perform very poorly during zero-load hours. While they are able to understand the general trend, they predict the trend to continue even when there is no actual load.

2.3.2 Norway shared charger dataset

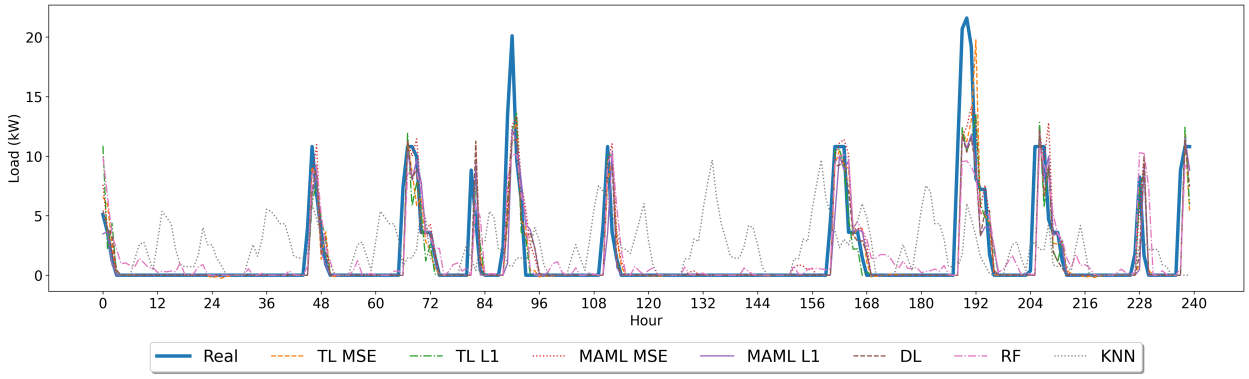


Figure 2.11: Results from the forecasting models compared to the true load value on a subset of the Norway shared charger dataset starting from February 21, 2019 for 10 days

Table 2.2: Mean MAE, RMSE and R2 scores of the forecasting models on the Norway shared charger dataset

Specification		**Mean Scores**		
Subset	**Model**	***MAE***	***RMSE***	***R2***
	TL MSE	0.96	2.38	0.63
	TL L1	0.91	2.39	0.63
	MAML MSE	0.91	2.38	0.63
21st February 2019, 10 Days	MAML L1	***0.89***	***2.32***	***0.65***
	DL	0.92	2.40	0.62
	RF	1.18	2.48	0.32
	KNN	2.28	4.3	-0.32
	TL MSE	3.77	5.64	0.59
	TL L1	3.66	5.50	0.61
	MAML MSE	***3.30***	***5.06***	***0.67***
17th September 2019, 10 Days	MAML L1	3.47	5.29	0.64
	DL	3.60	5.55	0.61
	RF	3.51	4.94	0.46
	KNN	5.88	8.36	-1.84
	TL MSE	1.01	2.43	0.59
	TL L1	1.03	2.44	0.59
	MAML MSE	0.93	2.35	0.62
21st February 2019, 20 Days	MAML L1	***0.88***	***2.25***	***0.65***
	DL	0.97	2.41	0.60
	RF	1.24	2.31	0.49
	KNN	2.17	3.83	-0.23
	TL MSE	3.70	5.64	0.65
	TL L1	3.38	5.50	0.67
	MAML MSE	***3.23***	***5.38***	***0.68***
17th September 2019, 20 Days	MAML L1	3.38	5.52	0.67
	DL	3.33	5.45	0.67
	RF	4.29	5.68	0.33
	KNN	5.93	8.18	-1.03

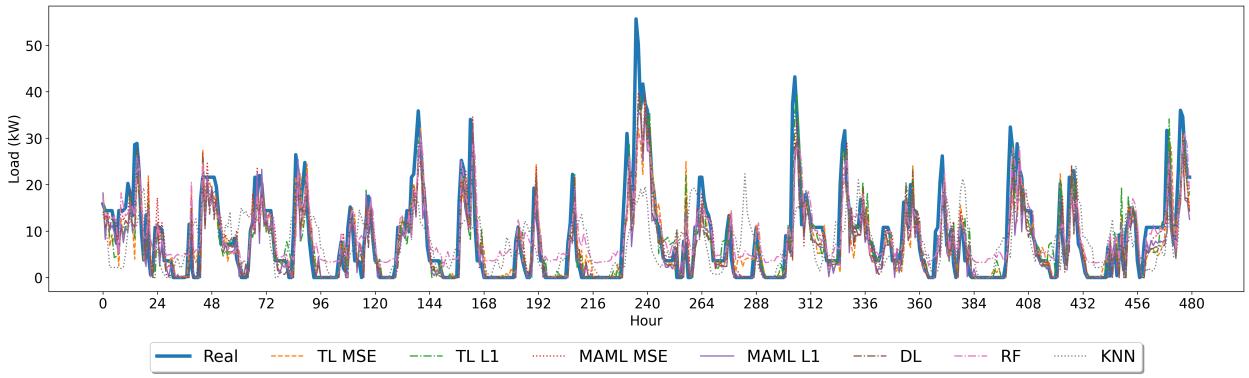


Figure 2.12: Results from the forecasting models compared to the true load value on a subset of the Norway shared charger dataset starting from September 17, 2019 for 20 days

Examining the Norway shared charger data presented in Table 2.2, it is that MAML demonstrates the most robust performance, specifically excelling in terms of MAE and RMSE. Interestingly, in this dataset, DL manages to outperform TL models, yet it still falls short when compared to the performance achieved by MAML models. CML models expectedly underperform, with KNN showing negative R2 scores. In the second subset of the dataset, the MAE exhibited by DL is 10% higher than that of MAML MSE but 5% lower than that of TL MSE. Additionally, the R2 scores affirm that MAML models tend to make predictions that closely align with the actual data trends, demonstrating their superior predictive capability.

From Fig. 2.11 and 2.12, we can assess how each model fits the real hourly load trend. We can see that the models under-perform at the two peaks greater than 15 kW in Fig. 2.11, and the CML models continue to predict loads even when there are none, as discussed previously. Additionally, Fig. 2.11 displays an interesting phenomenon - models appear to arrive with a delay of one timestep with respect to the peaks, suggesting that they are under-confident in predicting the starting edges of the peak periods.

Table 2.3: Mean MAE, RMSE, and R2 scores of the forecasting models on the Norway private charger dataset

Specification		**Mean Scores**		
Subset	**Model**	***MAE***	***RMSE***	***R2***
21st February 2019, 10 Days	TL MSE	2.8	4.95	0.51
	TL L1	***2.61***	***4.93***	***0.58***
	MAML MSE	3.1	6.35	0.2
	MAML L1	2.98	6.18	0.24
	DL	3.12	6.72	0.18
	RF	2.80	5.60	0.14
	KNN	3.66	7.28	-0.10
17th September 2019, 10 Days	TL MSE	5.01	7.73	0.59
	TL L1	***4.75***	***6.96***	***0.69***
	MAML MSE	6.18	9.23	0.46
	MAML L1	5.74	8.18	0.58
	DL	6.24	9.34	0.45
	RF	4.85	6.65	0.61
	KNN	6.24	9.34	0.45
21st February 2019, 20 Days	TL MSE	3.10	5.65	0.58
	TL L1	***2.98***	***5.64***	***0.58***
	MAML MSE	3.92	7.01	0.35
	MAML L1	3.39	6.38	0.45
	DL	3.59	6.66	0.41
	RF	3.23	6.28	0.43
	KNN	5.17	9.01	0.12
17th September 2019, 20 Days	TL MSE	5.56	8.95	0.69
	TL L1	***5.39***	***8.28***	***0.74***
	MAML MSE	5.61	8.45	0.72
	MAML L1	5.39	8.35	0.73
	DL	5.70	8.93	0.69
	RF	5.50	8.57	0.46
	KNN	7.36	10.21	-0.31

2.3.3 Norway private charger dataset

From the data outlined in Table 2.3, it becomes evident that TL L1 demonstrates the most robust performance across all subsets examined within the Norway private charger dataset. Conversely, DL exhibits relatively poorer performance in most instances.

For example, consider the MAE scores: TL L1 achieves scores that are 20% and 31% lower than those attained by DL for the first and second subsets within the dataset. Moreover, TL L1 outperforms MAML L1 (the better-performing MAML) by approximately 15% and 21% for the same subsets. CML models expectedly underperform again. Additionally, it's worth noting that both MAE and RMSE values for all models within the Norway private charger dataset are higher when compared to those of the Norway shared charger dataset and the ACN dataset. This discrepancy might be attributed to the Colorado dataset containing charging transactions acquired from shared chargers that might exhibit similar patterns to Norway shared charger dataset and the ACN dataset (shared chargers on campus). Achieving an optimal balance between private and shared charging data during pre-training may be necessary to enhance the final results.

Analyzing Fig. 2.13 and 2.14, we can evaluate how well each model aligns with the actual hourly load trends. Notably, all models, with the exception of TL L1 and TL MSE, exhibit significant underperformance. TL models struggle to accurately predict peaks exceeding 15 kW as seen in Fig. 2.13. However, Fig. 2.14 shows a relatively improved performance, though the models still face challenges in accurately predicting peaks exceeding 50 kW.

2.4 Discussion

This chapter demonstrates the effectiveness of MAML and TL models in short-term load forecasting, particularly in scenarios with limited data availability. These models exhibit the capability to forecast accurately across diverse geographical regions, scales, and data distributions by employing a pre-training strategy on a more extensive dataset followed by

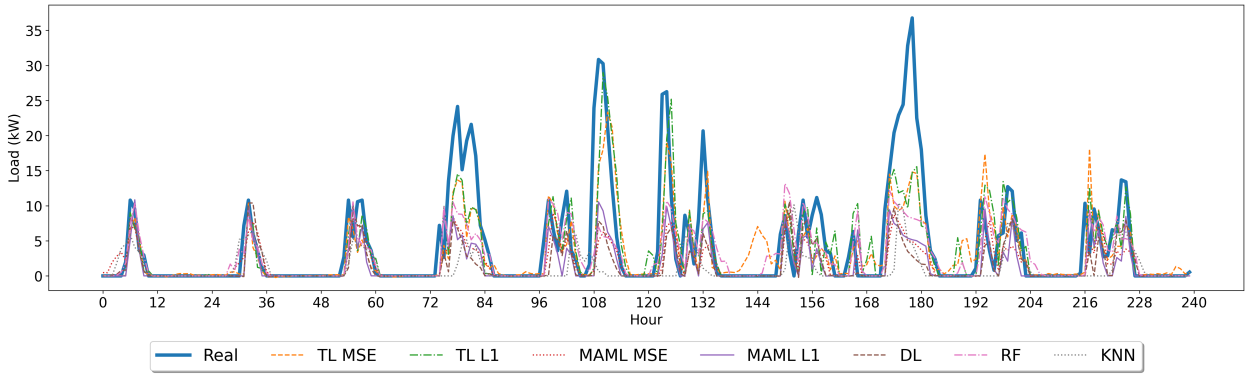


Figure 2.13: Results from the forecasting models compared to the true load value on a subset of the Norway private charger dataset starting from February 21, 2019 for 10 days

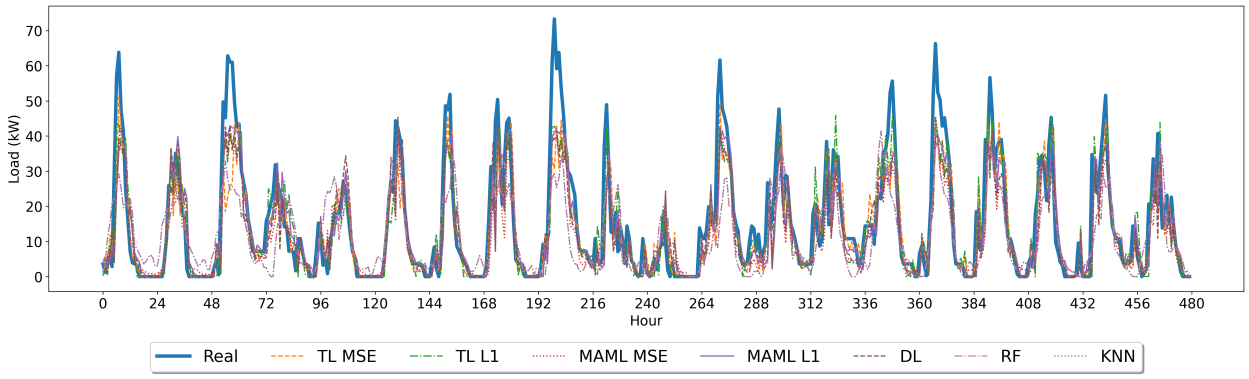


Figure 2.14: Results from the forecasting models compared to the true load value on a subset of the Norway private charger dataset starting from September 17, 2019 for 20 days

fine-tuning on the smaller target dataset. Notably, both MAML and TL models exhibit competitive performance, with MAML excelling for the Norway shared charger dataset and TL performing exceptionally well for the ACN dataset as well as the Norway private charger dataset. MAML seems to perform best when the target dataset closely matches the setting of the source dataset but this does not seem to matter too much for TL. The Colorado dataset was the only dataset used for pre-training and the data is obtained from shared chargers dispersed in Colorado which is similar to the Norway shared charger dataset with data from shared chargers in Trondheim. Achieving an optimal balance between private and shared charging data during pre-training may be necessary to enhance forecasting metrics Across all three evaluation metrics, both MAML and TL models consistently outperform traditional DL models. Classical Machine Learning CML models are clearly not adequate for the complexity of the task. The error metrics from TL and MAML are up to 24% and 61% lower than deep learning and classic machine learning models respectively. It's worth noting that while the differences in scores are generally significant, there may be instances where DL models outperform specific MAML and TL configurations.

We also see that models tend to exhibit suboptimal performance during peak load periods, occasionally either overestimating or underestimating the peak values. However, most models display a higher level of accuracy in predicting periods of zero load except CML models. While CML models are able to understand the general trend, they predict the trend to continue even when there is no actual load. It is also worth noting that sometimes the models appear to perform well after a delay of one timestep when the load jumps from zero to a higher value. This suggests that the models are under-confident in predicting the starting edges of the peak periods.

A few variations of the models were tested before arriving at the final models. We tried pre-training the models for MAML and TL on the same timespan as the test data i.e. if the test data was October to November 2019 then we pre-trained the models of data only from August to September 2019. The results were poor compared to the results

discussed above. Additionally, multiple variations of the models were tested by tuning various hyperparameters before settling on the model architectures utilized for forecasting.

While accurate forecasting of EV charging loads is crucial for grid stability, EVs can serve as more than just loads on the electrical network. The bidirectional power flow capability of EVs through V2G technology transforms EVs from passive consumers to active grid assets. This enables EVs to provide valuable grid services. In Chapter 3 we cover the use of V2G in the context of transmission and distribution network congestion. By strategically controlling when EVs charge and discharge, their aggregated flexibility can be harnessed to alleviate grid constraints during peak demand periods and defer costly infrastructure upgrades. However, realizing this potential requires careful consideration of battery degradation costs and charging behavior patterns identified through the forecasting.

CHAPTER 3

Congestion Relief

The growing integration of intermittent RES, particularly solar and wind, coupled with increasing EV adoption as part of global climate change mitigation efforts, presents significant challenges for energy grid management and stability [41]. Meeting sustainability goals through renewable energy integration and transportation electrification requires effective instruments and markets to maintain grid equilibrium across all timeframes. Battery energy storage systems (BESS) have emerged as a promising solution, driven by declining costs and improved battery longevity [42]. Grid-scale BESS offers versatile functionality, capable of rapid and cost-effective energy storage and supply at megawatt-hour scales while maintaining high efficiency, reliability, and safety standards [10]. These systems provide benefits across the energy ecosystem, from Independent System Operators (ISOs) and Regional Transmission Organizations (RTOs) to utilities and end-users [43]. Behind-the-meter (BTM) energy storage enables backup power, solar photovoltaic (PV) optimization, electricity cost reduction through time-of-use (TOU) pricing, and peak shaving for both residential and commercial consumers [44]. BESS can reduce load variance [45], minimize renewable energy curtailment costs [46], and support electric bus charging operations while reducing demand charges [25]. BESS applications extend to market participation through energy arbitrage in Day-Ahead Markets (DAM) and Real-Time Markets (RTM), generating revenue by charging at low prices and discharging at high prices [47]. These systems can also provide ancillary services including voltage support, reserves [43], frequency regulation [47], and reactive power compensation [48], with participation varying by jurisdiction and market structure. Additionally, BESS offers cost savings through transmission and distribution grid

upgrade deferral and congestion relief [43]. EVs represent another critical element in this evolving energy landscape. Operating solely on battery power, EVs offer reduced greenhouse gas (GHG) emissions when charged with renewable energy compared to conventional vehicles [49]. Smart charging coordination further reduces operational costs [50]. The U.S. Department of Transportation's National Household Travel Survey (NHTA) indicates that private vehicles remain stationary for approximately 96% of the day [51], creating substantial opportunities for grid services through V2G technology [52].

V2G technology enables bidirectional communication and power flow between EVs and the grid, allowing vehicles to serve as backup power sources [11]. Coordinated EV energy management enhances grid efficiency, performance, and power quality [53] while optimizing charging costs. When parked and connected, EVs can generate revenue through frequency regulation [12], voltage regulation, and TOU pricing arbitrage [13]. They can also store excess renewable energy for later grid support, reducing curtailment and peak load, particularly in regions with distinctive load profiles such as California's "duck curve" [54]. Through V2G capabilities, EVs contribute to emissions reduction both in transportation and by reducing reliance on peaking power plants [55].

Contemporary EV models feature battery capacities exceeding 90 kWh and power transfer capabilities above 250 kW [56], though actual power transfer rates remain limited by internal circuitry and manufacturer specifications. Growing EV adoption and potential V2G-related financial incentives may encourage more manufacturers to implement bidirectional power flow capabilities. While BESS and V2G-enabled EVs have been extensively studied for various grid applications, their potential for congestion relief remains relatively unexplored. Initial studies suggest significant economic potential, with EVs providing transmission congestion relief in CAISO potentially generating monthly savings up to $280.47 [14]. However, these analyses often assume constant EV availability and neglect battery degradation effects, necessitating more comprehensive investigation.

This chapter investigates the potential economic benefits of utilizing EVs for congestion

relief in aging electric grid infrastructure. We analyze charging and discharging strategies for congestion relief and energy arbitrage across multiple locations within the California Independent System Operator (CAISO) territory, incorporating battery degradation through a constant cost factor model. Our analysis focuses on two strategic types of nodes within the CAISO network: endpoints of heavily congested transmission lines and locations of major solar generation facilities in California. Using locational marginal pricing (LMP) data, we examine the temporal value distribution of EV-based congestion relief services on a monthly basis and analyze the trade-off between congestion minimization and arbitrage revenue maximization. This research represents a novel approach to evaluating EV contributions to congestion relief by specifically targeting identified congestion points and solar generation sites using actual pricing data. The strategic deployment of EVs for congestion management offers multiple benefits: EVs can charge during periods of excess renewable generation, potentially reducing solar curtailment, and discharge locally during peak demand, reducing reliance on expensive and polluting peaker plants. This dual functionality contributes to both grid efficiency and environmental sustainability. The chapter is organized as follows:

- Section 3.1 presents the theoretical framework for congestion relief, financial transmission rights, and LMPs, followed by our methodology for node selection, battery degradation modeling, and optimization formulations for total cost and congestion-related cost minimization
- Section 3.2 details optimization results across selected nodes, including per-EV value for congestion minimization, monthly temporal analysis, battery capacity degradation assessment, and V2G value metrics
- Section 3.3 synthesizes key findings

3.1 Framework and methodology

3.1.1 Congestion Relief and Financial Transmission Rights

Line congestion occurs when transmission lines operate at their limits due to thermal, voltage, or stability constraints. In various electricity markets worldwide, this congestion necessitates differential pricing, resulting in additional operational costs when transmission lines operate near capacity [9]. The congestion creates barriers to efficient electricity flow, particularly from low-cost RES to end-users. When congestion occurs, grid operators must activate more expensive generation sources to deliver power through non-congested routes, leading to increased electricity prices in affected regions. These price variations manifest as changes in LMPs at specific nodes throughout the electrical grid network [57]. The impact of congestion on pricing can be observed through contrasting scenarios in different markets. Figure 3.1 illustrates stable pricing across most of CAISO network during a Spring morning, indicating minimal congestion [58]. In stark contrast, Figure 3.2 demonstrates severe congestion in the Midcontinent Independent System Operator (MISO) network [59], where price disparities are extreme—ranging from -$500/MWh in some locations to over $500/MWh in others.

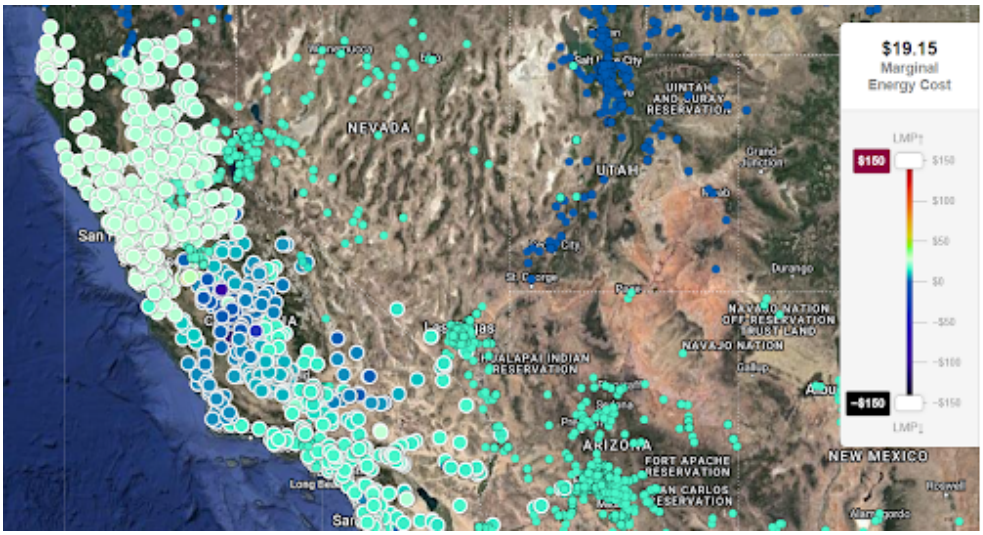


Figure 3.1: Low congestion across the CAISO grid on a Spring morning.

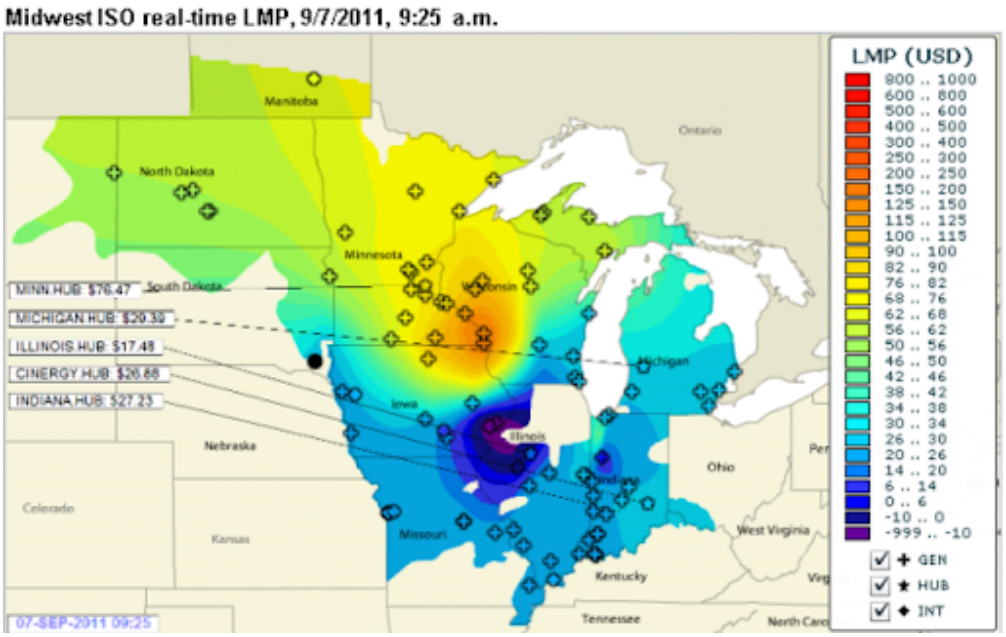


Figure 3.2: Extremely high congestion in the MISO grid in the morning of 9/7/2011.

Financial Transmission Rights (FTRs) represent market agreements between system operators and participants designed to mitigate price uncertainty from transmission congestion [60]. These financial instruments are distributed through auctions and allocations in the financial transmission market, with allocation volumes determined by simultaneous feasibility constraints within the market's security-constrained optimal power flow problem [61]. FTR holders receive payments based on the energy price differential between source and sink nodes for each MWh of transmitted energy. When congestion occurs, ISOs collect congestion rents and distribute them to FTR holders [60].

The fundamental design of FTRs centers on bilateral contracts with transmission charges for transactions between injection and withdrawal points [62]. In this system, loads pay the LMP at withdrawal points, while generators receive the LMP at injection points for each additional MWh. Congestion fees apply at both nodes when LMPs differ, with the ISO collecting and redistributing congestion rents to FTR holders. Different regions employ varying terminology and mechanisms: California uses Congestion Revenue Rights (CRR),

while New York operates with Transmission Congestion Contracts (TCC), each featuring distinct contract designs, durations, acquisition methods, trading rules, auction mechanisms, allocation criteria, and revenue distribution approaches [62].

However, the FTR market faces several significant challenges. First, FTRs function purely as financial instruments and do not resolve physical congestion. Second, regional ISOs operate under different rules and regulations for market participation, potentially excluding entities requiring congestion cost protection. Third, even approved participants may encounter difficulties in auctions. While ideally, under unconstrained transmission conditions, FTR allocation should align with Day-Ahead Market electricity flow to ensure FTR payouts match auction revenue [63], real-world conditions often deviate from this ideal scenario.

A persistent challenge is FTR underfunding, where collected LMP congestion costs fail to cover credits distributed to FTR holders [64]. This issue has affected multiple ISOs: PJM Pennsylvania Jersey Maryland (PJM) RTO experienced 31% underfunding in 2012-2013 and 28% in 2013-2014, while the Southwest Power Pool (SPP) reported 20% underfunding in 2014-2015, resulting in tens of millions of dollars in shortfalls.

Market regulation plays a crucial role in preventing market manipulation, as unchecked dominance can incentivize generation curtailment and artificially inflate FTR values [65]. One potential solution to address FTR market inefficiencies involves minimizing congestion rent through strategic deployment of energy storage or V2G, thereby optimizing existing grid asset utilization.

3.1.2 Utility Scale Energy Storage Projects for Congestion Relief

There have been attempts to study the use of energy storage to minimize transmission grid congestion without looking into FTRs. Del et al. used battery energy storage to relieve thermal constraints and hence provide congestion relief [66]. Khani et al. developed a real time optimal dispatch algorithm for privately owned large-scale BESS. This allowed BESS

to generate revenue primarily by arbitrage in the Day-Ahead Market and also prepared the BESS to maximize contribution to congestion relief as an ancillary service [67]. Arteaga et al. researched the potential for BESS to compete in an electricity market to trade energy and provide ancillary services. The BESS also has an opportunity to provide transmission congestion relief (TCR) under a long-term contract with a regional network operator [68]. They modeled the opportunity costs (difference between maximum profit with and without TCR) for TCR with the limitations imposed on participating in the electricity markets while providing TCR. The DOE (Department of Energy) Global Energy Storage Database also contains information on grid-connected energy storage projects used for transmission congestion relief [69]. Globally, 26 operational battery storage projects are used for transmission congestion relief, with 9 of them in the USA. Table 3.1 provides key information on the energy storage projects used for transmission congestion relief in the USA.

Table 3.1: Grid-scale battery projects in the USA resulting in transmission congestion relief.

Project Name	**Rated Power (kW)**	**Storage Capacity (kWh)**	**State**	**City**
Long Island Bus BESS—New York Power Authority	1000	6500	New York	Garden City
Redding Electric Utilities (Phase 1)—Ice Energy	1000	6000	California	Redding
SustainX Inc Isothermal Compressed Air Energy Storage	1500	1500	New Hampshire	Seabrook
Tehachapi Wind Energy Storage Project	8000	32000	California	Tehachapi
Glendale Water and Power/Skylar Energy BESS Pilot	2000	960	California	Glendale
University of Hawaii Smart Grid Regional and Energy Storage Demonstration Project (Maui Smart Grid)	1000	1000	Hawaii	Wailea
PDE Smart Microgrid System	90	29.7	California	Commerce
Borrego Springs Microgrid—SDG&E	500	1500	California	Borrego Springs
Redding Electric Utilities (Phase 2)—Ice Energy	6000	12000	California	Redding

With respect to EVs, Staudt et al. evaluated the effect of uncontrolled EV charging on the expansion of the German transmission grid and proposed a coordinated charging approach to relieve the transmission grid of congestion [70]. In order to calculate possible compensation

for participants, they reduced their model to one node per state. [71] developed a Day-Ahead Market framework for congestion management by using a decentralized mechanism for the collaboration of EV aggregators that utilized EVS as distributed storage. Their work focused on day-ahead congestion and ran their simulations for only 24-hour time periods in an unbalanced 136 bus system. Gowda et al. claimed that EVs supporting transmission congestion relief can lead to monetary savings as high as $280.47 in one month in CAISO [14]. This work was based on the assumption that each EV was always available to support the grid, treated the electric vehicle as a small battery and ignored the effects of battery degradation.

3.1.3 Locational Marginal Price

The LMP represents the marginal price of electricity at a specific location on the electric grid at any point in time. The total LMP_T can be broken down into 3 components—energy, congestion, and loss, as shown in Equation (3.1). Here, LMP_E, LMP_C, and LMP_L represent the energy component, congestion component, and the loss component.

$$LMP_T = LMP_E + LMP_C + LMP_L \tag{3.1}$$

The energy component, LMP_E, represents the cost of serving load with the least expensive available generation, assuming no transmission constraints or losses. This component is uniform across all nodes in the system and reflects the marginal cost of energy at the reference node. The loss component,LMP_L, accounts for the marginal cost of system losses caused by delivering energy to the specific location.

The congestion component, LMP_C, captures the marginal cost of congestion at a specific node relative to the reference node. LMP_C is positive when congested transmission lines do not allow electricity from cheaper sustainable sources of energy (like renewables) to reach a node, resulting in the usage of nearby or local higher-cost non-renewable sources to meet

the demand, resulting in increased energy prices and pollution. LMP_C is negative when there is excess transmission capacity at a location but little demand for electricity, leading to the underutilization of sources of energy like RES. The difference between the congestion components of the LMPs of two nodes is the congestion charge in moving energy between them [57]. The price of moving E MWh of energy between the source and sink node is given by Equation (3.2).

$$C_{FTR} = E(LMP_{C,\text{sink}} - LMP_{C,\text{source}}) \tag{3.2}$$

FTRs allow settlements based on the difference between source and sink congestion prices when the transmission line between them is congested in the Day-Ahead Market. In CAISO, FTRs are called CRRs. Load Serving Entities (LSE) can become CRR holders if they meet any of three minimum conditions—(1) $1 million tangible net worth, (2) $10 million total assets, or (3) post financial $500,000 cash or letter of credit. Completing the required applications is followed by registration, agreement policies, and training to obtain CRR. Each ISO have their own criteria to become FTR holders. As mentioned previously, FTRs protect a limited number of entities against price stochasticity, and the physical lines connecting nodes are still congested.

Given the challenges in the FTR market and the demonstrated potential of EVs with V2G for congestion relief, we evaluate EV-based congestion management that addresses previous studies' limitations. While prior research has established the basic feasibility of using EVs for congestion relief, most studies have overlooked critical real-world factors such as battery degradation costs, variable EV availability, and long-term economic implications. Our methodology incorporates these crucial elements by analyzing actual CAISO pricing data from March 2021 to September 2023 across multiple nodes at the ends of congested lines and at large solar generation plants. Using the gridstatus module in Python to obtain LMP data, we examine both seasonal variations and the impact of increasing renewable energy integration in the grid. This extended timeframe and real-world data, combined with our consideration of practical constraints and battery degradation modeling, enables a more

accurate assessment of the economic and technical viability of EV-based congestion relief under actual market conditions. The following section details our node selection process and presents the maximum monetary benefits obtainable by a single EV at these strategic locations.

3.1.4 Node Selection Process

CAISO releases a market performance report for each month, and the reports from 2021 onwards are available on their website [72]. The market performance report discusses trends in system peak load, resource adequacy, day-ahead and real-time prices, congestion, CRRs, and ancillary services. These reports discuss congestion rents on interties, transmission lines, transformers, nomograms, and nodal group constraints. The following three transmission lines show up most often in the reports from March 2021 to September 2023, (1) 230 kV line between Panoche and Gates, (2) 500 kV line between Los Banos and Gates, and (3) 230 kV line between Gates and Midway. The locations of these transmission lines, shown in figure 3.3, were identified from the California Electric Transmission Lines dataset hosted on the California State Geoportal [73]. The ends of the transmission lines were identified and mapped with the nodes on the CAISO price map [74]. The nodes at the two ends of the transmission lines are shown in Table 3.2.

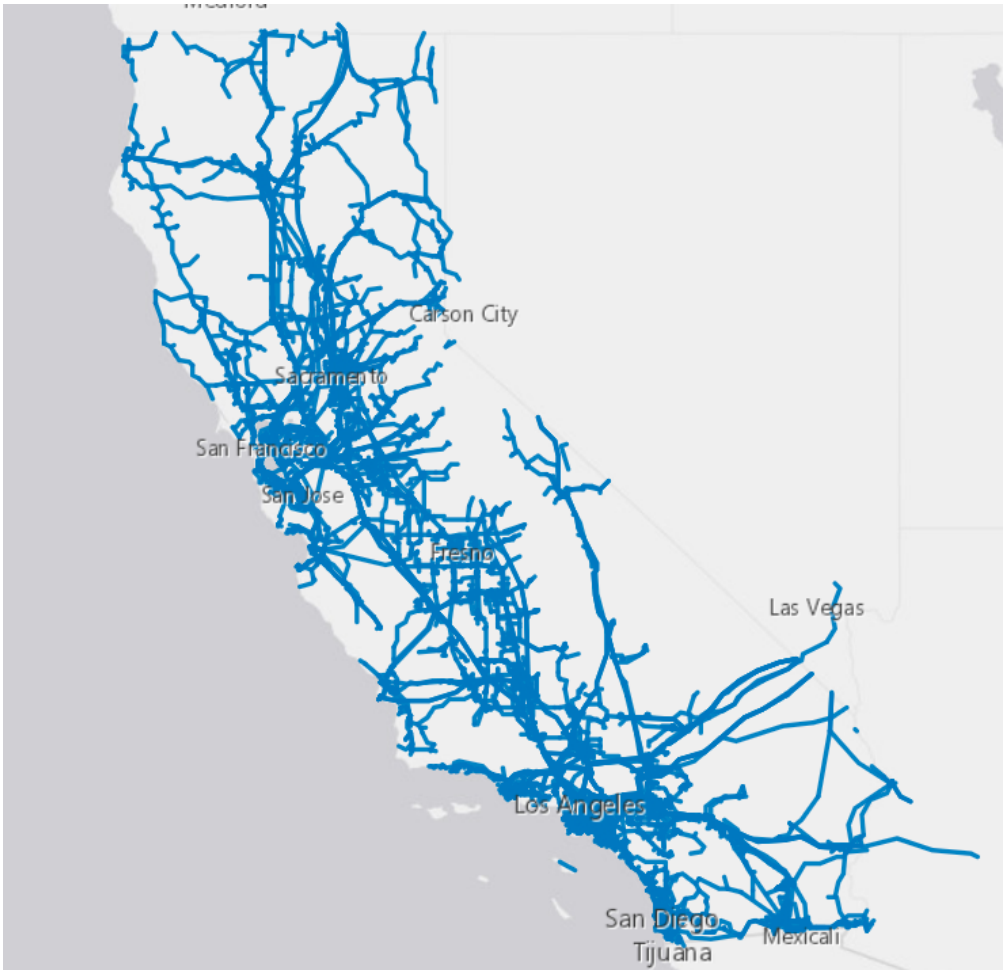


Figure 3.3: Transmission line network in CAISO.

Table 3.2: Congested transmission lines and nodes at the ends of the transmission lines.

Transmission Line	**Nodes**
230 kV Panoche–Gates	DGPAN1_7_B1, HURON_6_N001
500 kV Los Banos–Gates	SNTANLA_6_N001, HURON_6_N001
230 kV Gates–Midway	HURON_6_N001, MIDWAY_1_N047

In addition to congested transmission endpoints, we selected nodes representing five of California's largest solar PV plants to study V2G's potential for minimizing congestion losses and mitigating renewable energy curtailment. Figure 3.4 illustrates both the annual increase

in renewable energy curtailment as CAISO's renewable capacity grows and the seasonal patterns in curtailed energy [75]. Peak curtailment occurs during spring months when high solar generation coincides with a lower demand for electricity. A secondary curtailment peak emerges during fall months, though of lesser magnitude than spring curtailment.

We identified these solar PV plants using the California Power Plants dataset from the California State Geoportal [76], applying the following selection criteria:

- Minimum capacity of 250 MW
- Currently operational status
- Located away from system borders

The selected plants were then mapped to corresponding nodes on the CAISO price map [74]. Table 3.3 provides the names, capacities, and associated nodes of these solar power plants.

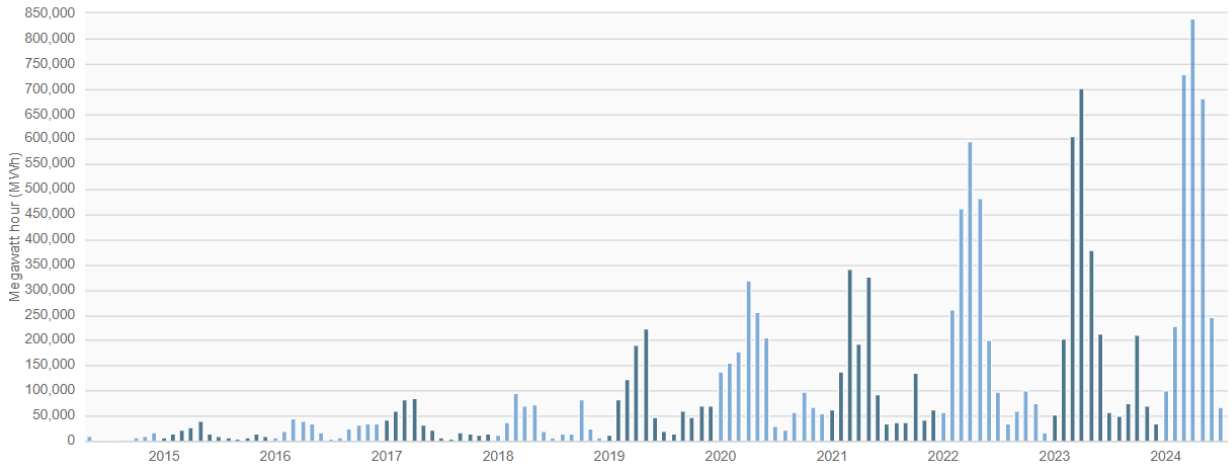


Figure 3.4: Wind and solar curtailment by month in CAISO.

Table 3.3: Chosen solar power plants from California for analysis.

Name	Capacity (MW)	Node
Topaz Solar Farm	550	TOPAZC1_7_N021
Antelope Valley Solar	250	AVSOLAR_7_N008
Desert Stateline Solar Facility	300	DSRTHV3_7_N003
California Valley Solar Ranch	250	CAVLSRGN_7_B1
Genesis Solar Energy Project	250	TOT223L2_7_N001

3.1.5 LMP Visualization

In this section, we will observe some of the characteristics of the LMPs at the chosen nodes. We focus on one transmission line and the nodes at the ends of it, as well as one node from the solar power plants for brevity. Typically, the units of LMP are $/MWh, but we plot them as $/kWh since the charging/discharging rate from the EV are in the order of kW.

In Figure 3.5, we can observe the energy component of LMP and the congestion component of LMP plotted across the given time frame (March 2021 to September 2023) for the node DGPAN1_7_B1. LMP_E is the average LMP for the entire grid and reflects, on average, the cost to add the next unit (MWh) of energy into the grid. We observe that LMP_E is mostly positive and generally higher in the summer months each year. Figure 3.5 also shows that there was a higher LMP_E in the winter months of December 2022 until March 2023. Meanwhile, at this particular node, LMP_C is negative most of the time and is mostly positive in the months of December 2022 until March 2023. We can observe that there are instances where it makes sense to charge the EV during time intervals with high LMP_E when the LMP_C is low to minimize congestion or renewable energy curtailment. We will delve into details in future sections.

Figure 3.6 shows the congestion components of LMPs at the two nodes at the ends of the transmission line 230 kV Panoche–Gates. It can be seen on multiple points in the

chosen time frame that EVs at the nodes need to perform the opposite task if the goal is to minimize congestion. During the month of December 2022, we would expect the EVs at node HURON_6_N001 to charge at certain hours, while the EVs at node DGPAN1_7_B1 would discharge at the same hours. The optimized actions of EVs will be discussed in future sections.

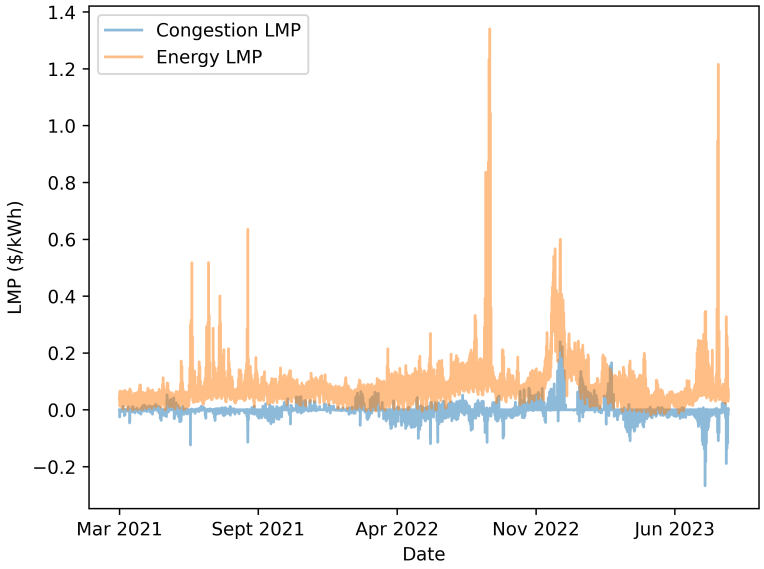


Figure 3.5: Congestion and energy components of LMP visualized for DGPAN1_7_B1.

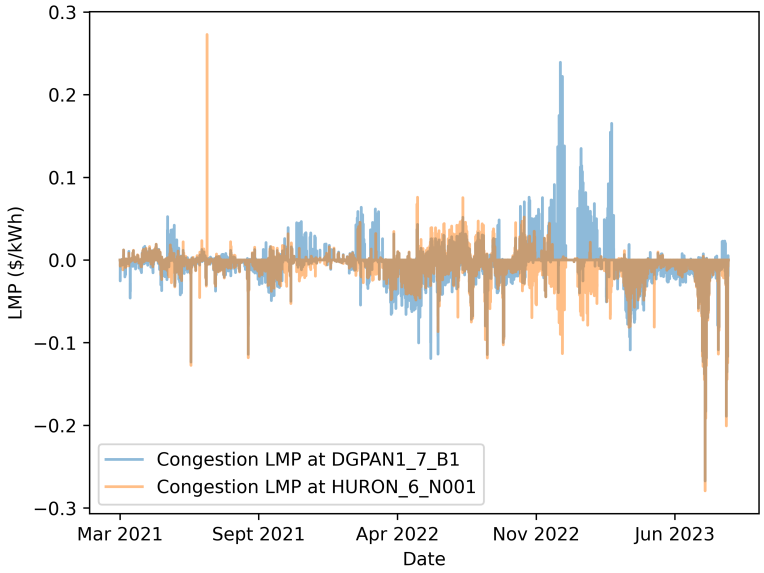


Figure 3.6: Congestion components of LMP visualized for the ends of the 230 kV Panoche–Gates transmission lines at nodes DGPAN1_7_B1 and HURON_6_N001.

Finally, we look at Figure 3.7 to observe LMP_C at large solar power plants. We can see that LMP_C is predominantly negative. We see that there is a seasonal component to it. LMP_C is largely negative during the spring months of the year, and some positive spikes in LMP_C can be observed during summer. This indicates seasonal curtailment in renewable energy in the nodes near the solar power plants due to lack of demand. However, existing transmission capacity does not allow for this energy to be transported to other nodes, perhaps due to a lack of demand.

CAISO provides data on renewable energy curtailment each year [77]. With increasing penetration of renewable energy in the grid, the curtailment in the months of February to June for both 2022 and 2023 have been over 200,000 MWh. In 2021, the maximum amount of curtailment occurred in the month of March, about 240,000 MWh. In 2023, the curtailed energy in the month of March almost tripled to 700,000 MWh. By potentially creating markets that incentivize electricity consumption at local nodes based on congestion pricing, sustainable energy curtailment and reliance on expensive polluting power plants could be

minimized.

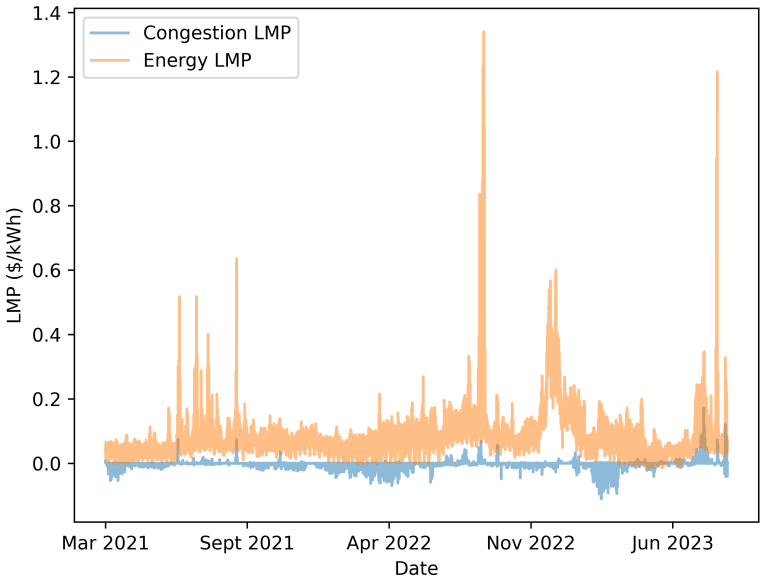


Figure 3.7: Congestion and energy components of LMP visualized for DSRTHV3_7_N003.

3.1.6 Battery Degradation

Participation in V2G applications reduces the service life of the batteries housed by EVs due to the increased number of charging cycles. There are multiple approaches that have been used to account for battery degradation in V2G, like equivalent circuit models, electrochemical models, performance based models, neural networks, and so on [15]. In our case, we choose to use a degradation model represented as a constant degradation cost factor that can be directly utilized in the objective function of the optimization model [78]. While battery degradation consists of both calendar and cyclic aging, we focus on the capacity loss purely due to the increased cycles and ignore the degradation that occurs from calendar aging. This enables the use of a constant degradation parameter in the optimization objective instead of a variable degradation parameter that depends on the current state of health of the battery [13]. Our battery degradation model is based on recent work in [15] that describes a weighted Ah-throughput model (wAh model) using a constant degradation cost factor.

The wAh model used here is based on curve fitting performed on measured experimental data in [79]. The fitting function describing capacity loss C_{loss} is shown in Equation (3.3).

$$C_{loss} = k_C k_D f^{1/2} \tag{3.3}$$

In Equation (3.3), k_C describes the influence of C-rate and k_D describes the influence of depth of cycle (DoC). f represents the number of full equivalent cycles. The fitting functions of k_C and k_D are described in Equations (3.4) and (3.5), respectively.

$$k_C = 0.063 C_{rate} + 0.0971 \tag{3.4}$$

$$k_D = 4.0253(DoC - 0.5)^3 + 1.0923 \tag{3.5}$$

k_C is a linear function of the C-rate of the battery, and k_D depends non-linearly on the depth of cycle. f is a function of cell capacity C_{cell} and charge quantity throughput Q, as shown in Equation (3.6).

$$f = \frac{Q}{2C_{cell}} \tag{3.6}$$

The battery cell under consideration has a nominal capacity (C_{cell}) of 2.85Ah. The effect of temperature on degradation is ignored since EVs are equipped with a Battery Thermal Management Systems (BTMS) that ensure that the battery pack operates at an optimal range [79]. [80] reviews the latest advancements in BTMS for EVs and discusses in detail how combinations of passive and active cooling/heating methods are used by BTMS to meet the stringent thermal requirements.

The opportunity cost from battery aging is determined using the initial cost of the battery, assuming that the battery is valued at 0$ when it reaches the end of its life at 20% capacity loss (or 80% of its initial capacity). The specific price of the battery pack C^{inv} is set at \$118/kWh based on [15]. With this information, we can obtain a constant degradation cost

factor CF_{deg} in \$/kWh using Equation (3.7).

$$CF_{deg} = \frac{C^{inv} E^{rat}}{E^{life}} \tag{3.7}$$

E^{rat} is the rated capacity of the battery, and E^{life} is the maximum possible lifetime energy throughput until the battery reaches the end of its life. E^{life} can be computed using Equation (3.8) by utilizing Equation (3.3) and the fact that the battery is valued at 0\$ at 20% capacity loss.

$$E^{life} = 2E^{rat}(\frac{20\%}{k_C k_D})^2 \tag{3.8}$$

The constant degradation cost factor CF_{deg} will be directly utilized in the objective of the optimization problem. We estimate the CF_{deg} for a Nissan Leaf EV with a battery capacity 40 kWh that can be charged/discharged at 6.6 kW using the described methodology as 0.18 cents/kWh.

3.1.7 Optimization

At each node under consideration, we optimize for two outcomes. Firstly, we use a Nissan Leaf EV for the minimization of the congestion component of the LMP at the node and then for the minimization of the total LMP at the node by means of charging and V2G. Minimization of the congestion component results in greater utilization of local cheaper sustainable energy, and potential reduction in sustainable energy curtailment and stress on transmission lines. The minimization of total LMP results in maximum revenue or minimum charging cost to the EV by trading energy at the appropriate times. Here, we only look at the benefits to a single EV and the tradeoff between the outcomes with these two methods. The usage of a large number of EVs for V2G (hundreds of kW or MW) can potentially update the LMPs significantly and drastically affect the power flow in the entire grid. Hence, we pick a single EV for our analysis to identify the value that it brings to congestion relief.

For our study, we consider a Nissan Leaf with a battery capacity of 40 kWh that can be charged/discharged at at a maximum rate of 6.6 kWh with 90% efficiency. We assume that the minimum possible state of charge of the EV is 10% and a maximum possible state of charge is 90%. Within these constraints, the charging or discharging profile is assumed to be linear. Time is discretized into hourly intervals, and we work with a simple uncertainty that the EV is not available for charging or V2G for a one hour interval interval between 8–10 AM, as well as another hour between 4–6 PM to be used for transportation, creating 4 scenarios typical for an average workday. The minimized congestion-related costs or charging costs, the total energy discharged by the EVs, the battery degradation, and the $ value per kWh of discharge is calculated at each of the nodes for all the months between March 2021 to September 2023 and reported as an average value from all scenarios. We also assume that the EVs do not travel far enough to another node's service area. The optimization problem is described below.

$$\text{Minimize} \quad \sum_{k=1}^{T} (LMP_{i,k}(P_{ch,k} - P_{dch,k}) - CF_{deg}(P_{ch,k} + P_{dch,k}))\Delta_T \tag{3.9}$$

subject to

$$E_k = E_{k-1} + (P_{ch,k}\eta_{ch} - P_{dch,k}/\eta_{dch} - P_{driv,k})\Delta_T \quad \forall k \in \{T\} \tag{3.10}$$

$$E_{min} \leq E_k \leq E_{max} \quad \forall k \in \{T\} \tag{3.11}$$

$$0 \leq P_{ch,k} \leq \delta_{ch,k} P_{ch,max} \quad \forall k \in \{T\} \tag{3.12}$$

$$0 \leq P_{dch,k} \leq \delta_{dch,k} P_{dch,max} \quad \forall k \in \{T\} \tag{3.13}$$

$$\delta_{ch,k} \in \{0,1\} \quad \forall k \in \{T\} \tag{3.14}$$

$$\delta_{dch,k} \in \{0,1\} \quad \forall k \in \{T\} \tag{3.15}$$

$$\delta_{ch,k} + \delta_{dch,k} \leq 1 \quad \forall k \in \{T\} \tag{3.16}$$

$$\delta_{ch,k} = 0 \quad \forall k \in \{T_{driv}\} \tag{3.17}$$

$$\delta_{dch,k} = 0 \quad \forall k \in \{T_{driv}\} \tag{3.18}$$

$$E_k \geq E_{dep,k} \quad \forall k \in \{T_{dep}\} \tag{3.19}$$

The optimization problem is formulated as a mixed integer linear program (MILP) that is run multiple times for each node for all the months chosen (with no change in timings of EV departure, arrival, and energy consumed driving). The day-ahead LMP data including the 3 components—energy, congestion, and loss for every time interval at each node—is obtained using the gridstatus module in Python. Equation (3.9) states that the objective function minimizes the charging cost with $LMP_{i,k}$ using the EV with V2G. The i in $LMP_{i,k}$ can be T, with $LMP_{T,k}$ representing the total LMP or i can be C to represent the congestion component $LMP_{C,k}$ for time interval k at the node. The timeline under consideration is discretized to T time intervals of size Δ_T, which, in this case, is 1 h. $P_{ch,k}$ and $P_{dch,k}$ are the charging and discharging power of the EV at time interval k. CF_{deg} is the constant degradation cost factor of the EV battery. The cost of charging/discharging the energy from the EV and/or the prevented congestion-related costs are incorporated in this objective.

Equations (3.10)–(3.19) represent the constraints of the optimization model. Equation (3.10) is based on the law of conservation of energy—it states that the energy stored in the EV at time k depends on the energy in the EV at time $(k-1)$, energy expenditure due to driving in time k, as well as the power flow into or out of the EV at time k when plugged in. The EV can be charged with power $P_{ch,k}$ with efficiency η_{ch}, discharged with power $P_{dch,k}$ with efficiency η_{dch}, or the EV consumes power $P_{driv,k}$ when driven at time interval k. $P_{driv,k}$ is randomly set in the range of 5 to 10 kW to reflect a driven distance in the range of 15 to 30 miles but is fixed at that value for a given scenario. Both η_{ch} and η_{dch} are set at 90%. Equation (3.11) sets limitations on the maximum and minimum energy stored in the battery of the EV. The energy in the EV at any time interval k is assumed to lie between 10% (E_{min}) and 90% (E_{max}) of the EV battery's rated capacity E^{rat}. Equations (3.12) and (3.13) set the

charging and discharging power limitations of the EV as $P_{ch,max}$ and $P_{dch,max}$, respectively, which, in this case, is 6.6 kWh. $\delta_{ch,k}$ and $\delta_{dch,k}$ are binary decision variables as shown in Equations (3.14) and (3.15). When $\delta_{ch,k}$ equals 1, the EV is charging, and when it equals 0, the EV is not charging. The same rule applies to $\delta_{dch,k}$. The sum of $\delta_{ch,k}$ and $\delta_{dch,k}$ is always less than or equal to 1, as shown in Equation (3.16), ensuring that the EV can either charge, discharge, or remain idle when plugged in. Equation (3.17) and (3.18) ensure that the EV cannot charge or discharge during the time intervals when it is driven. Equation (3.19) states that the EV must hit a minimum amount of energy $E_{dep,k}$ before its departure from a charging station.

The optimization is set up and solved using the gurobipy module in Python [81]. The only input data to the program are the LMP_T and LMP_C data of the nodes for the months of March 2021 to September 2023. The other parameters are set as stated in the assumptions. The outputs obtained are the average maximum revenue from the EV, the congestion-related savings, the charging schedule of the EV, the total discharged power, benefit per kWh of V2G, and battery degradation as capacity loss.

3.2 Results

In this section, we will first look at the total benefits from V2G-enabled EVs at each node. Following this, we will explore seasonality and the behavior of EVs at smaller time scales in these nodes.

The blue bars in Figure 3.8 shows the total savings (or revenue) earned by a single EV at each node that participates in energy arbitrage with LMP_T pricing. The orange bars in the figure represent the congestion savings as an outcome of minimizing total charging cost. We can see that in each of the nodes, the EV earns over 200 dollars, with a maximum of \$290.37 at node HURON_6_N001. However, the congestion savings are only in the range of 110–190 dollars for these nodes.

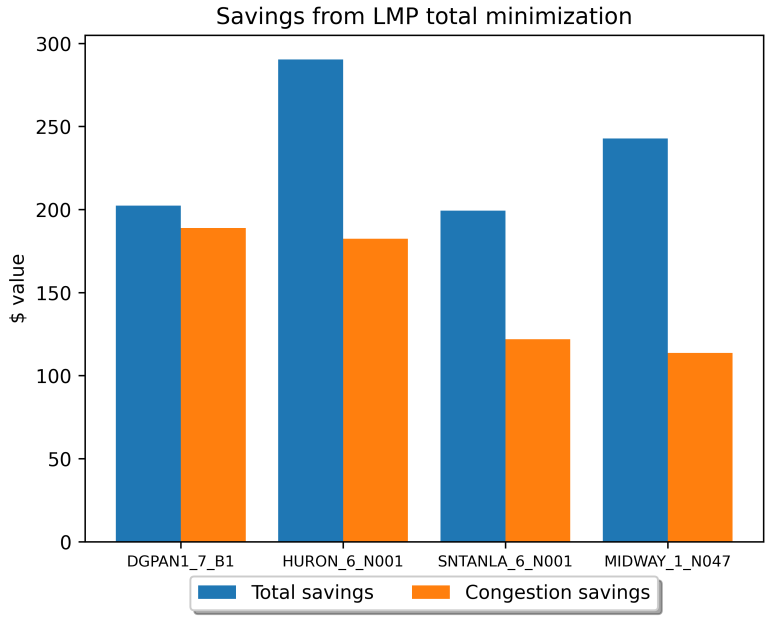


Figure 3.8: Savings from LMP_T minimization at the nodes at the ends of the transmission lines.

The results of the LMP_C optimization in Figure 3.9 shares an interesting find. Here, the blue bars show the total congestion savings by a single EV at the appropriate node that participates in congestion minimization with LMP_C pricing. The orange bars represent the minimized total congestion costs. We see that congestion minimization comes at a significant cost based on the current market design. In each of the nodes, we can see congestion savings over \$380, except for one node at \$259.8. However, based on the current electricity market design, the EVs have to pay in the range of \$670–950 to help minimize local congestion. This is one of the main reasons why EVs with V2G capability will not participate in local congestion minimization with the current LMP pricing, unless they can be incentivized to do so.

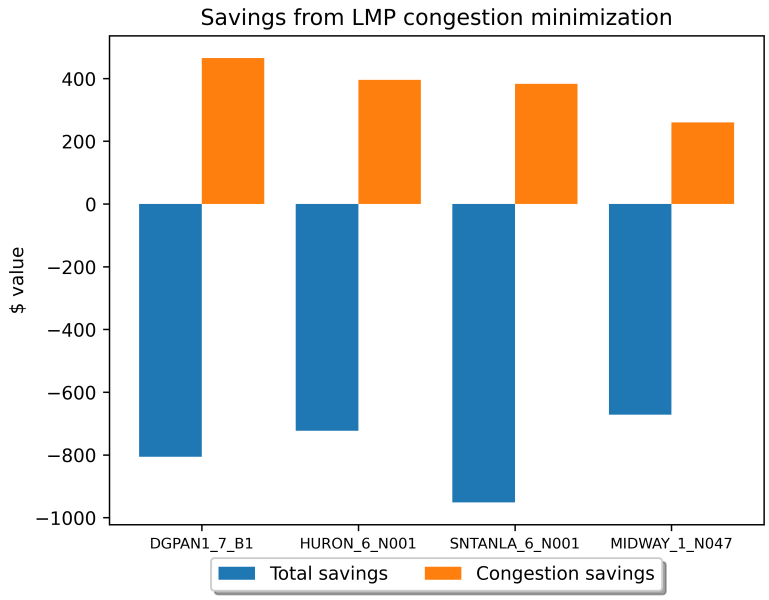


Figure 3.9: Savings from LMP_C minimization at the nodes at the ends of the transmission lines.

The blue and orange bars in Figure 3.10 show the capacity degradation from the LMP_T and LMP_C optimization, respectively. The capacity losses for the LMP_T optimization are in the range of 3.7–3.8% for the timeline in consideration (March 2021 to September 2023), while the capacity losses for the LMP_C optimization are less than 2.7%. This suggests that the EV discharges in fewer instances for the LMP_C optimization when compared to the LMP_T optimization.

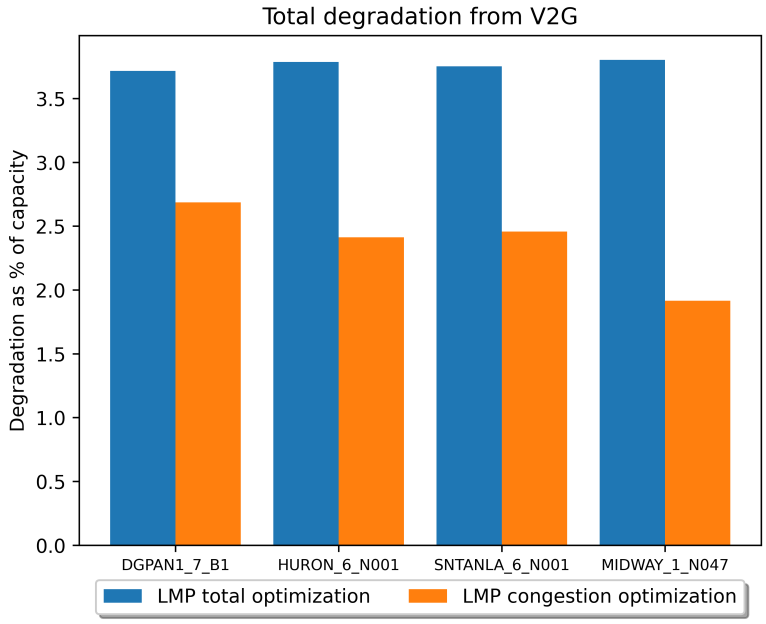


Figure 3.10: Battery capacity loss (%) from LMP_T and LMP_C minimization at the nodes at the ends of the transmission lines.

The blue bars in Figure 3.11 shows the total savings (or revenue) earned by a single EV at each solar power plant node that participates in energy arbitrage with LMP_T pricing. The orange bars in the figure represent the congestion savings. We can see that in each of the cases, the EV earns over 275 dollars, with a maximum of $420.1 at node DSRTHV3_7_N003. However, the congestion savings are only in the range of 120–255 dollars.

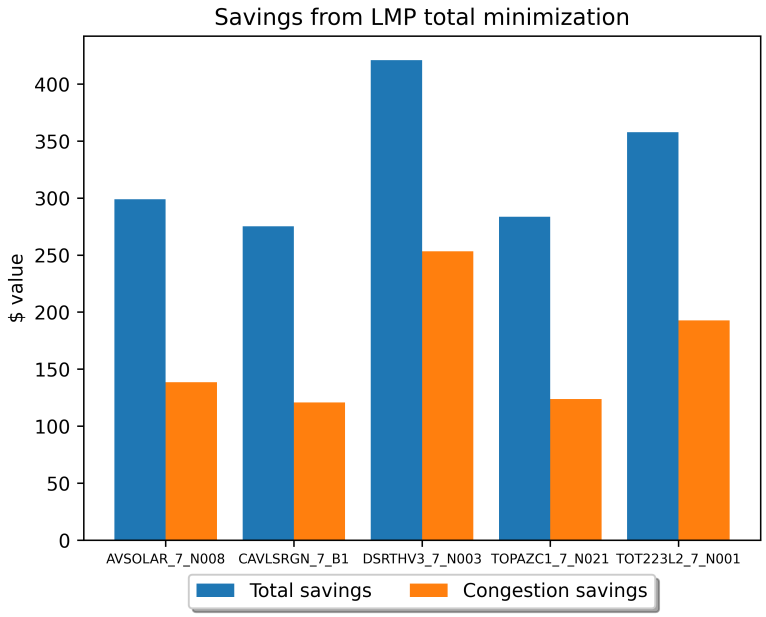


Figure 3.11: Savings from LMP_T minimization at the solar power plant nodes.

Figure 3.12 shares a similar finding as Figure 3.9. Here, the blue bars show the total savings earned by a single EV at the appropriate node that participates in congestion minimization with LMP_C pricing. The orange bars represent the minimized total congestion costs. We can observe congestion savings in the range of \$150–290 depending on location. However, the EVs have to pay in the range of \$400–660 to help minimize local congestion. This again shows that local congestion minimization may come at a cost to earning revenue from total LMP and highlights the need to incentivize action at a nodal level.

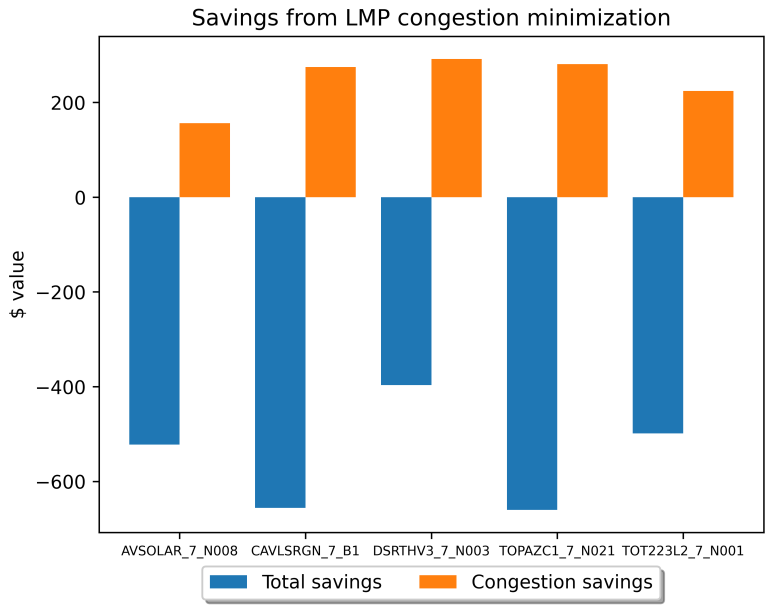


Figure 3.12: Savings from LMP_C minimization at the solar power plant nodes.

The blue and orange bars in Figure 3.13 show the capacity degradation from the LMP_T and LMP_C optimization, respectively, at the solar power plant nodes. The capacity losses for the LMP_T optimization are close to 3.8% for the timeline in consideration (March 2021 to September 2023), while the capacity losses for the LMP_C optimization are around 1.7–2%.

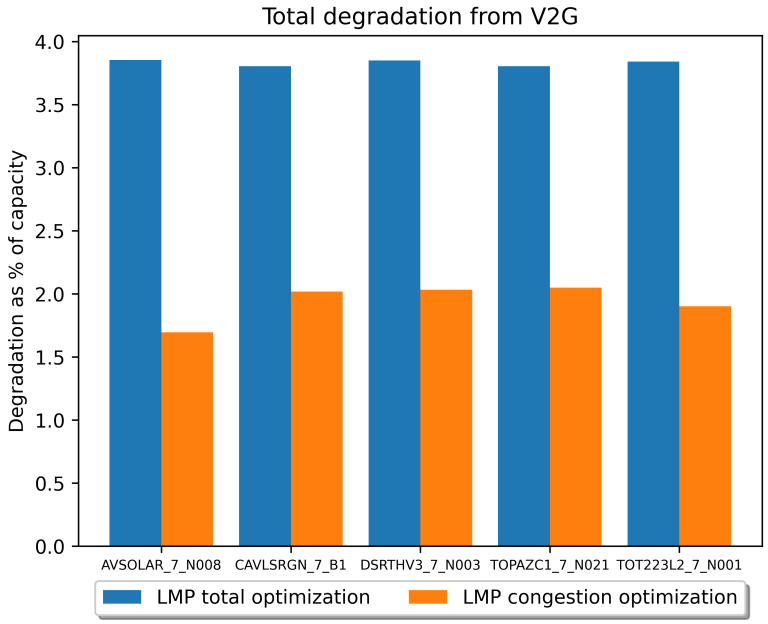


Figure 3.13: Battery capacity loss (%) from LMP_T and LMP_C minimization at the solar power plant nodes.

For conciseness, we focus on the nodes whose LMPs were highlighted in Figures 3.5–3.7 to observe the monthly trends in EV behavior. The monthly distribution of arbitrage revenue and congestion savings from both the LMP_T and LMP_C optimization as well as the distribution of V2G commitment and degradation from nodes DGPAN1_7_B1, HURON_6_N001, and DSRTHV3_7_N003 are discussed.

Figures 3.14–3.16 show the monthly distribution of revenue or congestion savings. A EV optimized for LMP_T at DGPAN1_7_B1 can earn over \$50 in the months of May 2022, September 2022, and April 2023, but the congestion savings are much larger in May 2022 and April 2023 compared to September 2022. This shows that the LMP_T optimal charging strategy for a EV results in both higher earnings and congestion savings during the spring season, but during summer, there is an opportunity to earn a higher amount with minimal influence on congestion. We also see that during the winter months, the congestion savings are higher than the revenue from arbitrage. This indicates a lower opportunity to earn revenue from arbitrage during winter. A drastic example in this case is during the months

of December 2022 and January 2023, where \$84 and \$49 are required to charge the EVs. Figure 3.15 shows a similar promise with higher earnings (greater than \$40) in the months of May 2022, September 2022, and April 2023, but congestion savings peak mostly during the spring months (though the value is much lower). Here again, the congestion savings are higher than the revenue from arbitrage during the winter months. We see a similar outcome for the solar power plant node DSRTHV3_7_N003 in Figure 3.16, showing potential earnings in May 2022, September 2022, and April 2023 being greater than \$35. However, we see that the revenue continues to remain high except for a dip in June 2023. We also see that the congestion savings are higher one month earlier compared to nodes DGPAN1_7_B1 and HURON_6_N001.

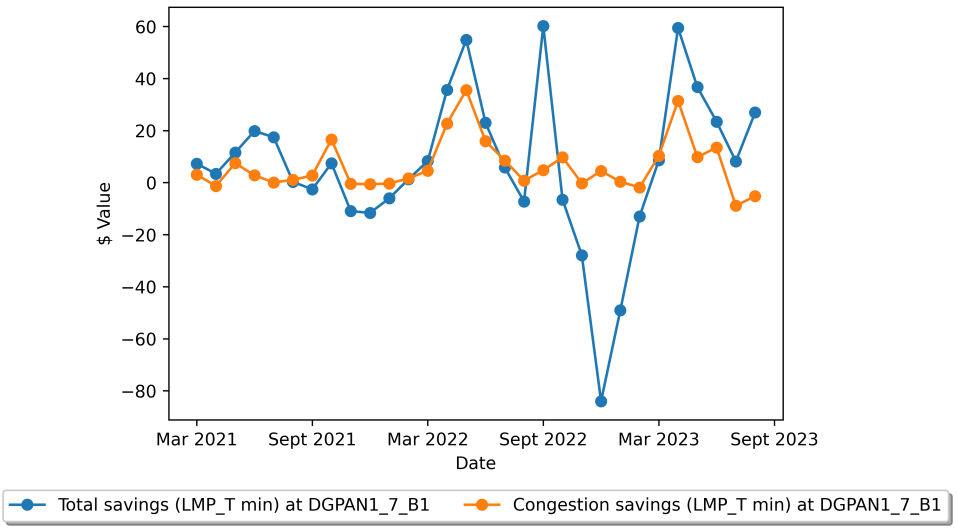


Figure 3.14: Monthly savings from LMP_T minimization at DGPAN1_7_B1.

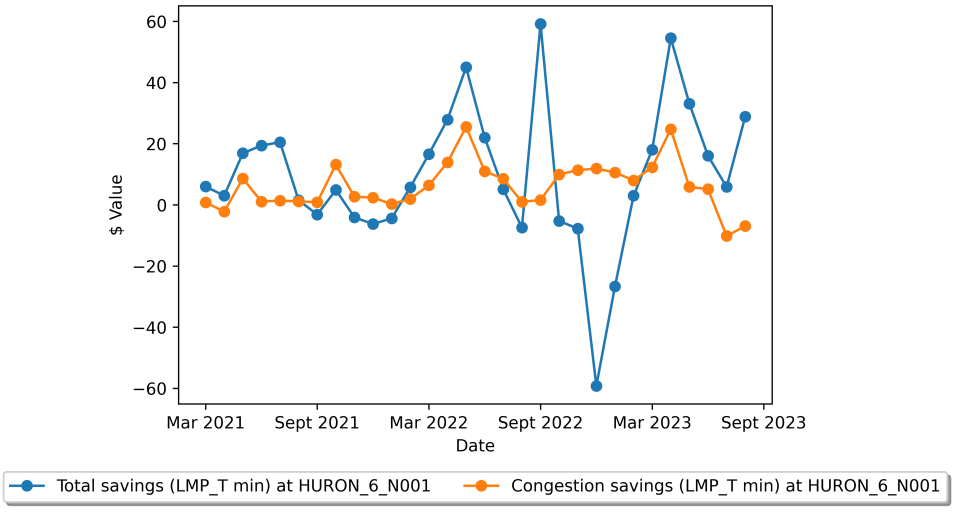


Figure 3.15: Monthly savings from LMP_T minimization at HURON_6_N001.

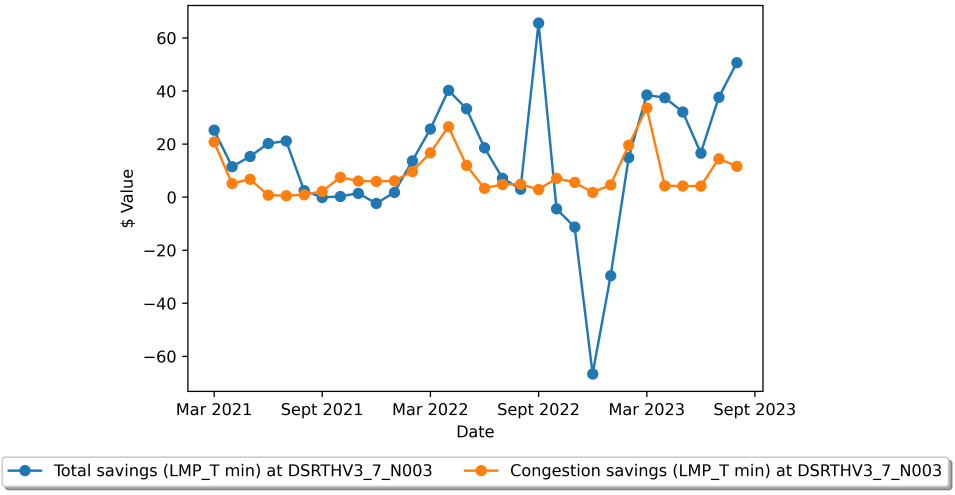


Figure 3.16: Monthly savings from LMP_T minimization at DSRTHV3_7_N003.

Figures 3.17–3.19 show the monthly distribution of revenue or congestion savings under LMP_C optimization. As seen previously, LMP_C minimization results in congestion savings but significantly increases charging costs. In both DGPAN1_7_B1 and HURON_6_N001, the congestion savings spike close to the months of April and May each year. During these months, the charging costs are not significant as well. However, for most other months from early summer to early spring, there are negligible congestion savings for a very large rise in

charging costs, especially during December 2022, with charging costs as high as $174 and $117 in DGPAN1_7_B1 and HURON_6_N001, respectively. We see a similar trend with the solar power plant node DSRTHV3_7_N003. In the case of DGPAN1_7_B1 and HURON_6_N001, congestion minimization leads to revenue on the order of $8 and above (up to $35) for the months of April and May 2022 and 2023. The positive revenue for DSRTHV3_7_N003 shows up in March 2021, March–April 2022, March 2023, and July–August 2023.

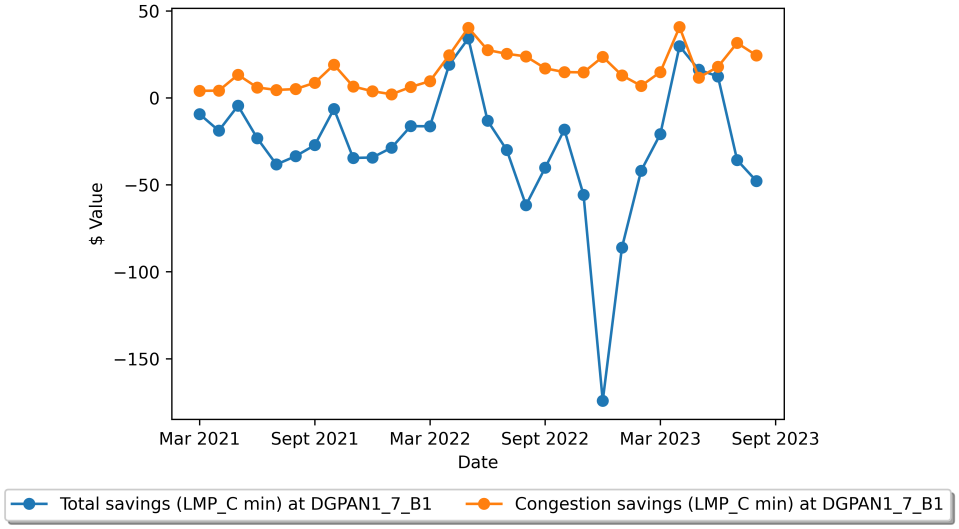


Figure 3.17: Monthly savings from LMP_C minimization at DGPAN1_7_B1.

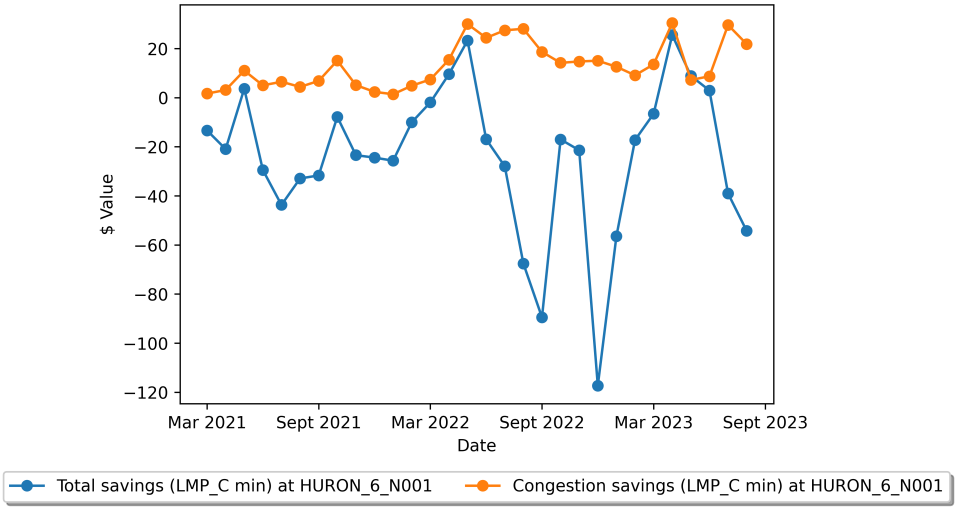


Figure 3.18: Monthly savings from LMP_C minimization at HURON_6_N001.

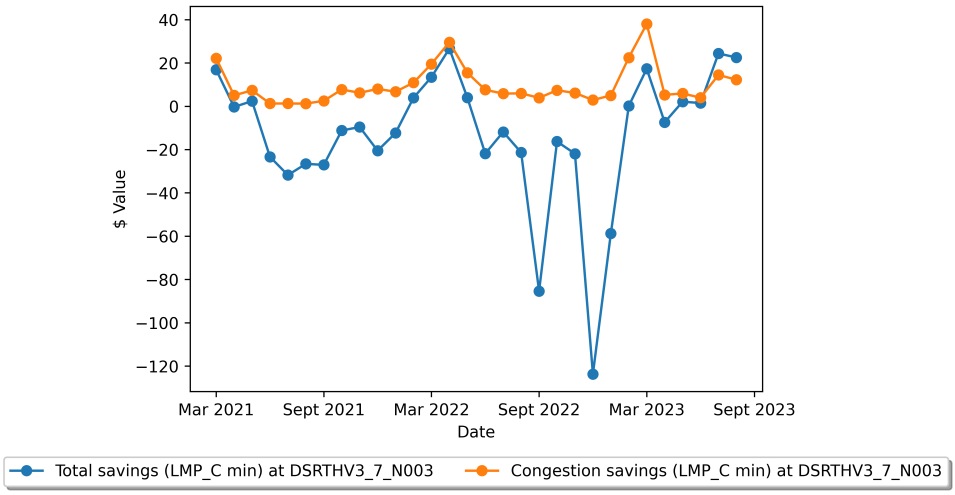


Figure 3.19: Monthly savings from LMP_C minimization at DSRTHV3_7_N003.

Figures 3.20–3.22 show the total amount of V2G throughput provided by the EV at the node for both LMP_T and LMP_C optimization. For the three nodes with LMP_T optimization, the V2G throughput is in the range of 500–900 kWh per month, with the exception of the months from October 2022 to January 2023 for DGPAN1_7_B1. For the three nodes with LMP_C optimization, the V2G throughput is in the range of 0–600 kWh per month, with the exception of the months from November 2022 to January 2023, where it is closer to 800 kWh for DGPAN1_7_B1 and HURON_6_N001. With respect to LMP_C optimization, we see a much smaller throughput of V2G in the range of 0–250 kWh for the months of June 2021 to March 2022, with an exception in October 2021, as well as from January 2023 to March 2023 for all three nodes. Additionally, in DSRTHV3_7_N003, we see a low V2G throughput from September 2022 to June 2023, with an exception in March 2023.

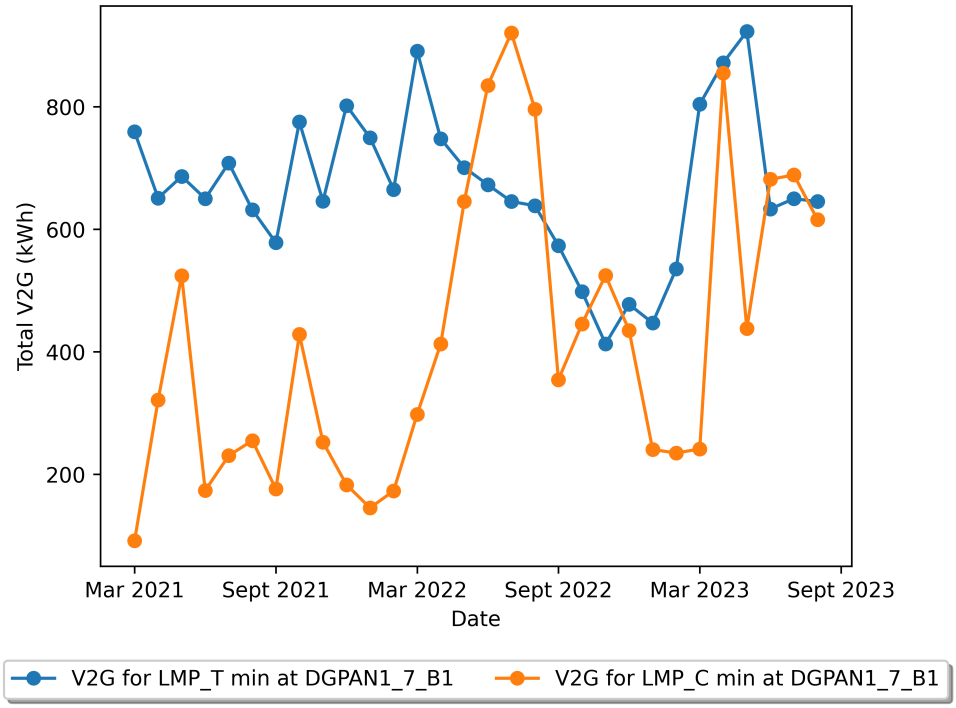


Figure 3.20: Monthly total V2G power throughput at DGPAN1_7_B1.

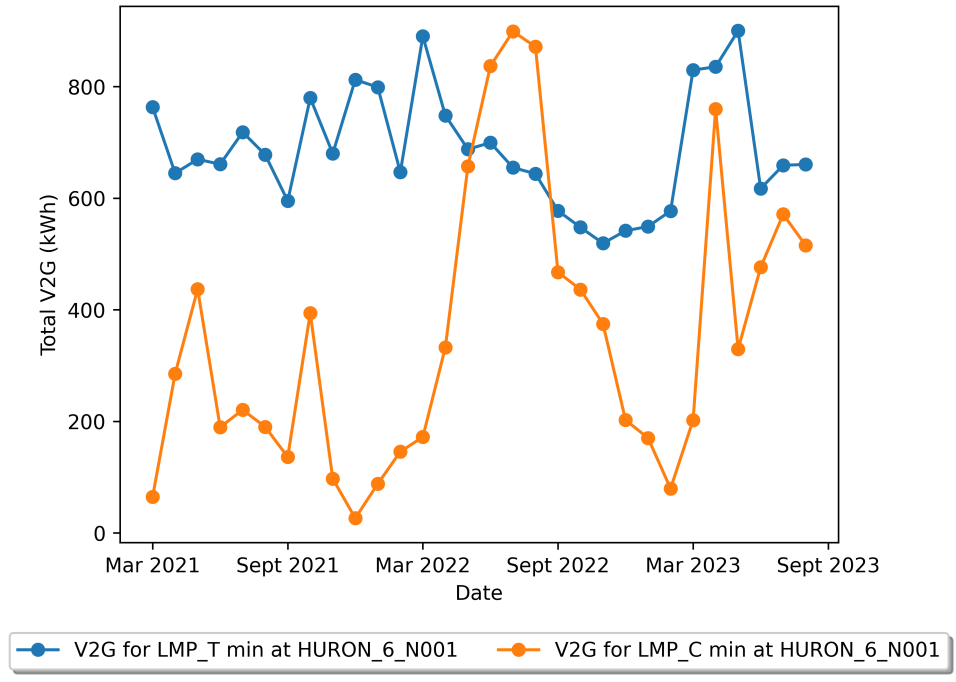


Figure 3.21: Monthly total V2G power throughput at HURON_6_N001.

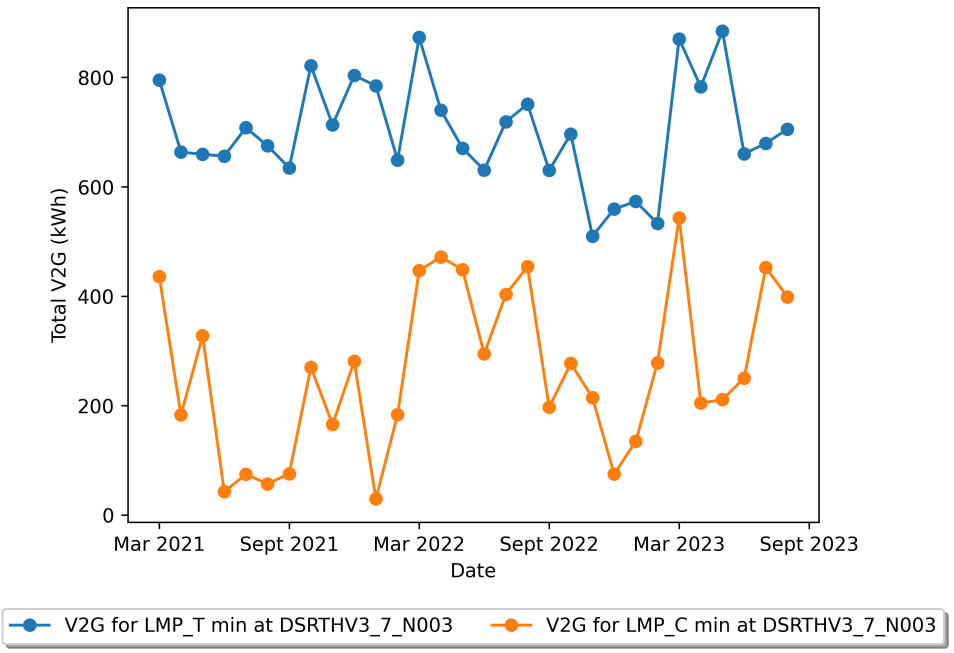


Figure 3.22: Monthly total V2G power throughput at DSRTHV3_7_N003.

Figures 3.23–3.25 show the value of congestion savings per units of V2G provided by the EV at the nodes for both LMP_T and LMP_C minimization. We see a seasonal variation for the benefits per unit of V2G. As expected, the congestion savings from LMP_C minimization are higher than those from LMP_T minimization since the focus is to reduce congestion in the former optimization. In all the cases, the benefits from LMP_C minimization are positive, but for some months, LMP_T optimization increases congestion, like July and August 2023 in DGPAN1_7_B1 and HURON_6_N001. The value from LMP_C optimization is in the range of 0.01–0.07 \$/kWh for most months for the three nodes. While no exceptions are seen at DGPAN1_7_B1, we observe a higher value (upto \$0.12/kWh) at HURON_6_N001 in the months of December 2021 and December 2022 to March 2023 and a very large spike in DSRTHV3_7_N003 in the month of January 2022, with a value of \$0.23/kWh.

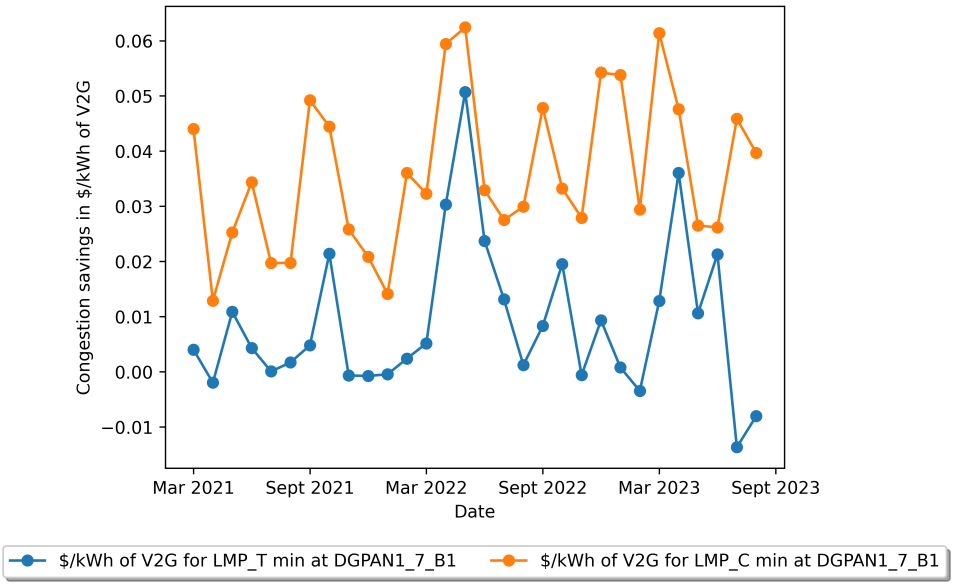


Figure 3.23: Congestion savings in $/kWh of V2G at DGPAN1_7_B1.

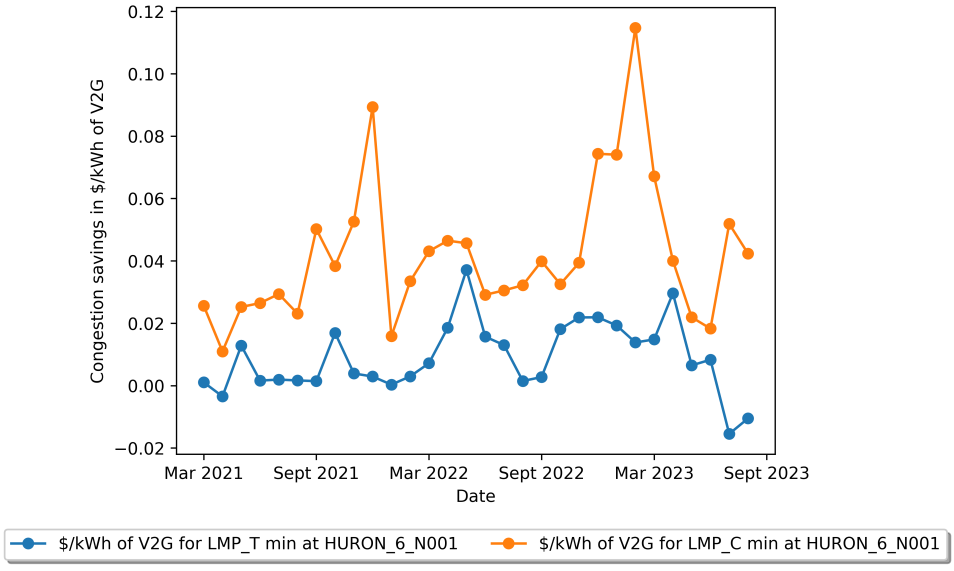


Figure 3.24: Congestion savings in $/kWh of V2G at HURON_6_N001.

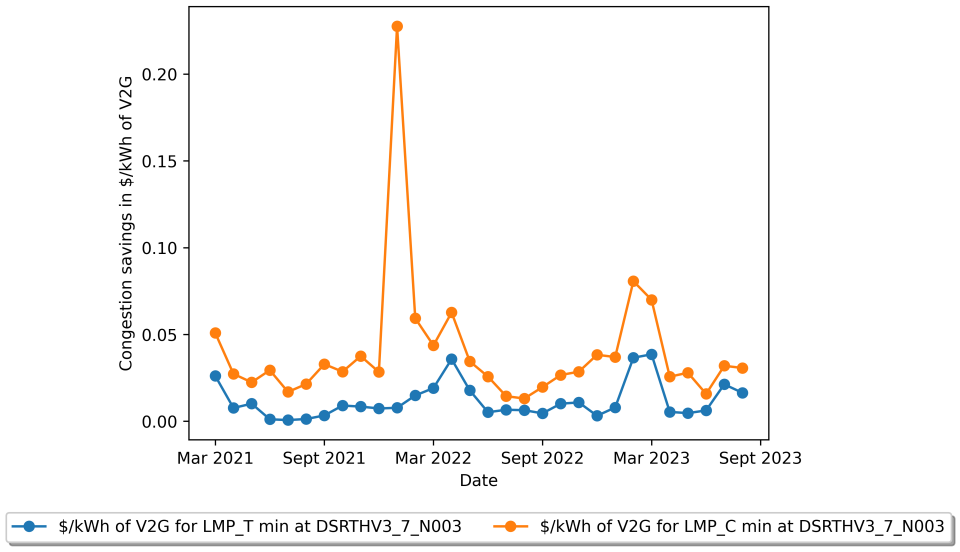


Figure 3.25: Congestion savings in $/kWh of V2G at DSRTHV3_7_N003.

The other nodes listed in Tables 3.2 and 3.3 show similar findings as reported for DG-PAN1_7_B1, HURON_6_N001, and DSRTHV3_7_N003. We show that local congestion at nodes can potentially be minimized using EVs and V2G with LMP_C minimization. The benefits seem to be larger during certain months of the year. Strong incentives to utilize V2G for congestion minimization could lead to lower stress on the grid and minimize sustainable energy curtailment and pollution.

3.3 Discussion

In this study, our initial focus centers on electric grid congestion and the limitations of FTRs in mitigating price uncertainties that arise from the inability of certain locations to access nearby sustainable energy sources due to transmission congestion. The large amounts of RES installed in the grid to combat climate change and air pollution are intermittent in nature, leading to frequent supply-demand mismatch and price fluctuations within the existing transmission infrastructure and electricity markets. We examined the shortcomings of FTR markets, emphasizing that they do not fully address transmission congestion

challenges. After exploring utility-scale energy storage applications for transmission congestion relief, we investigated V2G technology's potential for minimizing local congestion through analysis of LMPs. We identified three of the most congested transmission lines within CAISO and designated the nodes at their endpoints as potential focal points for our analysis. Additionally, we incorporated nodes representing several of California's largest solar power facilities. We developed a battery degradation quantification approach using a constant degradation cost factor and created optimization programs incorporating either the total LMP (LMP_T) or the congestion component of LMP (LMP_C) within their objective functions. For the period from March 2021 to September 2023, LMP_T optimization resulted in EV earnings of \$200-290 at transmission line nodes and \$275-420 at solar power plant nodes, with congestion savings of \$110-190 and \$120-255 respectively. Under LMP_C optimization, congestion savings increased to \$260-430 for transmission line nodes and \$150-290 for solar power plant nodes. However, this came at significantly higher charging costs of $670 - 950 and 400-660$ respectively, highlighting the need to incentivize action at the nodal level. Solar power plant nodes demonstrated greater revenue potential from arbitrage with LMP_T optimization, while congested transmission line nodes showed substantially higher congestion savings with LMP_C minimization. Battery capacity losses under LMP_T optimization ranged from 3.7-3.8% across all nodes, while LMP_C optimization showed losses of 1.8-2.7% for transmission line nodes and 1.7-2% for solar power plant nodes, indicating less frequent discharge events. Monthly analysis revealed that LMP_T optimal charging strategies yielded both higher earnings and congestion savings during spring months, with summer offering increased earning potential but minimal congestion impact. Winter months showed higher congestion savings relative to arbitrage revenue. Solar power plant nodes exhibited congestion savings peaks one month earlier compared to transmission line nodes. Under LMP_C minimization, late spring/early summer showed high congestion savings with low charging costs, while other months demonstrated minimal congestion savings despite significantly increased charging costs. V2G throughput under LMP_C optimization remained lower than LMP_T optimization for transmission line nodes except during May-July 2022,

suggesting acute transmission congestion during this period.

These findings on the total benefits of V2G-enabled EVs at different nodes, including financial savings and congestion cost reductions, highlight spatio-temporal patterns in local congestion. This work provides another lens to evaluate V2G's value in a real-world context for alleviating congestion, complementing other V2G services like frequency regulation, voltage regulation, and energy arbitrage. We hope that this work helps promote V2G adoption by the automotive industry and government entities, encouraging the launch of more V2G-enabled car models and charging stations, ultimately contributing to a more sustainable planet. The battery degradation and capacity losses due to V2G participation were also studied to observe the trade-off between benefits and EV battery longevity.

While our analysis demonstrates the significant potential of V2G for grid congestion relief, the impact of V2G services on battery degradation remains a critical concern for EV owners and fleet operators. The financial benefits of grid services must be weighed against battery lifetime costs, requiring accurate tracking and valuation of battery health over time. Traditional battery health monitoring systems often lack transparency and can be subject to manipulation, potentially discouraging EV owners from participating in V2G services. Additionally, EVs can go through multiple charge/discharge cycles when being charged by profit seeking entities. To address these challenges, we propose a blockchain-based framework for tracking and validating EV battery degradation. This approach provides an immutable record of battery health metrics, enabling fair compensation for V2G participants while ensuring transparency and trust in the battery degradation assessment process.

CHAPTER 4

Blockchain for EV battery degradation

The increasing adoption of EVs with V2G capability presents multiple opportunities for power system optimization. V2G technology enables EVs to provide essential grid services, including renewable energy integration, peak load reduction, frequency regulation, voltage support, emergency power supply, and congestion relief as described in Chapter 3. However, this paradigm introduces complex challenges regarding battery degradation and fair compensation mechanisms.

Battery degradation from frequent charging and discharging cycles represents a significant barrier to widespread V2G adoption. The economic implications of this degradation create uncertainty about V2G's cost-effectiveness, as grid operators must balance multiple variables including degradation costs, electricity prices, grid service revenues, and renewable energy availability [15]. This complexity is further compounded by the market structure, where individual EVs cannot directly participate in ancillary service markets but must instead work through EV aggregators (EVAs) since a single EV does not provide sufficient power or energy to meet minimum market requirements [16].

EVAs serve as intermediaries between individual EVs and electricity markets, aggregating modular EV resources into larger units. EVAs perform several critical functions in the V2G ecosystem. They bid into wholesale electricity and ancillary service markets on behalf of their EV fleet, coordinate charging and discharging schedules across multiple vehicles, and manage power delivery commitments [82]. EVAs are responsible for handling market settlements and payments, predicting EV availability and capacity, and optimizing fleet performance while

meeting grid requirements. By pooling resources, EVAs enable individual EVs to participate in markets they couldn't access independently.

Charging Station Operators (CSOs) manage the physical infrastructure connecting EVs to the grid and serve as the direct interface with EV owners. CSOs are responsible for operating and maintaining charging stations, managing local power distribution, and implementing charging and discharging commands received from EVAs [83]. They collect charging data, handle direct customer transactions, and ensure charging station availability and reliability. CSOs also play a crucial role in monitoring equipment health and safety, serving as the primary point of contact for EV owners using their facilities.

The hierarchical relationship typically flows from EVAs to CSOs to individual EVs, with each level having distinct roles and economic interests. Figure 4.1 highlights the relationship among EVAs, CSOs, EVs and the grid Distribution System Operator (DSO). EVAs aggregate sufficient capacity to meet minimum market participation thresholds, often in hundreds of kilowatts to megawatts, that individual EVs cannot achieve alone. CSOs provide the physical connection points and handle the actual power transfers, while also serving as the primary point of contact for EV owners. This multi-tiered structure enables market participation but also introduces challenges in ensuring fair compensation and transparent operations throughout the value chain. EVAs might maximize their profits while providing minimal compensation to CSOs, who in turn might undercompensate EV owners. This misalignment of incentives particularly affects EV owners, who bear the cost of battery health degradation without guaranteed fair compensation.

To address these challenges, blockchain technology emerges as a promising solution for tracking battery health and ensuring fair compensation. By creating an immutable, transparent record of battery state of health and grid service contributions, blockchain can help establish trust between all participants in the V2G ecosystem. This chapter explores how blockchain technology can be leveraged to create a fair, transparent, and efficient system for tracking EV battery degradation and ensuring appropriate compensation for V2G services.

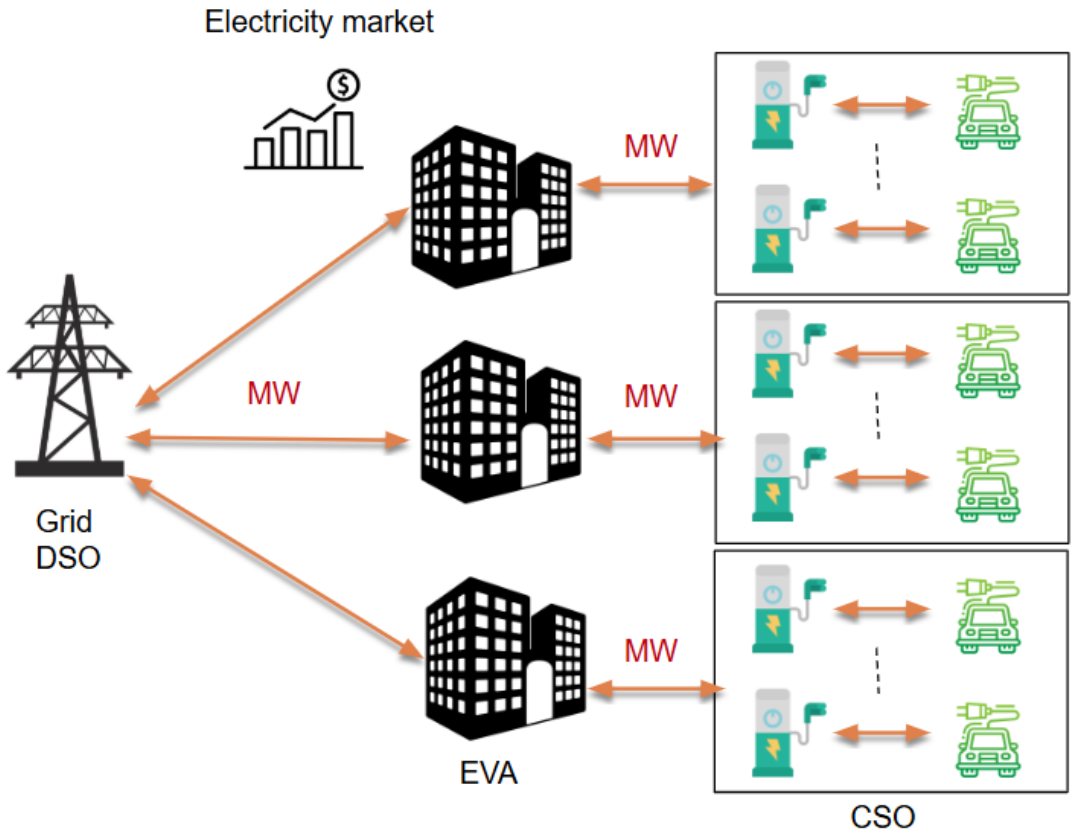


Figure 4.1: Schematic highlighting the relationship among EVAs, CSO and EVs with the grid.

This chapter is organized as follows:

- Section 4.1 introduces blockchain technology, public, private and consortium blockchain, and the relationship among various stakeholders (EVs, CSOs and EVAs) with the blockchain.
- Section 4.2 introduces calendar aging and cycle degradation in Li-ion batteries and dicusses a model to calculate and track battery degradation through a blockchain-based system for accurate state-of-health estimation and cost calculation.
- Section 4.3 discusses the optimization model that minimizes charging and battery degradation costs for 20 EVs over three years by considering both calendar and cycle aging,

- Section 4.4 discusses results comparing dynamic degradation cost modeling to constant degradation cost
- Section 4.5 synthesizes key findings

4.1 Blockchain

Blockchain is an immutable distributed ledger that maintains an ordered list of records, contracts, events, data, or transactions in blocks. First introduced with Bitcoin [84], blockchain enables decentralized digital transactions verified by network nodes through cryptographic signatures and stored in a public distributed ledger. The technology employs consensus algorithms in decentralized networks for transaction verification and authentication, eliminating single points of failure while protecting user privacy. Through cryptographic hashing, each block links to the previous block's hash, creating an unbreakable chain that ensures chronological ordering and prevents transaction modification [85].

The security architecture of blockchain relies on asymmetric cryptography, with each participant having public and private keys. While public keys are visible to all and used for encryption, private keys remain confidential and enable decryption [86]. Blockchain wallets store these key pairs and transaction details. The system uses cryptographic hashing (like SHA-256) to create fixed-length, unique hashes of data, organized in Merkle trees. Each block combines a header containing the Merkle root and previous block's hash with a body containing transaction data. Transaction verification utilizes various consensus mechanisms, from Bitcoin's Proof-of-Work [84] to alternatives like Proof-of-Stake [87] and Byzantine Fault Tolerance [88]. Smart contracts enhance this system by automating agreement execution based on predefined conditions, enabling trustless interactions between participants [89].

Blockchain systems are categorized into three types: public, consortium, and private. Public blockchains maximize transparency but sacrifice privacy and processing speed, while private blockchains limit participation to selected entities. Consortium blockchains offer a

middle ground, requiring validation from a group of equal stakeholders rather than a single entity or all participants. This consortium model has successfully supported energy sector applications, including energy trading [90], battery swapping [91], and Internet of Things integration [92].

For EV battery lifetime tracking, the consortium blockchain model is particularly suitable as it accommodates multiple stakeholders in the charging ecosystem. CSOs manage the physical charging infrastructure and operations. EVAs coordinate with multiple CSO facilities and participate in grid service markets by aggregating EV resources to meet power requirements, typically in the range of hundreds of kW or a few MW. EV Mobility Service Providers (MSP) enable EV connectivity across different CSOs and EVAs, facilitating charging and V2G participation across multiple locations.

Each stakeholder operates under specific authorizations and restrictions within the network. Without regulation, these actors might prioritize individual profit maximization at others' expense. The consortium blockchain's requirement for multi-stakeholder transaction validation ensures transparent, verifiable tracking of both transactions and battery lifecycle events.

The blockchain system tracks two primary types of EV data: operational metrics (charging/discharging power and operating temperature) and financial transactions. This data enables calculation of battery degradation costs, which EVAs use to optimize V2G participation decisions. EV owners receive compensation for V2G services and the blockchain records both power transactions and daily profit distribution among participants.

Access rights within the system are structured hierarchically. EV users have READ access limited to their own vehicle's data, including charging/discharging logs, V2G income, and charging expenses. CSOs and EVAs possess broader READ access to all EV charging transactions and battery degradation costs. Additionally, they have WRITE access for recording power transactions, degradation costs, and monetary distributions. EVAs interface directly with DSO on specific V2G applications.

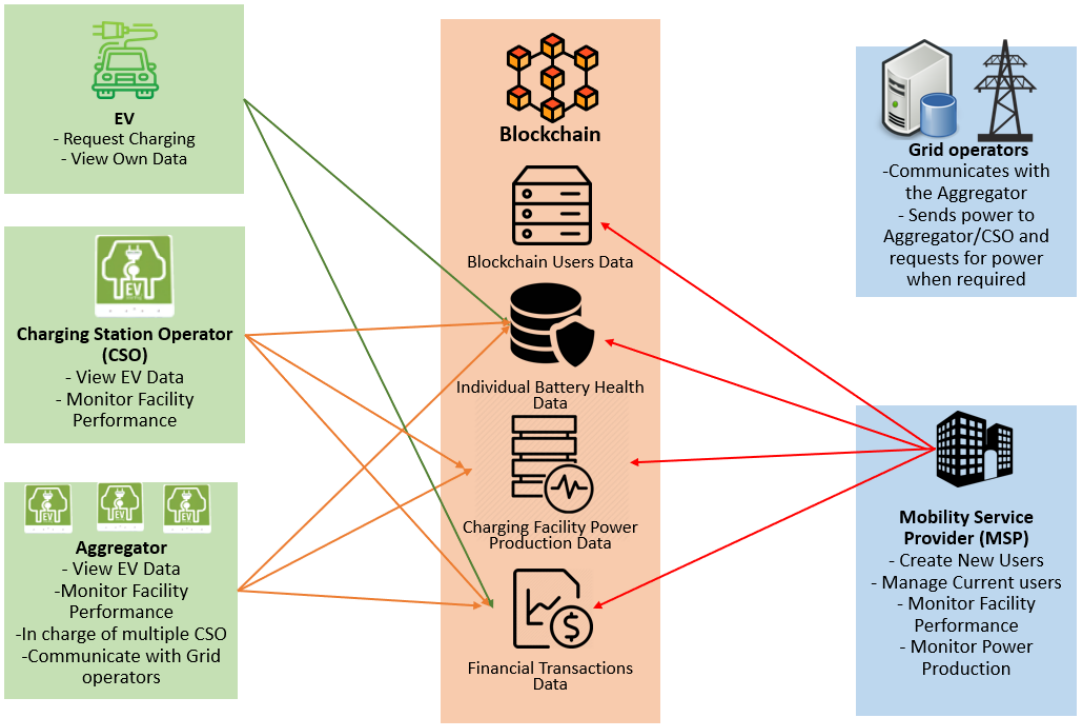


Figure 4.2: A network fabric diagram showing the different data access authorizations for all actors in a blockchain consortium network.

Our implementation utilizes Hyperledger Fabric, an open-source blockchain platform selected for its optimal balance of transparency, security, and performance. Network transaction logic is implemented in Javascript, defining transaction types and actor roles, with initial testing conducted through Hyperledger Composer. Unlike public blockchains such as Bitcoin and Ethereum, which process only 5 and 15 transactions per second (TPS) respectively, Hyperledger Fabric achieves up to 10,000 TPS—essential for managing frequent EV charging transactions and associated data.

Fabric operates as a permissioned network where validated nodes of equal authority verify transactions through smart contracts. The platform's RAFT consensus mechanism follows a three-step process: first executing and endorsing transactions after verifying correctness, then ordering transactions through a pluggable consensus protocol, and finally validating transactions against application-specific endorsement policies before ledger commitment. All

participants, including EVs and CSOs, must obtain verified unique identifiers before joining the network, enhancing security while maintaining operational efficiency.

This architecture, combined with the elimination of transaction fees and comprehensive testing of user privileges and data integrity, makes Hyperledger Fabric particularly suitable for EV battery tracking applications where frequent, small transactions need to be processed efficiently and cost-effectively. The system's permissioned structure provides robust protection against cyber-attacks while maintaining controlled network access.

4.2 Variable Battery Degradation Model

Battery degradation is an important parameter since it indicates how quickly the battery ages and loses its range. Multiple research articles have ignored battery degradation while studying the feasibility of V2G [93, 94]. H. Farzin et al. presented a methodology for calculating battery degradation due to V2G in terms of depreciation cost for charging/discharging optimization [95]. While this method is used in recent research [17], it has several drawbacks: it requires an iterative procedure to compute battery degradation cost, ignores calendar aging, and overlooks the effects of charge/discharge rates. The degradation cost is not constant and depends on the number of charging/discharging cycles and depth of discharge, with each future cycle and varying depth of discharge affecting the degradation cost [95]. Additionally, as more vehicles participate in V2G, optimization programs require longer convergence times. Calendar aging significantly influences V2G decisions, and without tracking battery age, degradation cost values cannot accurately reflect battery state. Fast charging rates further accelerate battery degradation [17].

EVs primarily utilize Li-ion batteries, which are complex systems where capacity fade may occur due to multiple factors including cycling, temperature, and operating conditions. The Battery Management System (BMS) tracks state variables like voltages, currents, and temperature to estimate State of Charge (SOC) and State of Health (SOH). Three main

types of models estimate SOH: data-driven models, physics-based models, and equivalent circuit models [96]. The BMS employs simple equivalent circuit models for computational efficiency, as physics-based models, while accurate, are computationally intensive, and data-driven models require historical operation data.

In this chapter, we use the model developed in [97], which has been validated for comparing battery degradation in normal operation versus V2G [98]. The current SOH can be estimated based on the EV's range and age, provided as one-time user inputs that initialize the blockchain process tracking battery degradation cost. The calendar loss Q_{cal} is calculated using equation (4.1) [97]:

$$Q_{cal} = \mu e^{\frac{-E_a}{RT}} \ t^{0.5} \tag{4.1}$$

where μ is 14876 day$^{-1/2}$, E_a is 24.5 kJ/mol, R is 8.314 J/mol K, T is absolute temperature in Kelvin, and t is time in days. The cycle loss incorporates temperature, charge/discharge rate, and current throughput effects.

The cycle loss is a function of temperature (T) and charge/discharge rate and current throughput [97]. It is estimated based on equations (4.2), (4.3), and (4.4). Equation (4.2) estimates the cycle loss while equations (4.3) and (4.4) find the pre-exponential factor B_1 and the exponential factor B_2 respectively, both of which are functions of temperature. The values of a,b,c,d and e are obtained from the model developed in [97]. The C_{rate} is the charge/discharge factor expressed as C-rate and the A_h is the cumulative current throughput in Ah.

$$Q_{cycle} = B_1 e^{B_2 C_{rate}} A_h \tag{4.2}$$

$$B_1 = aT^2 + bT + c \tag{4.3}$$

$$B_2 = dT + e \tag{4.4}$$

4.3 Optimization framework

A MILP (Mixed Integer Linear Program) is used to schedule the charging/discharging behavior of EVs with an objective to minimize the cost of charging and degradation of 20 EVs in an EV CSO facility. Python and Gurobipy are chosen as main programming/simulation environments. A degradation cost that captures EV battery cycle degradation as a $/kWh value is introduced in the objective. The optimization is run for a 3 year period with discrete time intervals of 1 hour. Equations (4.1) and (4.2) are discretized to follow the same hourly intervals, and rewritten as equations (4.5) and (4.6). Equations (4.5) and (4.6) represent the calendar aging and cycle aging for time $\hat{t}$. The cumulative cycle and calendar losses are the sum of all the losses at the various time intervals values as shown in equation (4.7).

$$\Delta Q_{cal}\left(\hat{t}\right) = 0.5\mu e^{\frac{-E_a}{RT}}\hat{t}^{-0.5}\Delta t \tag{4.5}$$

$$\Delta Q_{cycle}\left(\hat{t}\right) = B_1 e^{B_2 C_{rate}} I_{rate}\Delta t \tag{4.6}$$

$$Q_{net}\left(t\right) = \Sigma_{\hat{t}=0}^{t}\left(\Delta Q_{cal}\left(\hat{t}\right) + \Delta Q_{cycle}\left(\hat{t}\right)\right) \tag{4.7}$$

Thermal models can be used to supplement battery degradation models. However, this model assumes the battery temperature to be ambient temperature. The temperature data for each day in the model is assumed to be the average temperature in Los Angeles for that day for the years 2017-2019.

The optimization objective and constraints are listed in equations (4.8) to (4.18). The optimal value for the 24-hour period is used to calculate the total cycle loss for that day based on equation (4.6) and then the degradation cost based on equation (4.19). Assume a 24-hour cycle is divided into T time intervals and the number of EVs willing to provide V2G services is N_{ev}. For day i, EV j, and time interval k, the MILP objective is equation (4.8). The objective minimizes the charging cost and degradation cost. For the day i, $P_{ch,k,j}$ and $P_{dch,k,j}$ represent the charging power and discharging power in kW for EV j at

time interval k. $C_{ch,k,j}$ and $C_{dch,k,j}$ are the cost of charging and profits from discharging respectively in \$/kWh for EV j at time interval k on the day i. The charging rates are based on LADWP R1B 2019 rate structure. Without loss of generality, we assume that the EV will be participating in energy arbitrage, but the revenue from discharging can be set to the value representing other applications at the various time intervals. η_{ch} and η_{dch} are the charging and discharging efficiencies which are set at 90%. $w_{i,j}$ is the degradation cost with units of \$/kWh.

$$\min \sum_{j=1}^{Nev} \sum_{k=1}^{T} [(P_{ch,k,j} C_{ch,k,j} - P_{dch,k,j} C_{dch,k,j}) + (P_{ch,k,j} \eta_{ch} + P_{dch,k,j} / \eta_{dch}) w_{i,j}] \tag{4.8}$$

The constraints are represented in equations (4.9) to (4.18). Equation (4.9) states that the energy in EV j at time k is the sum of the energy in EV j at time $k-1$ and the power transferred to or from the EV for the duration ΔT. Equation (4.10) sets limitations on the maximum and minimum energy stored in the battery of EV j. The energy in the EV j at any time interval k is assumed to lie between 10% and 90% of the EV battery's nominal capacity. Equation (4.11) and (4.12) set limitations on the charging and discharging power of the EV when it is plugged into an EV charger with charging and discharging power limitations of $P_{ch,max}$ and $P_{dch,max}$ respectively. $\delta_{ch,k,j}$ and $\delta_{dch,k,j}$ are binary decision variables as shown in equations (4.13) and (4.14). The sum of $\delta_{ch,k,j}$ and $\delta_{dch,k,j}$ is always less than or equal to 1 as shown in equation (4.15). This indicates that the EV can have one of three statuses for a time interval k when plugged in – charging, discharging, or idle. Equation (4.16) defines the energy in the EV j on arrival on the day i and equations (4.17) states that the energy in the EV j at departure on the day i should be at minimum the desired charge expected by the EV user. Equation (4.18) sets limits on the total power into and out of the EV CSO infrastructure. Constraints (4.9)-(4.18) hold when the EV is plugged into the charger. When the EV is unplugged, $\delta_{ch,k,j}$ and $\delta_{dch,k,j}$ are set to zero.

$$E_{k,j} = E_{k-1,j} + (P_{ch,k,j}\eta_{ch} - P_{dch,k,j}/\eta_{dch})\,\Delta T \tag{4.9}$$

$$E_{min,j} \leq E_{k,j} \leq E_{max,j} \tag{4.10}$$

$$0 \leq P_{ch,k,j} \leq \delta_{ch,k,j} P_{ch,max} \tag{4.11}$$

$$0 \leq P_{dch,k,j} \leq \delta_{dch,k,j} P_{dch,max} \tag{4.12}$$

$$\delta_{ch,k,j} \in 0, 1 \tag{4.13}$$

$$\delta_{dch,k,j} \in 0, 1 \tag{4.14}$$

$$\delta_{ch,k,j} + \delta_{dch,k,j} \leq 1 \tag{4.15}$$

$$E_{arr,j} = E_{ini,j} \tag{4.16}$$

$$E_{dep,j} \geq E_{des,j} \tag{4.17}$$

$$-P_{inf} \leq \sum_{j=1}^{Nev} P_{ch} - \sum_{j=1}^{Nev} P_{dch} \leq P_{inf} \tag{4.18}$$

At the end of the day, based on data including charging/discharging schedules and the capacity losses, a new estimate will be made for battery degradation costw for the following day. Equation (4.19) estimates the degradation cost $w_{i,j}$ for day i and EV j with units of \$/kWh, based on the cumulative calendar and cycle losses. ΔBP is the difference in the original battery price and the salvage price (assumed to be 20% of the original battery price) in \$. The battery's end of life is assumed to occur when the battery loses 30% of its initial capacity. $E_{cap,j}$ is the EV's original battery capacity in kWh and $Q_{tot,i-1,j}$ is the cumulative capacity losses for EV j from day 0 to day $i-1$. Each day's EV energy transactions, monetary transactions, and End of Day (EoD) battery degradation cost will be added to and maintained in the consortium blockchain.

$$w_{i,j} = \frac{\Delta BP}{30(100 - Q_{tot,i-1,j})E_{cap,j}} \tag{4.19}$$

The optimization is run for twenty new Nissan Leaf EVs for a three-year period to generate daily charging costs, estimate battery degradation costs, transfer the information to the blockchain and read the degradation cost information for the next day's optimization program. The nominal battery capacity of all the EVs is 40 kWh. The EV is charged at the workplace between 7 am and 7 pm. The EV arrives with 40% SOC and requires a minimum of 60% SOC at departure. The optimization is run for two different degradation costs – (i) constant degradation cost at 0.04 $/kWh and (ii) dynamic degradation cost as obtained from equation (4.19) for a maximum charging/discharging rate of 6.6 kW. The V2G application considered here is energy arbitrage.

4.4 Results

The results for constant and dynamic degradation costs over the three-year period are summarized in Table 1. The revenue from participating in energy arbitrage is $2447.6 for the case with dynamic degradation cost which is 31.7% higher than the $1880.9 in the constant degradation cost case. The total energy supplied by V2G is 381.6 MWh for the case with dynamic degradation cost which is only 2.5% higher than the 372.3 MWh in the constant degradation cost case. The V2G energy per EV is in the range of 7.23 to 27.37 MWh in case of the constant degradation cost while the range is between 19.07 and 19.09 MWh for the dynamic degradation cost. Effectively all the EVs in the dynamic degradation cost are contributing equally because they all started with the same initial battery energy capacity. Figure 4.3 and Table 1 highlight the difference in the battery energy capacity of the EVs at the end of the three-year period. The dynamic degradation cost prioritizes EVs with lower battery degradation for V2G in each 24-hour cycle resulting in all the EVs having similar remaining battery capacity around 70% while the EVs using the constant degradation cost

have remaining battery capacity in the range 67.8 to 75.6%.

Table 4.1: Results from the degradation costs at the end of three-year period.

Degradation cost	**Constant**	**Dynamic**
Revenue ($)	1880.9	2477.6
Total V2G energy (MWh)	372.3	381.6
V2G energy per EV (MWh)	7.23 to 27.37	19.07 to 19.09
EV battery capacity (%)	67.8 to 75.6	71.02 to 71.03

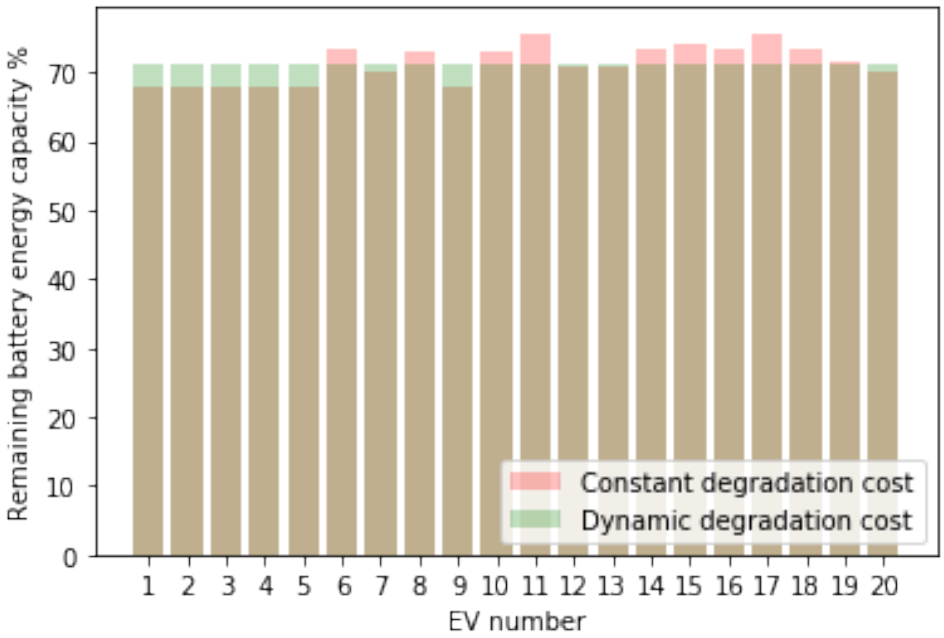


Figure 4.3: Bar chart highlighting the remaining battery energy capacity in the EVs utilized for V2G using the constant and dynamic degradation costs.

While the EVs can participate in various V2G applications to support the grid, financial incentives must outweigh the losses due to degradation that support the grid event. The simulations are run for just one V2G application – energy arbitrage and just twenty EVs that charge at a single CSO facility. This can be extended to multiple EVs and optimizing for multiple V2G applications governed by Aggregators that work with various CSO facilities. Also, the battery model used is an empirical model, different battery models with thermal models can be tried and tested with blockchains to realize the full extent of possibility.

4.5 Discussion

The results comparing constant and dynamic degradation costs over the three-year period reveal several key differences, as summarized in Table 4.1. The dynamic degradation cost approach generates 31.7% increase from energy arbitrage while delivering 2.5% more energy through V2G. More significantly, the V2G energy contribution per EV shows marked differences: the dynamic cost approach results in nearly uniform contributions (19.07-19.09 MWh per EV) compared to the wide range (7.23-27.37 MWh per EV) under constant cost.

As illustrated in Figure 4.3, the dynamic degradation cost methodology leads to more uniform battery degradation across the EV fleet. By prioritizing EVs with lower battery degradation for V2G services in each 24-hour cycle, this approach maintains remaining battery capacity around 71% for all EVs, compared to the 67.8-75.6% range observed with constant degradation cost.

The blockchain implementation successfully tracked and validated all battery degradation transactions throughout the three-year period, maintaining an immutable record of each EV's charging patterns, degradation rates, and V2G participation. For the twenty EVs in the study, the system processed approximately 175,200 hourly transactions (24 hours $\times$ 365 days $\times$ 3 years $\times$ 20 EVs), demonstrating robust scalability. The consortium blockchain's structure proved particularly effective in managing the hierarchical relationships between EVs, CSOs, and Aggregators, while ensuring transparent and verifiable degradation cost calculations.

The dynamic degradation cost model's implementation within the blockchain framework enabled real-time updates of battery health status and automated cost adjustments, facilitating more efficient V2G participation decisions. This automated tracking and validation system not only enhanced transparency but also reduced computational overhead in degradation cost calculations, as each EV's historical performance data was readily accessible and verifiable by all authorized participants. The system's ability to maintain consistent per-

formance while handling both constant and dynamic degradation cost models suggests its viability for larger-scale implementations involving more EVs and multiple V2G applications.

These findings, while promising, represent only initial results from a limited scenario: twenty EVs participating in energy arbitrage at a single CSO facility. Future research could extend to multiple V2G applications across different Aggregators and CSO facilities, larger EV fleets with diverse usage patterns, integration of thermal models with the current empirical battery model, and enhanced blockchain implementations for broader application scenarios.

In contrast to light-duty EVs, electric buses operate on fixed routes and schedules, making their charging demands more predictable. However, their high-power charging requirements can significantly strain local grid infrastructure. Grid-scale battery energy storage systems (BESS) emerge as a promising solution to support electric bus charging infrastructure, offering consistent high-power support while reducing demand charges and facilitating renewable energy integration. The following chapter examines optimal BESS sizing strategies to enable bus fleet electrification while minimizing grid impacts and operating costs.

CHAPTER 5

BESS support for electric buse charging

California Public Utilities Code (CPUC) Section 9621 requires publicly-owned utilities to adopt Integrated Resource Plans (IRP) that include greenhouse gas reduction objectives and renewable energy requirements. In response, LADWP has expanded its electric transportation program to support Los Angeles Metro bus fleet electrification through depot (overnight) and en-route charging facilities, aligning with its goal of 100 percent renewable energy by 2030 [18]. However, high capital costs remain a significant barrier to electric bus (E-Bus) market penetration, prompting numerous cost-benefit analyses.

Zhou et al. examined emissions and lifetime costs of commercial E-Bus models in China, considering factors such as traffic conditions, passenger load, air conditioning, and charging efficiency [19]. Despite high capital costs, E-Buses' low fuel costs proved competitive with diesel buses. However, fast-charging technologies, while enabling continuous operation, can increase electricity costs [20]. Electricity costs typically comprise two main components: energy charges and demand charges. Energy charges are calculated by multiplying total electricity consumption (kWh) by the current rate ($/kWh). Demand charges, billed monthly, are based on peak power demand, typically measured over 15 to 60-minute intervals [99]. These charges can reach $90/kW for commercial and industrial sectors in the United States [21].

Recent research has explored the use of a BESS as a solution for managing E-Bus charging costs. Ding et al. demonstrated that BESS can reduce DC fast charger investment and operating costs [100]. Pan et al. proposed day-ahead charging strategies with BESS to opti-

mize charging station economics [101], while Trocker et al. showed cost reduction potential depends significantly on peak demand pricing mechanisms [102]. Additional studies have examined optimal BESS power allocation [103], charging schedule optimization [104] and charging station placement [105]. This chapter investigates BESS applications for demand charge reduction in E-Bus charging.

This chapter is organized as follows:

- Section 5.1: introduces en-route charging and depot charging
- Section 5.2: describes the optimization model used to find the optimal BESS specifications to support E-bus charging
- Section 5.3: describes a case study of bus electrification along the LA Metro Orange line that includes both depot and en-route charging
- Section 5.4: identifies the optimal BESS configurations to support E-bus integration at 4 sites. It also highlights the benefits like annual savings and peak reduction
- Section 5.5: synthesizes key findings

This chapter investigates the application of a BESS for a demand charge reduction (a.k.a. peak shaving) for E-Bus charging demand. The end user's goals are first to reduce peak load and second, reduce their monthly utility bills. To determine the optimal BESS, one must consider the following factors: operating range, charging load demands, schedules, flexibility, charging time, cost, grid capacity, fleet size, and charging interfaces to minimize operational costs, purchase and installation costs, and demand charges, and facility charges on the electric bus charging infrastructure.

Therefore, in this study, an optimization program is developed as a MILP [105], variations of which have been previously used for optimal renewable energy scheduling [106], optimal electric vehicle (EV) charging [13] and optimal battery storage for Photovoltaic (PV) systems [107], to identify energy and power ratings of the BESS to support realistic en-route and

depot charging scenarios of E-Bus charging load within LADWP territory, and in particular for Metro G-line (Orange) as the primary E-Bus line.

5.1 E-bus charging infrastructure

Electric bus charging infrastructure consists of two main approaches: en-route (opportunity) charging and depot charging. En-route charging occurs during brief passenger stops, requiring high-power DC chargers operating between 150kW and 600kW to deliver sufficient charge in short time intervals. These systems can utilize conventional chargers at terminals or along routes, magnetic induction, catenary, or overhead charging systems at bus stops. Due to frequent charging cycles, opportunity chargers typically maintain battery levels between 80-85% State of Charge (SOC) throughout operational hours, with a full charge to 100% occurring once daily, usually overnight.

Depot charging, in contrast, operates at lower power levels (50-100kW) during extended overnight periods of 8-10 hours. This approach particularly suits single-shift transit operations, such as school buses that typically cover 60-70 miles per day with extended idle periods. While depot-charging infrastructure costs less than fast-charging systems, the lengthy charging times can impact operational flexibility. For multi-shift operations, buses may require additional battery capacity to maintain service schedules. Each charging approach presents distinct trade-offs. En-route charging enables continuous operation with smaller battery sizes, as vehicles need only enough capacity to reach the next charging point. However, this requires more extensive charging infrastructure along routes. Depot charging offers simpler infrastructure requirements but may necessitate larger battery capacities and careful schedule management to ensure sufficient charging time.

5.2 BESS sizing optimization

The optimal BESS specifications are determined by identifying battery power and energy capacities that minimize annual costs for supporting specific E-Bus charging patterns. We developed a Mixed Integer Linear Program in Python using the gurobipy module. The program utilizes LADWP A-2 prices for summer, adjusted to 2025 values [108], with a 24-hour optimization period.

The following assumptions were considered for the simulation:

1. The energy rating of a battery is at the most 4 times the power rating of the battery [109]).
2. The upper limit of energy rating and power rating are set as 6000 kWh and 1500 kW, respectively.
3. Discrete-time intervals of 5 minutes are used.
4. The battery cost based on energy is $285/kWh and the cost based on power is $306/kW [109].
5. The total charged energy per day is less than the battery capacity. The same holds for total discharged energy per day.
6. The charging and discharging efficiency of the battery storage are assumed to be 90%.

5.2.1 Optimization objective and constraints

A 24-hour cycle is broken into T 5-minute time intervals. The BESS must make optimal decisions for each of the time intervals i. To achieve this, the objective function is:

$$minimize \quad (C^{energy} + C^{inv} + C^{demand}) \tag{5.1}$$

where:

$$C^{energy} = \sum_{i=1}^{T} (P_i^{eb} + P_i^{ch} - P_i^{dch}) c_i \Delta_t \tag{5.2}$$

$$C^{inv} = \frac{r(r+1)^L}{(r+1)^L - 1}(E^{b,rat} \cdot c^E + P^{b,rat} \cdot c^P) \tag{5.3}$$

$$C^{demand} = P^{inf,max}(c^{dem} + c^{fac}) \tag{5.4}$$

subject to:

$$\delta_i^{ch} \in \{0,1\} \quad \forall_i \tag{5.5}$$

$$\delta_i^{dch} \in \{0,1\} \quad \forall_i \tag{5.6}$$

$$\delta_i^{dch} + \delta_i^{ch} \leq 1 \quad \forall_i \tag{5.7}$$

$$P_i^{ch} \geq 0 \quad \forall_i \tag{5.8}$$

$$P_i^{dch} \geq 0 \quad \forall_i \tag{5.9}$$

$$P_i^{ch} \leq P^{b,max} \cdot \delta_i^{ch} \quad \forall_i \tag{5.10}$$

$$P_i^{dch} \leq P^{b,max} \cdot \delta_i^{dch} \quad \forall_i \tag{5.11}$$

$$P_i^{ch} \leq P^{b,rat} \quad \forall_i \tag{5.12}$$

$$P_i^{dch} \leq P^{b,rat} \quad \forall_i \tag{5.13}$$

$$P_i^{ch} \geq P^{b,rat} - (1 - \delta_i^{ch}) \cdot P^{b,max} \quad \forall_i \tag{5.14}$$

$$P_i^{dch} \geq P^{b,rat} - (1 - \delta_i^{dch}) \cdot P^{b,max} \quad \forall_i \tag{5.15}$$

$$E^{b,rat} \geq 0 \tag{5.16}$$

$$E_1 = 0.2E^{b,rat} \tag{5.17}$$

$$E_i \leq E^{b,rat} \quad \forall_i \tag{5.18}$$

$$E_i \geq 0.2E^{b,rat} \quad \forall_i \tag{5.19}$$

$$E_T \geq 0.2E^{b,rat} \tag{5.20}$$

$$E_{i+1} = E_i + (P_i^{ch}\eta_{ch} - P_i^{dch}/\eta_{dch})\Delta_t \quad \forall_i \setminus \{T\} \tag{5.21}$$

$$P_i^{eb} + P_i^{ch} - P_i^{dch} \leq P^{inf,max} \quad \forall_i \tag{5.22}$$

$$P_i^{eb} - P_i^{dch} \geq 0 \quad \forall_i \tag{5.23}$$

$$\sum_{i=1}^{T} P_i^{ch}\Delta_t \leq E^{b,rat} \tag{5.24}$$

$$\sum_{i=1}^{T} P_i^{dch}\Delta_t \leq E^{b,rat} \tag{5.25}$$

The various variables, constants, and indices are described in the following:

i indicates the time interval index, Δ_t represents time interval duration in hours, and T indicates the last time interval index. δ_i^{ch} and δ_i^{dch} are binary variables indicating if the battery is charging or discharging at time interval i. E_i is the level of energy in the battery storage at time interval i in kWh. $E^{b,rat}$ and $P^{b,rat}$ are the energy and power ratings of the battery in kWh and kW respectively. P_i^{eb} represents E-bus demand requested at time interval i in kW. P_i^{ch} and P_i^{dch} indicate the charging power and the discharging power respectively of the battery at time interval i in kW. $P^{b,max}$ is the upper limit of the battery capacity in kW under consideration. $P^{inf,max}$ represents the maximum power flow into the infrastructure in kW. c_i is the electricity price at time interval i in \$/kWh. c^P and c^E represent the cost of battery investment, installation, and maintenance based on battery power and energy ratings respectively as obtained from [109]. c^{dem} represents the demand charges (based on monthly demand charge) in \$/kW and c^{fac} indicates the equivalent facility charge (based on annual facility charge) in \$/kW.

Equation (5.1) is the objective that minimizes the cost of investment as well as the energy and demand charges. C^{energy} corresponds to the operation cost to charge the E-buses, charge the battery, and discharge the battery as seen in equation (5.2). C^{inv} in equation (5.3) is

the amortized annual costs for purchase and installation of the BESS. Here, r is the interest rate, which is set to 7.6% [109], and L is the lifespan of the battery which is set to 10 years. C^{demand} in equation (5.4) corresponds to the annual equivalent of demand charge and facility charge on the electric bus charging infrastructure. The period considered for optimization is only 24 hours.

Equations (5.5) to (5.20) represent the constraints on the optimization problem. Equations (5.5) and (5.6) state that a binary variable will be responsible for the status of the battery as charging and discharging respectively. In equation (5.5), if the variable holds the value 1, then the battery is charging, and if the value is 0, then the battery is not charging. Equation (5.6) works the same way as equation (5.5), but the variable holds the status of discharging. Equation (5.7) ensures that the battery cannot charge and discharge at the same time for any time interval. Equations (5.8) and (5.9) ensure the non-negativity of charging and discharging power flow, respectively. Equations (5.10) to (5.15) linearize the following non-linear constraints that include a product of a binary variable and a continuous variable with a fixed upper limit : $P_i^{ch} \leq P^{b,rat} \cdot \delta_i^{ch}$ and $P_i^{dch} \leq P^{b,rat} \cdot \delta_i^{dch}$. These equations place upper limits on charging and discharging power respectively based on the maximum power flow of the rated optimal battery. Equation (5.16) ensures a positive optimal rated energy capacity for the BESS. Equation (5.17) represents the assumption that we start the simulation (at midnight) with the battery at 20% SOC at time period 1. Equations (5.18) and (5.19) ensure that the battery operates within defined energy capacity limits. Equation (5.20) states that the battery must be at least 20% SOC at time period T. Equation (5.21) is the conservation of energy in the battery based on power flow. Equation (5.22) states that the total power flow into the charging infrastructure is limited. Equation (5.23) ensures that the battery cannot discharge to make money from arbitrage; the battery can only discharge to support the electric bus charging load. Equations (5.24) and (5.25) limit the total energy charged and discharged by the battery to its rated energy capacity per day to ensure a minimum of 10-year operation.

5.3 Case study

Multiple electric buses and their charging site details to be deployed on the LA Metro G line (Orange) are shown in figure (5.1) [110]. 3 locations were identified along the route with 2-4 chargers at each location. Each en-route charger supplies 450 kW of charging power. 1 depot location was identified to house 10 150 kW chargers.

The LA Metro G Line (Orange), connecting North Hollywood's Red Line station to Chatsworth, serves as the primary E-Bus route for this study, as shown in Figure 5.1 [110]. Operating seven days a week with weekend service following weekday schedules, the line is scheduled for complete electrification by 2025, with an anticipated 30% increase in bus frequency [111]. The planned charging infrastructure includes:

Chatsworth station: Two 450 kW en-route chargers Canoga station: Two 450 kW en-route chargers North Hollywood station: Four 450 kW en-route chargers Chatsworth depot: Ten 150 kW depot chargers

The line utilizes New Flyer's Xcelsior CHARGE 60' buses, each equipped with 160 kWh battery capacity [112]. En-route charging occurs for 15 minutes at maximum charging rate upon arrival at stations, while depot charging operates at lower rates for extended periods. The analysis assumes predictable bus arrival and departure times and consistent charger availability at each location. To optimize energy costs, BESS implementation enables load shifting from peak to off-peak hours. The economic analysis uses LADWP A-2 TOU rate structure projected to 2025, based on 2016 rates with an assumed 2

Installation of a BESS will include several parts, including Cost of Capital for Energy Capacity (COC), Construction and Commissioning (C&C), power conversion systems (PCS), inverters, and miscellaneous costs (Misc.) such as the balance of plant. According to a report by Pacific Northwest National Laboratory (PNNL), estimates of the battery costs per kWh and kW for Li-ion battery types, as the primary choice of BESS technologies [109], are shown as follows for the year 2025 in Table 5.1. The Li-ion battery expected life span of 3650 cycles

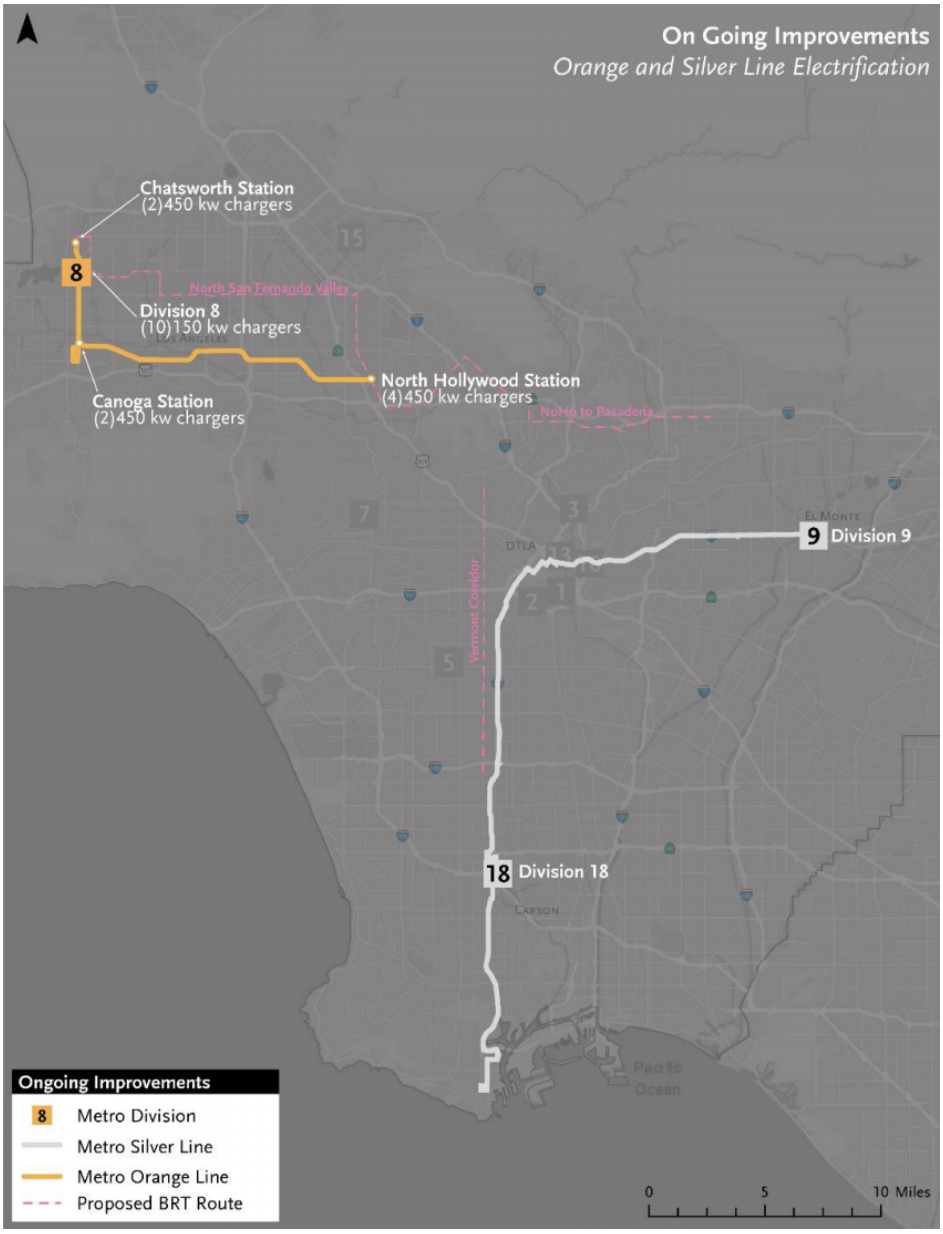


Figure 5.1: Metro G Line (Orange Line) connecting Chatsworth to North Hollywood in Los Angeles.

is also considered according to the assumption of one cycle per day and 10 years of operation [113].

Table 5.1: BESS cost and parameter ranges per kWh and kW for Li-Ion battery types, for the year 2025

	COC($/kWh)	**C&C($/kWh)**	**PCS($/kW)**	**Misc.($/kW)**
Cost Range	156-203	87-105	184-329	75-115
Cost Mean Estimate	189	96	211	95
Total Cost	**Total Cost ($/kWh) = 285**		**Total Cost ($/kW) = 306**	

The E-bus charging schedule aligns with route endpoints, where buses charge for 15 minutes after passengers disembark and before boarding the next group of travelers. Charging begins immediately upon arrival at designated stations, which are strategically located at route terminals. The charging load patterns were developed using the G Line (Orange) bus schedules, ensuring minimal impact on service frequency and passenger convenience.

5.4 Results

The E-bus charging schedule aligns with route endpoints, where buses charge for 15 minutes after passengers disembark and before boarding the next group of travelers. Charging begins immediately upon arrival at designated stations, which are strategically located at route terminals. The charging load patterns were developed using the G Line (Orange) bus schedules, ensuring minimal impact on service frequency and passenger convenience.

Depot charging - BESS #1

LADWP A-2 rate structure defines three pricing periods: base period (5 PM to 10 AM), low peak (10 AM to 1 PM), and high peak (1 PM to 5 PM). During the base period, buses can be charged from 20% to 100% State of Charge, resulting in a uniform grid load of approximately

165 kW. However, no BESS configuration provides annual savings for this particular charging pattern. Figure 5.2 demonstrates this by showing overlapping E-bus charging and grid load patterns across a 24-hour period.

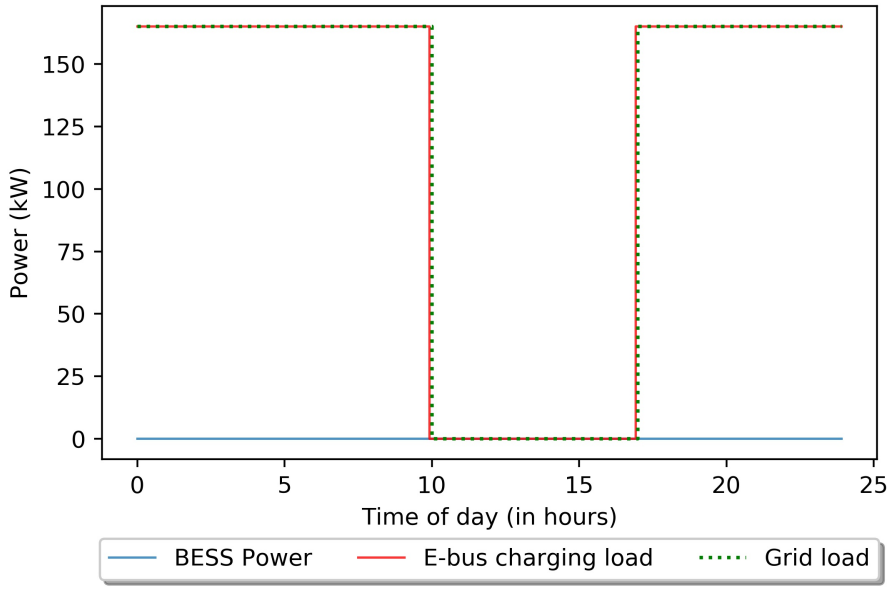


Figure 5.2: BESS power, E-bus charging load, and electric grid load at the Chatsworth Depot charging station during a 24-hour cycle. The BESS load curve is non-existent since no BESS specification results in savings over 10 years.

Chatsworth station - BESS #2

The round trip between the Chatsworth station and the North Hollywood station is 36 miles and requires about 112 kWh. Since the buses have an energy capacity of 160 kWh they would need to be charged at the end of each round trip at about 450 kW for 15 minutes. 450 kW and 1125 kWh are the optimal power and energy ratings of BESS #2. Figure 5.3 shows the BESS power profile, E-bus charging load pattern as well as the electric grid load for a 24-hour period. **Canoga station - BESS #3**

The round trip between the Canoga station and the North Hollywood station is about 28 miles and requires about 100 kWh. Since the buses have an energy capacity of 160 kWh,

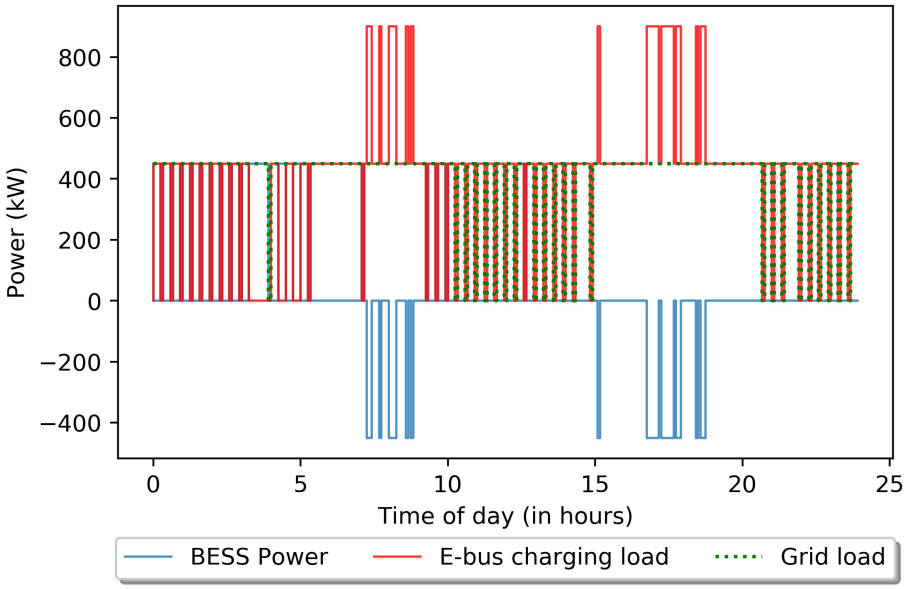


Figure 5.3: BESS power, E-bus charging load, and electric grid load at the Chatsworth en-route charging station during a 24-hour cycle. The BESS responsible for the BESS load profile results in savings over 10 years.

they would need to be charged at the end of each round trip at about 400 kW for 15 minutes. 400 kW and 166.67 kWh are the optimal power and energy ratings of BESS #3. Figure 5.4 shows the E-bus charging load, BESS power profile as well as electric grid load for a 24-hour period.

North Hollywood station - BESS #4

The North Hollywood station will charge E-buses that arrive from both Canoga station and Chatsworth station, resulting in a larger load profile compared to both stations. Since the buses have an energy capacity of 160 kWh, they would need to be charged at the end of each round trip at about 400 kW for 15 minutes if they arrive from Canoga station, and at 450 kW for 15 minutes if they arrive from Chatsworth station. 400 kW and 466.67 kWh are the optimal power and energy ratings of BESS #4. Figure 5.5 shows the E-bus charging load, BESS power profile as well as electric grid load for a 24-hour period.

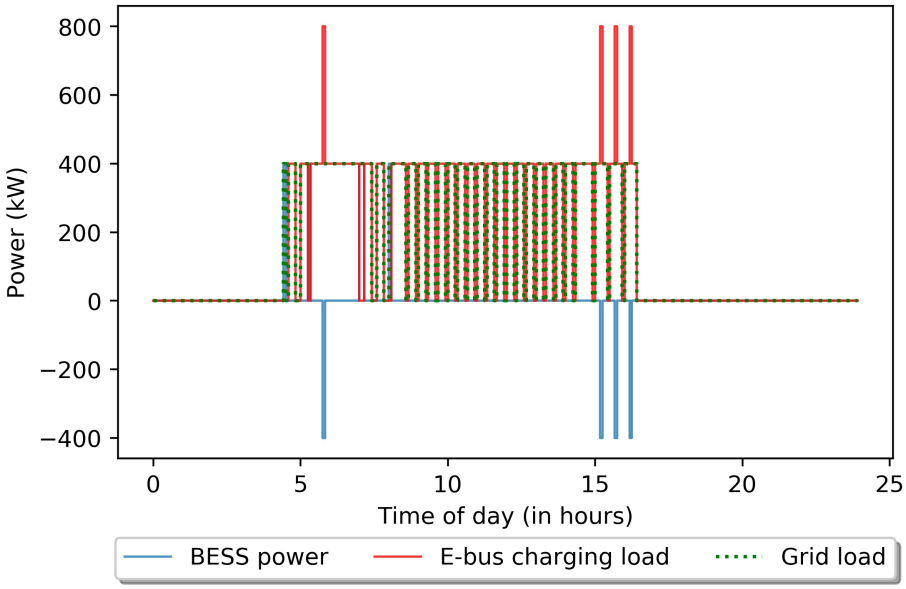


Figure 5.4: BESS power, E-bus charging load, and electric grid load at the Canoga en-route charging station during a 24-hour cycle. The BESS responsible for the BESS load profile results in savings over 10 years.

Table 5.2: Optimal BESS specifications and cost savings over a 10-year period

BESS#	**Energy (kWh)**	**Power (kW)**	**% Annual Savings**
1	0	0	0
2	166.67	400	20.68
3	1125	450	1.91
4	466.67	400	6.64

The results of all optimal BESS energy and power ratings, as well as the percentage annual savings, are summarized in Table 5.2. While the optimization program only considered the peak prices from the rate structure, the annual savings took into account both the peak and the non-peak periods for the optimal BESS and the no BESS case. Of the 4 sites in consideration, the optimal BESS sizing can results in 32-55% peak reduction and 2-20% in

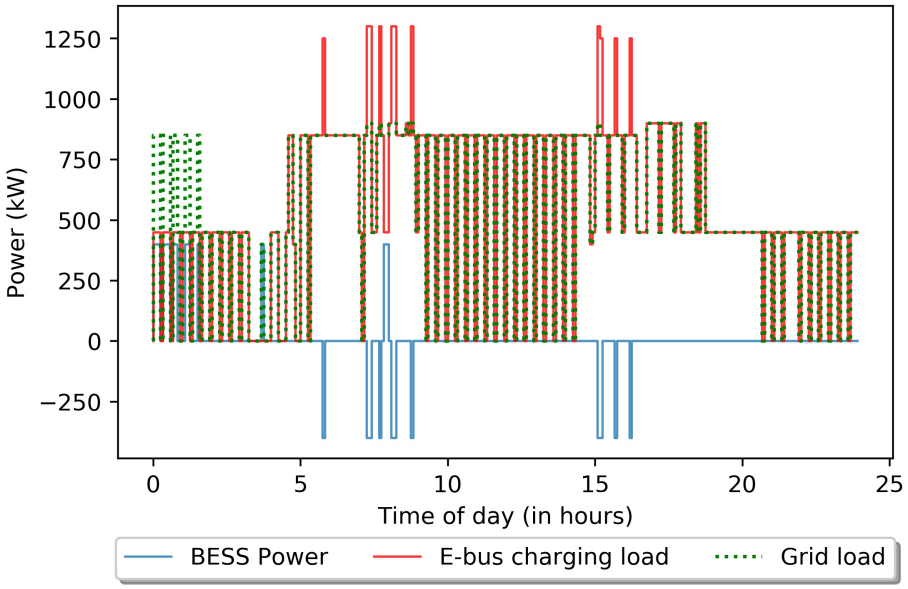


Figure 5.5: BESS power, E-bus charging load, and electric grid load at the North Hollywood en-route charging station during a 24-hour cycle. The BESS responsible for the BESS load profile results in savings over 10 years.

charging cost mitigation for day-time en-route charging. No such benefits were obtained in the case of overnight depot charging since no configuration of BESS could result in cost reduction.

5.5 Discussion

Despite the growth in adoption of E-buses and the continuous decline in the prices associated with the Li-ion batteries, the high cost of E-Bus charging infrastructure, the peak power demand of the E-Bus chargers, and their actual impact on future grids are challenges for the E-Bus mass deployment. The potential impact of BESS deployment, in conjunction with the installed depot and en-route chargers, on the annual costs was determined, and the optimal BESS power and energy ratings were identified. However, the potential for integrating other renewable energy resources, particularly photovoltaic panels, along with BESS, to support

realistic en-route and depot charging scenarios for E-Bus charging and load curtailment within LADWP territory needs to be realized.

Additionally, when trying to find out optimal BESS specifications to mitigate the peak demands and cut the electricity bills associated with E-Buses, it is essential to specify a reasonable power-to-energy ratio window for BESS operation; as the high ratio of power-to-energy leads to BESS degradation impacting the life span, consequently changing the optimal BESS size and the associated realistic daily operational costs to support E-Bus charging.

CHAPTER 6

Conclusion

This dissertation explores various strategies and methodologies for optimizing the integration of EVs and BESS into electric grids, focusing on applications such as load forecasting, congestion relief, battery degradation management, and electric bus charging infrastructure. The rapid adoption of EVs and the increasing penetration of renewable energy sources have introduced complexities in grid management. These challenges highlight the need for advanced optimization and forecasting models that can handle the inherent uncertainties in demand, supply, and infrastructure costs.

6.1 Summary

Chapter 2 investigates the application of Model-Agnostic Meta-Learning (MAML) and Transfer Learning (TL) techniques for short-term EV load forecasting. These models are pretrained on a larger dataset and fine-tuned on smaller target datasets to enhance performance across diverse geographical regions and charging environments. The findings indicate that both MAML and TL models consistently outperform traditional deep learning and classic machine learning models, with MAML excelling in settings where the target dataset closely resembles the source dataset. Conversely, TL is less sensitive to differences between the source and target datasets, making it particularly effective in heterogeneous settings.

Chapter 3 examines how EVs with V2G capabilities can be leveraged to alleviate congestion and optimize LMPs. By identifying key nodes in CAISO territory that are prone to congestion, optimization models are developed to either maximize revenue through energy

arbitrage or minimize congestion-related costs. The results show that optimizing for total LMP yields higher revenue, while optimizing for the congestion component of LMP significantly reduces congestion but at a higher charging cost for the EVs. Seasonal variations also play a crucial role, with spring and summer months offering better opportunities for both revenue generation and congestion mitigation. The study underscores the need for incentivizing nodal-level action to achieve optimal outcomes in congestion management.

Chapter 4 proposed the use of blockchain technology to track and assess dynamic battery degradation costs for V2G applications. Traditional methods treat degradation as a constant cost, but this approach fails to capture the variability introduced by factors such as cycle aging and calendar aging. By incorporating dynamic degradation costs into an optimization program that maximizes arbitrage revenue, the study demonstrates improved decision-making for smart charging and discharging strategies. The blockchain ledger logs data related to power flow, monetary transactions, and battery health, providing stakeholders with secure and transparent information. Simulated results show that using dynamic degradation costs leads to better battery utilization and less variability in battery capacity loss across multiple EVs compared to constant degradation cost scenarios. Additionally, this approach offers potential applications in second-life battery tracking and battery swap programs.

Chapter 5 analyzes the integration of BESS with E-Bus charging stations to determine the optimal power and energy ratings needed to manage both depot and en-route charging while minimizing operational costs. The high capital costs associated with E-Bus infrastructure and peak demand charges are significant barriers to mass deployment. By optimizing the power-to-energy ratio of BESS, the study finds that peak demand charges can be reduced while maintaining system efficiency.

6.2 Future Work

Future research directions should focus on several key areas. First, in the domain of load forecasting, efforts should concentrate on developing more robust Transfer Learning (TL) and Model-Agnostic Meta-Learning (MAML) models. This could be achieved by utilizing larger, geographically diverse datasets that encompass various climate zones and charging behaviors, including both private and shared charging scenarios. Data from regions with established EV adoption, such as California, could provide valuable insights for pre-training. The development of hybrid models combining TL and MAML approaches could potentially leverage the strengths of both methodologies while addressing their limitations.

In terms of Vehicle-to-Grid (V2G) operations and congestion management, future work should investigate the impact of different battery degradation models on V2G effectiveness. Key areas include implementing variable degradation cost factors and developing congestion-driven pricing incentives at the distribution level. The integration of high-power charging and heavy-duty electric vehicles into congestion relief strategies warrants exploration, particularly in areas experiencing significant transmission line congestion. Research should also consider optimizing the ratio of monetary benefits to V2G throughput, establishing mechanisms to ensure V2G actions are initiated only when benefits exceed predefined thresholds.

Regarding blockchain implementation for battery degradation tracking, scaling challenges need to be addressed as the system expands from twenty to thousands of vehicles. This may require developing hierarchical or distributed optimization approaches and modifying the blockchain architecture through side-chains or sharding techniques to handle increased transaction volumes efficiently.

Finally, research should focus on integrating renewable energy sources, particularly solar power, with Battery Energy Storage Systems (BESS) for electric bus charging infrastructure. This includes studying optimal power-to-energy ratios that balance peak demand reduction with battery degradation, incorporating lifecycle cost analyses, and developing smart charg-

ing strategies and dynamic load management systems to optimize the interaction between renewable sources, BESS, and charging infrastructure while maintaining grid stability.

REFERENCES

[1] J. Curtin, C. McInerney, B. Ó. Gallachóir, C. Hickey, P. Deane, and P. Deeney, "Quantifying stranding risk for fossil fuel assets and implications for renewable energy investment: A review of the literature," *Renewable and Sustainable Energy Reviews*, vol. 116, p. 109402, 2019.

[2] IRENA, "Data:installed capacity for different renewable technologies." `https://ourworldindata.org/grapher/installed-global-renewable-energy-capacity-by-technology?country=Wind+energy~Solar+energy#reuse-this-work`. Accessed: 2023-09-30.

[3] H. Ritchie and M. Roser, "Tracking global data on electric vehicles," *Our World in Data*, 2024.

[4] V. P. Singh, V. Vijay, S. Gaurishankar, D. Chaturvedi, and N. Rajkumar, "Analysis of solar power variability due to seasonal variation and its forecasting for jodhpur region using artificial neural network," *Power Research-A Journal of CPRI*, pp. 423–430, 2013.

[5] X. Huang, D. Wu, and B. Boulet, "Ensemble learning for charging load forecasting of electric vehicle charging stations," in *2020 IEEE Electric Power and Energy Conference (EPEC)*, pp. 1–5, IEEE, 2020.

[6] S. Balasubramanian and P. Balachandra, "Effectiveness of demand response in achieving supply-demand matching in a renewables dominated electricity system: A modelling approach," *Renewable and Sustainable Energy Reviews*, vol. 147, p. 111245, 2021.

[7] N. Sadeghianpourhamami, N. Refa, M. Strobbe, and C. Develder, "Quantitive analysis of electric vehicle flexibility: A data-driven approach," *International Journal of Electrical Power & Energy Systems*, vol. 95, pp. 451–462, 2018.

[8] E. Lee and W. Rhee, "Individualized short-term electric load forecasting with deep neural network based transfer learning and meta learning," *IEEE Access*, vol. 9, pp. 15413–15425, 2021.

[9] R. H. Byrne, T. A. Nguyen, D. A. Copp, B. R. Chalamala, and I. Gyuk, "Energy management and optimization methods for grid energy storage systems," *IEEE Access*, vol. 6, pp. 13231–13260, 2017.

[10] M. Sufyan, N. A. Rahim, M. M. Aman, C. K. Tan, and S. R. S. Raihan, "Sizing and applications of battery energy storage technologies in smart grid system: A review," *Journal of Renewable and Sustainable Energy*, vol. 11, no. 1, p. 014105, 2019.

[11] M. D. Galus, M. G. Vayá, T. Krause, and G. Andersson, "The role of electric vehicles in smart grids," *Wiley Interdisciplinary Reviews: Energy and Environment*, vol. 2, no. 4, pp. 384–400, 2013.

[12] E. Sortomme and M. A. El-Sharkawi, "Optimal charging strategies for unidirectional vehicle-to-grid," *IEEE Transactions on Smart Grid*, vol. 2, no. 1, pp. 131–138, 2011.

[13] S. N. Gowda, B. A. Eraqi, H. Nazaripouya, and R. Gadh, "Assessment and tracking electric vehicle battery degradation cost using blockchain," in *2021 IEEE Power & Energy Society Innovative Smart Grid Technologies Conference (ISGT)*, pp. 1–5, IEEE, 2021.

[14] S. N. Gowda, T. Zhang, C. J. Kim, R. Gadh, and H. Nazaripouya, "Transmission, distribution deferral and congestion relief services by electric vehicles," in *2019 IEEE Power & Energy Society Innovative Smart Grid Technologies Conference (ISGT)*, pp. 1–5, IEEE, 2019.

[15] V. Preis and F. Biedenbach, "Assessing the incorporation of battery degradation in vehicle-to-grid optimization models," *Energy Informatics*, vol. 6, no. Suppl 1, p. 33, 2023.

[16] Y. Zheng, H. Yu, Z. Shao, and L. Jian, "Day-ahead bidding strategy for electric vehicle aggregator enabling multiple agent modes in uncertain electricity markets," *Applied Energy*, vol. 280, p. 115977, 2020.

[17] K. Chaudhari, A. Ukil, K. N. Kumar, U. Manandhar, and S. K. Kollimalla, "Hybrid optimization for economic deployment of ess in pv-integrated ev charging stations," *IEEE Transactions on Industrial Informatics*, vol. 14, no. 1, pp. 106–116, 2017.

[18] G. Newsom, "STAFF REPORT Review of Los Angeles Department of Water and Power's 2017 Power Integrated Resource Plan," tech. rep., California Energy Commission, 2019.

[19] B. Zhou, Y. Wu, B. Zhou, R. Wang, W. Ke, S. Zhang, and J. Hao, "Real-world performance of battery electric buses and their life-cycle benefits with respect to energy consumption and carbon dioxide emissions," *Energy*, vol. 96, pp. 603–613, 2016.

[20] R.-C. Leou and J.-J. Hung, "Optimal charging schedule planning and economic analysis for electric bus charging stations," *Energies*, vol. 10, no. 4, p. 483, 2017.

[21] N. R. E. Laboratory, "Maximum demand charge rates for commercial and industrial electricity tariffs in the United States — NREL Data Catalog."

[22] S. Narayana Gowda, K. Nath, C. Zhang, R. Gowda, and R. Gadh, "Short-term aggregate electric vehicle charging load forecasting in diverse conditions with minimal data using transfer and meta-learning," *Energy Systems*, pp. 1–20, 2024.

[23] K. Nath, S. N. Gowda, C. Zhang, R. S. Gowda, and R. Gadh, "Short-term electric vehicle charging load forecasting using transfer and meta-learning," in *2024 IEEE Power & Energy Society Innovative Smart Grid Technologies Conference (ISGT)*, pp. 1–5, IEEE, 2024.

[24] S. Narayana Gowda, H. Nazaripouya, and R. Gadh, "Congestion relief services by vehicle-to-grid enabled electric vehicles considering battery degradation," *Sustainability*, vol. 15, no. 24, p. 16733, 2023.

[25] S. N. Gowda, A. Ahmadian, V. Anantharaman, C.-C. Chu, and R. Gadh, "Power management via integration of battery energy storage systems with electric bus charging," in *2022 IEEE Power & Energy Society Innovative Smart Grid Technologies Conference (ISGT)*, pp. 1–5, IEEE, 2022.

[26] H. Hewamalage, C. Bergmeir, and K. Bandara, "Recurrent neural networks for time series forecasting: Current status and future directions," *International Journal of Forecasting*, vol. 37, no. 1, pp. 388–427, 2021.

[27] K. Weiss, T. M. Khoshgoftaar, and D. Wang, "A survey of transfer learning," *Journal of Big data*, vol. 3, no. 1, pp. 1–40, 2016.

[28] A. Forootani, M. Rastegar, and H. Zareipour, "Transfer learning-based framework enhanced by deep generative model for cold-start forecasting of residential ev charging behavior," *IEEE Transactions on Intelligent Vehicles*, 2023.

[29] P. Banda, M. A. Bhuiyan, K. N. Hasan, and K. Zhang, "Assessment of hybrid transfer learning method for forecasting ev profile and system voltage using limited ev charging data," *Sustainable Energy, Grids and Networks*, vol. 36, p. 101191, 2023.

[30] C. Finn, P. Abbeel, and S. Levine, "Model-agnostic meta-learning for fast adaptation of deep networks," in *International conference on machine learning*, pp. 1126–1135, PMLR, 2017.

[31] Y. He, F. Luo, and G. Ranzi, "Transferrable model-agnostic meta-learning for short-term household load forecasting with limited training data," *IEEE Transactions on Power Systems*, vol. 37, no. 4, pp. 3177–3180, 2022.

[32] X. Xiao, H. Mo, Y. Zhang, and G. Shan, "Meta-ann–a dynamic artificial neural network refined by meta-learning for short-term load forecasting," *energy*, vol. 246, p. 123418, 2022.

[33] Z. J. Lee, T. Li, and S. H. Low, "Acn-data: Analysis and applications of an open ev charging dataset," in *Proceedings of the tenth ACM international conference on future energy systems*, pp. 139–149, 2019.

[34] Å. L. Sørensen, K. B. Lindberg, I. Sartori, and I. Andresen, "Analysis of residential ev energy flexibility potential based on real-world charging reports and smart meter data," *Energy and Buildings*, vol. 241, p. 110923, 2021.

[35] C. of Boulder Open Data, "Electric vehicle charging station data." `https://open-data.bouldercolorado.gov/datasets/95992b3938be4622b07f0b05eba95d4c_0/explore`.

[36] Å. L. Sørensen, K. B. Lindberg, I. Sartori, and I. Andresen, "Residential electric vehicle charging datasets from apartment buildings," *Data in Brief*, vol. 36, p. 107105, 2021.

[37] Y. Dong, Y. Chen, X. Zhao, and X. Huang, "Short-term load forecasting with distributed long short-term memory," in *2023 IEEE Power & Energy Society Innovative Smart Grid Technologies Conference (ISGT)*, pp. 1–5, IEEE, 2023.

[38] S. P. Arango, F. Heinrich, K. Madhusudhanan, and L. Schmidt-Thieme, "Multimodal meta-learning for time series regression," in *Advanced Analytics and Learning on Temporal Data: 6th ECML PKDD Workshop, AALTD 2021, Bilbao, Spain, September 13, 2021, Revised Selected Papers 6*, pp. 123–138, Springer, 2021.

[39] M. Fernández-Delgado, M. S. Sirsat, E. Cernadas, S. Alawadi, S. Barro, and M. Febrero-Bande, "An extensive experimental survey of regression methods," *Neural Networks*, vol. 111, pp. 11–34, 2019.

[40] S. M. Arnold, P. Mahajan, D. Datta, I. Bunner, and K. S. Zarkias, "learn2learn: A library for meta-learning research," *arXiv preprint arXiv:2008.12284*, 2020.

[41] A. Priessner and N. Hampl, "Can product bundling increase the joint adoption of electric vehicles, solar panels and battery storage? explorative evidence from a choice-based conjoint study in austria," *Ecological Economics*, vol. 167, p. 106381, 2020.

[42] O. Y. Edelenbosch, A. F. Hof, B. Nykvist, B. Girod, and D. P. Van Vuuren, "Transport electrification: the effect of recent battery cost reduction on future emission scenarios," *Climatic change*, vol. 151, no. 2, pp. 95–108, 2018.

[43] G. Fitzgerald, J. Mandel, J. Morris, and H. Touati, "The economics of battery energy storage: How multi-use, customer-sited batteries deliver the most services and value to customers and the grid," *Rocky Mountain Institute*, vol. 6, 2015.

[44] M. Rezaeimozafar, R. F. Monaghan, E. Barrett, and M. Duffy, "A review of behind-the-meter energy storage systems in smart grids," *Renewable and Sustainable Energy Reviews*, vol. 164, p. 112573, 2022.

[45] T. Li, S. Tao, K. He, M. Lu, B. Xie, B. Yang, and Y. Sun, "V2g multi-objective dispatching optimization strategy based on user behavior model," *Frontiers in Energy Research*, p. 494, 2021.

[46] F. R. S. Sevilla, D. Parra, N. Wyrsch, M. K. Patel, F. Kienzle, and P. Korba, "Techno-economic analysis of battery storage and curtailment in a distribution grid with high pv penetration," *Journal of Energy Storage*, vol. 17, pp. 73–83, 2018.

[47] S. Englberger, A. Jossen, and H. Hesse, "Unlocking the potential of battery storage with the dynamic stacking of multiple applications," *Cell reports physical science*, vol. 1, no. 11, p. 100238, 2020.

[48] Y. P. Gusev and P. Subbotin, "Using battery energy storage systems for load balancing and reactive power compensation in distribution grids," in *2019 International Conference on Industrial Engineering, Applications and Manufacturing (ICIEAM)*, pp. 1–5, IEEE, 2019.

[49] H. Ma, F. Balthasar, N. Tait, X. Riera-Palou, and A. Harrison, "A new comparison between the life cycle greenhouse gas emissions of battery electric vehicles and internal combustion vehicles," *Energy policy*, vol. 44, pp. 160–173, 2012.

[50] O. Van Vliet, A. S. Brouwer, T. Kuramochi, M. van Den Broek, and A. Faaij, "Energy use, cost and co2 emissions of electric cars," *Journal of power sources*, vol. 196, no. 4, pp. 2298–2310, 2011.

[51] N. A. McGuckin and A. Fucci, *Summary of travel trends: 2017 national household travel survey*. US Department of Transportation, Federal Highway Administration, 2018.

[52] W. Kempton and S. E. Letendre, "Electric vehicles as a new power source for electric utilities," *Transportation Research Part D: Transport and Environment*, vol. 2, no. 3, pp. 157–175, 1997.

[53] J. A. P. Lopes, F. J. Soares, and P. M. R. Almeida, "Integration of electric vehicles in the electric power system," *Proceedings of the IEEE*, vol. 99, no. 1, pp. 168–183, 2011.

[54] P. Denholm, M. O'Connell, G. Brinkman, and J. Jorgenson, "Overgeneration from solar energy in california. a field guide to the duck chart," tech. rep., National Renewable Energy Lab.(NREL), Golden, CO (United States), 2015.

[55] R. Sioshansi and P. Denholm, "Emissions impacts and benefits of plug-in hybrid electric vehicles and vehicle-to-grid services," *Environmental science & technology*, vol. 43, no. 4, pp. 1199–1204, 2009.

[56] S. Rivera, S. Kouro, S. Vazquez, S. M. Goetz, R. Lizana, and E. Romero-Cadaval, "Electric vehicle charging infrastructure: From grid to battery," *IEEE Industrial Electronics Magazine*, vol. 15, no. 2, pp. 37–51, 2021.

[57] J. M. Eyer, G. P. Corey, and J. J. Iannucci Jr, "Energy storage benefits and market analysis handbook: a study for the doe energy storage systems program.," tech. rep., Sandia National Laboratories, 2004.

[58] CAISO, "Today's outlook: Price map." https://www.caiso.com/todays-outlook/prices, 2024.

[59] U. E. I. Administration, "Wholesale power price maps reflect real-time constraints on transmission of electricity," 2011.

[60] K. Lyons, H. Fraser, and H. Parmesano, "An introduction to financial transmission rights," *The Electricity Journal*, vol. 13, no. 10, pp. 31–37, 2000.

[61] A. M. Rudkevich, M. C. Caramanis, E. A. Goldis, X. Li, P. A. Ruiz, and R. D. Tabors, "Financial transmission rights in changing power networks," in *System Sciences (HICSS), 2016 49th Hawaii International Conference on*, pp. 2326–2334, IEEE, 2016.

[62] T. Kristiansen, "Markets for financial transmission rights," *Energy Studies Review*, vol. 13, no. 1, 2004.

[63] W. W. Hogan, "Contract networks for electric power transmission," *Journal of regulatory economics*, vol. 4, no. 3, pp. 211–242, 1992.

[64] H. Ye, Y. Ge, M. Shahidehpour, and Z. Li, "Uncertainty marginal price, transmission reserve, and day-ahead market clearing with robust unit commitment," *IEEE Transactions on Power Systems*, vol. 32, no. 3, pp. 1782–1795, 2016.

[65] G. W. Leslie, "Who benefits from ratepayer-funded auctions of transmission congestion contracts? evidence from new york," *Energy Economics*, vol. 93, p. 105025, 2021.

[66] A. D. Del Rosso and S. W. Eckroad, "Energy storage for relief of transmission congestion," *IEEE Transactions on Smart Grid*, vol. 5, no. 2, pp. 1138–1146, 2013.

[67] H. Khani, M. R. D. Zadeh, and A. H. Hajimiragha, "Transmission congestion relief using privately owned large-scale energy storage systems in a competitive electricity market," *IEEE Transactions on Power Systems*, vol. 31, no. 2, pp. 1449–1458, 2015.

[68] J. Arteaga, H. Zareipour, and N. Amjady, "Energy storage as a service: Optimal pricing for transmission congestion relief," *IEEE Open Access Journal of Power and Energy*, vol. 7, pp. 514–523, 2020.

[69] T. Nguyen, "Doe global energy storage database." https://sandia.gov/ess-ssl/gesdb/public/projects.html, 2021. Accessed: 2023-04-08.

[70] P. Staudt, M. Schmidt, J. Gärttner, and C. Weinhardt, "A decentralized approach towards resolving transmission grid congestion in germany using vehicle-to-grid technology," *Applied energy*, vol. 230, pp. 1435–1446, 2018.

[71] A. Asrari, M. Ansari, J. Khazaei, and P. Fajri, "A market framework for decentralized congestion management in smart distribution grids considering collaboration among electric vehicle aggregators," *IEEE Transactions on Smart Grid*, vol. 11, no. 2, pp. 1147–1158, 2019.

[72] CAISO, "Monthly market performance reports." `https://www.caiso.com/Pages/DocumentsByGroup.aspx?GroupID=A9180EE4-8972-4F3B-9CB8-21D0809B645E`, 2023.

[73] C. S. Geoportal, "California electric transmission lines." `https://gis.data.ca.gov/datasets/260b4513acdb4a3a8e4d64e69fc84fee/explore`, 2023.

[74] CAISO, "Today's outlook - price map." `https://www.caiso.com/TodaysOutlook/Pages/prices.html`, 2023.

[75] CAISO, "Managing the evolving grid: Renewable curtailment." `https://www.caiso.com/about/our-business/managing-the-evolving-grid#renewable-curtailment`, 2024.

[76] C. S. Geoportal, "California electric transmission lines."

[77] CAISO, "Managing oversupply." `https://www.caiso.com/informed/Pages/ManagingOversupply.aspx`, 2023.

[78] H. Farzin, M. Fotuhi-Firuzabad, and M. Moeini-Aghtaie, "A practical scheme to involve degradation cost of lithium-ion batteries in vehicle-to-grid applications," *ieee transactions on sustainable energy*, vol. 7, no. 4, pp. 1730–1738, 2016.

[79] M. Naumann, F. B. Spingler, and A. Jossen, "Analysis and modeling of cycle aging of a commercial lifepo4/graphite cell," *Journal of Power Sources*, vol. 451, p. 227666, 2020.

[80] Q. Yue, C. He, M. Wu, and T. Zhao, "Advances in thermal management systems for next-generation power batteries," *International Journal of Heat and Mass Transfer*, vol. 181, p. 121853, 2021.

[81] Gurobi Optimization, LLC, "Gurobi Optimizer Reference Manual," 2022.

[82] X. Duan, Z. Hu, and Y. Song, "Bidding strategies in energy and reserve markets for an aggregator of multiple ev fast charging stations with battery storage," *IEEE Transactions on Intelligent Transportation Systems*, vol. 22, no. 1, pp. 471–482, 2020.

[83] C. B. Saner, A. Trivedi, and D. Srinivasan, "A cooperative hierarchical multi-agent system for ev charging scheduling in presence of multiple charging stations," *IEEE Transactions on Smart Grid*, vol. 13, no. 3, pp. 2218–2233, 2022.

[84] S. Nakamoto, "Bitcoin: A peer-to-peer electronic cash system," tech. rep., Manubot, 2019.

[85] N. Z. Aitzhan and D. Svetinovic, "Security and privacy in decentralized energy trading through multi-signatures, blockchain and anonymous messaging streams," *IEEE transactions on dependable and secure computing*, vol. 15, no. 5, pp. 840–852, 2016.

[86] D. Drescher, *Blockchain basics*. Ascent Audio, 2020.

[87] Y. Li, W. Yang, P. He, C. Chen, and X. Wang, "Design and management of a distributed hybrid energy system through smart contract and blockchain," *Applied Energy*, vol. 248, pp. 390–405, 2019.

[88] S. Wang, A. F. Taha, J. Wang, K. Kvaternik, and A. Hahn, "Energy crowdsourcing and peer-to-peer energy trading in blockchain-enabled smart grids," *IEEE Transactions on Systems, Man, and Cybernetics: Systems*, vol. 49, no. 8, pp. 1612–1623, 2019.

[89] E. Münsing, J. Mather, and S. Moura, "Blockchains for decentralized optimization of energy resources in microgrid networks," in *2017 IEEE conference on control technology and applications (CCTA)*, pp. 2164–2171, IEEE, 2017.

[90] C. Chen, J. Wang, F. Qiu, and D. Zhao, "Resilient distribution system by microgrids formation after natural disasters," *IEEE Transactions on smart grid*, vol. 7, no. 2, pp. 958–966, 2015.

[91] S. Hua, E. Zhou, B. Pi, J. Sun, Y. Nomura, and H. Kurihara, "Apply blockchain technology to electric vehicle battery refueling," in *Proceedings of the 51st Hawaii International Conference on System Sciences*, 2018.

[92] K. Christidis and M. Devetsikiotis, "Blockchains and smart contracts for the internet of things," *Ieee Access*, vol. 4, pp. 2292–2303, 2016.

[93] S. Han, S. Han, and K. Sezaki, "Development of an optimal vehicle-to-grid aggregator for frequency regulation," *IEEE Transactions on smart grid*, vol. 1, no. 1, pp. 65–72, 2010.

[94] E. Sortomme and M. A. El-Sharkawi, "Optimal scheduling of vehicle-to-grid energy and ancillary services," *IEEE Transactions on Smart Grid*, vol. 3, no. 1, pp. 351–359, 2011.

[95] H. Farzin, M. Fotuhi-Firuzabad, and M. Moeini-Aghtaie, "A practical scheme to involve degradation cost of lithium-ion batteries in vehicle-to-grid applications," *ieee transactions on sustainable energy*, vol. 7, no. 4, pp. 1730–1738, 2016.

[96] S. Pelletier, O. Jabali, G. Laporte, and M. Veneroni, "Battery degradation and behaviour for electric vehicles: Review and numerical analyses of several models," *Transportation Research Part B: Methodological*, vol. 103, pp. 158–187, 2017.

[97] J. Wang, J. Purewal, P. Liu, J. Hicks-Garner, S. Soukazian, E. Sherman, A. Sorenson, L. Vu, H. Tataria, and M. W. Verbrugge, "Degradation of lithium ion batteries employing graphite negatives and nickel–cobalt–manganese oxide+ spinel manganese oxide positives: Part 1, aging mechanisms and life estimation," *Journal of Power Sources*, vol. 269, pp. 937–948, 2014.

[98] D. Wang, J. Coignard, T. Zeng, C. Zhang, and S. Saxena, "Quantifying electric vehicle battery degradation from driving vs. vehicle-to-grid services," *Journal of Power Sources*, vol. 332, pp. 193–203, 2016.

[99] R. Hledik, "Rediscovering residential demand charges," *The Electricity Journal*, vol. 27, no. 7, pp. 82–96, 2014.

[100] H. Ding, Z. Hu, and Y. Song, "Value of the energy storage system in an electric bus fast charging station," *Applied Energy*, vol. 157, pp. 630–639, 2015.

[101] J. Pan, X. Wu, Q. Feng, and Y. Ji, "Optimization of electric bus charging station considering energy storage system," in *2020 8th International Conference on Power Electronics Systems and Applications (PESA)*, pp. 1–5, IEEE, 2020.

[102] F. Trocker, O. Teichert, M. Gallet, A. Ongel, and M. Lienkamp, "City-scale assessment of stationary energy storage supporting end-station fast charging for different bus-fleet electrification levels," *Journal of Energy Storage*, vol. 32, p. 101794, 2020.

[103] X. Ding, W. Zhang, S. Wei, and Z. Wang, "Optimization of an energy storage system for electric bus fast-charging station," *Energies*, vol. 14, no. 14, p. 4143, 2021.

[104] Y. He, Z. Liu, and Z. Song, "Optimal charging scheduling and management for a fast-charging battery electric bus system," *Transportation Research Part E: Logistics and Transportation Review*, vol. 142, no. July, pp. 1–24, 2020.

[105] A. Kunith, R. Mendelevitch, and D. Goehlich, "Electrification of a city bus network—An optimization model for cost-effective placing of charging infrastructure and battery sizing of fast-charging electric bus systems," *International Journal of Sustainable Transportation*, vol. 11, no. 10, pp. 707–720, 2017.

[106] H. Morais, P. Kádár, P. Faria, Z. A. Vale, and H. Khodr, "Optimal scheduling of a renewable micro-grid in an isolated load area using mixed-integer linear programming," *Renewable Energy*, vol. 35, no. 1, pp. 151–156, 2010.

[107] A. S. Hassan, L. Cipcigan, and N. Jenkins, "Optimal battery storage operation for pv systems with tariff incentives," *Applied Energy*, vol. 203, pp. 422–441, 2017.

[108] F. H. Pickel, "OPA Ratepayer Advocate report on DWP 2015 Power Rate Proposal 2016-01-15," tech. rep., City of Los Angeles, Los Angeles, jan 2016.

[109] K. Mongird, V. V. Viswanathan, P. J. Balducci, M. J. E. Alam, V. Fotedar, V. S. Koritarov, and B. Hadjerioua, "Energy storage technology and cost characterization report," tech. rep., Pacific Northwest National Lab.(PNNL), Richland, WA (United States), 2019.

[110] Metro, "Metro G Line (Orange)." https://www.metro.net/riding/guide/G-line/. Accessed: 2021-06-06.

[111] M. Transit, "Electric Bus Update." https://metrocouncil.org/Council-Meetings/Committees/Metropolitan-Council/2021/3-10-21/Electric-Bus-PPT.aspx. Accessed: 2021-09-04.

[112] R. Jager, "Electric bus debuts on G Line (Orange) today in San Fernando Valley — The Source." https://thesource.metro.net/2020/07/27/electric-bus-debuts-on-g-orange-line-today-in-san-fernando-valley/(accessed:Nov.04,2021). Accessed: 2021-09-04.

[113] P. J. Balducci, M. Alam, V. Viswanathan, D. Wu, A. J. Crawford, K. Mongird, M. R. Weimar, A. Somani, and K. Whitener, "The salem smart power center: An assessment of battery performance and economic potential," tech. rep., Pacific Northwest National Lab.(PNNL), Richland, WA (United States), 2017.